An effective theory of driven high T_c superconductors via an alternative Magnus expansion approach

Dissertation
zur Erlangung des Doktorgrades
an der Fakultät für Mathematik,
Informatik und Naturwissenschaften
Fachbereich Physik
der Universität Hamburg

vorgelegt von

Tobias Rexin

Hamburg
2018

Gutachterin / Gutachter der Dissertation:	Prof. Dr. Michael Thorwart PD. Dr. Axel Pelster
Gutachterin / Gutachter der Disputation:	Prof. Dr. Michael Thorwart PD. Dr. Axel Pelster Prof. Dr. Michael Potthoff Prof. Dr. Daniela Pfannkuche Prof. Dr. Henning Moritz
Datum der Disputation:	07.12.2018
Vorsitzender der Prüfungskomission:	Prof. Dr. Michael Potthoff
Vorsitzender des Fach-Promotionsausschusses Physik:	Prof. Dr. Michael Potthoff
Leiter des Fachbereiches Physik:	Prof. Dr. Michael Potthoff
Dekan der Fakultät MIN:	Prof. Dr. Heinrich Graener

Kurzzusammenfassung

Neuste Fortschritte in der Lasertechnologie und der Experimentaltechnik machen es möglich Systeme in Nicht-Gleichgewichtszuständen zu untersuchen und sogar kohärent zu kontrollieren. Ein Beispiel dafür sind künstliche Eichfelder in ultrakalten Atomsystemen, welche durch ausgeklügeltes Treiben des optischen Gitters erzeugt werden konnten [1]. Mit dem Aufkommen von präzisen Starkfeld-THz-Pulsen ist man in der Anregungs- und Untersuchungsspektroskopie in der Lage Festkörpersysteme jenseits vom chemischen und thermischen Gleichgewicht zu untersuchen [2, 3]. Insbesondere Hochtemperatursupraleiter, wie Kuprate, weisen unter Anregung mit ultraschnellen THz-Pulsen neuartige Nicht-Gleichgewichtseigenschaften auf [4, 5, 6, 7, 8, 9, 10, 11, 12]. Eine der vielversprechenden Erscheinungen ist die kohärente Gitterkontrolle zur Begünstigung der Supraleitung, und das teilweise bei Temperaturen deutlich oberhalb der kritischen Temperatur T_c im Gleichgewicht [13].
Diese Dissertationsschrift bietet ein theoretisches Gerüst um Nicht-Gleichgewichtszustände zu untersuchen und liefert einen Beitrag zur Diskussion um diese sogenannten transienten supraleitenden Zustände. Die entwickelte effektive Theorie für den Niedrigenergiebereich basiert auf der Magnus-Entwicklung und der Floquettheorie und approximiert letzendlich den Floquet-Hamilton-Operator im Hochfrequenzgrenzbereich [14, 15, 16][1]. Die Theorie wird auf das Standardproblem des parametrischen Oszillators und das getriebene Lawrence-Doniach Modell angewandt. Letzteres ist ein vereinfachtes Modell eines getriebenen stark anisotropen geschichteten Supraleiters. Durch Neuanordnung der Störterme aus der Magnus-Entwicklung liefert die alternative Magnus-Entwicklung eine systematische Entwicklung in der Treibamplitude und dem Inversen der Treibfrequenz, das wiederum erweitert etwas den Anwendbarkeitsbereich der Magnus-Entwicklung.
Mit Hilfe des hergeleiteten effektiven Floquet-Hamilton-Operators erlangt man Zugang zu thermodynamischen und statistischen Größen wie dem Josephsonstrom und die Fluktuationen um diesen im Nicht-Gleichgewichtszustand. Innerhalb dieser Theorie findet man, dass das Treiben Systemparameter effektiv renormiert. Des Weiteren führt es zu dynamischer Stabilisierung und einem erhöhten kohärenten Transport in geschichteten Supraleitern.
Die hergeleiteten generellen Formeln der alternativen Magnus-Entwicklung können benutzt werden um den Effekt von unterschiedlichen Treibprotokollen zu testen und vorauszuberechnen. In diesem Sinne stellt diese Dissertationsschrift einen weiteres

[1] In Ref. [16] Abschnitt 3 habe ich einen Beitrag zur analytischen Herleitung der Magnus-Entwicklung geliefert. Des Weiteren habe ich Ausdrücke für den parametrischen Oszillator in Abschnitt 4 aus Ref. [16] berechnet. Alle Beiträge sind in Kollaboration mit B.Zhu and meinem ehemaligen Betreuer Prof. Ludwig Mathey.

Versuchsfeld in Richtung Floquet-Design.

Abstract

Recent advances in laser technology and experimental techniques made it feasible to study and coherently control systems in non-equilibrium states. For example, by means of elaborated driving of the optical lattice, an effective synthetic gauge field in a system of ultra-cold atoms has been established [1]. With the emergence of precise strong-field THz pulses, pump-probe spectroscopy allows to study solid state systems beyond chemical and thermal equilibrium [2, 3].
In particular high T_c superconductors (HTSC) such as cuprates, stimulated with ultrafast-THz pulses exhibit novel non-equilibrium features [4, 5, 6, 7, 8, 9, 10, 11, 12]. Among the most promising ones is coherent lattice control to favor superconductivity, sometimes at temperatures significantly above the equilibrium T_c [13].
This thesis provides a theoretical framework to study non-equilibrium states and contributes to the debate on these transient superconducting states. The developed low-energy effective theory is based on the Magnus expansion and the Floquet theory and effectively approximates Floquet Hamiltonians in the high-frequency limit [14, 15, 16][2]. It is employed to the standard problem of the parametric oscillator and the driven Lawrence-Doniach model, a simplified model of a driven highly anisotropic layered superconductor. Via a rearrangement of the perturbative terms from the Magnus expansion the alternative Magnus expansion yields a systematic expansion in the driving amplitude and the inverse of the driving frequency, which slightly increases the range of applicability of the Magnus expansion.
By means of the derived effective Floquet Hamiltonian one gains analytical access to thermodynamic and statistical quantities such as the Josephson current and its fluctuations for non-equilibrium states. Within this framework, one finds that the driving effectively renormalizes system parameters. Furthermore it gives rise to dynamical stabilization and enhanced coherent transport in layered superconductors.
The derived general formulas of the alternative Magnus expansion can be used to test and predict the effect of different driving protocols [17]. In this sense the thesis provides a further test ground towards Floquet engineering.

[2] In Ref. [16], I contributed to the analytic derivation of the Magnus expansion in Section 3 and I derived the expressions for the parametric oscillator in Sec. 4 of Ref. [16]. All contributions are in collaboration with B. Zhu and my former supervisor Prof. Ludwig Mathey.

Contents

Chapter 1

Introduction

Recent advances in laser technology and experimental techniques made it possible to study and coherently control systems in non-equilibrium states. For example, by means of elaborated lattice driving an effective synthetic gauge field in a system of ultra-cold atoms has been established [1]. Generally it is desirable to analyze and predict the effective lattice potential for a system of driven trapped atoms [17].
With the emergence of precise strong-field THz pulses, pump-probe spectroscopy allows to study solid-state systems beyond chemical and thermal equilibrium [2]. Of particular interest are pump-probe experiments which drive collective modes in solids. This enables interesting applications such as the dynamical manipulation of competing orders and the creation of non-equilibrium phases of matter. High T_c superconductors (HTSC) such as cuprates, stimulated with ultrafast-THz pulses exhibit novel non-equilibrium features [4, 5, 6, 7, 8, 9, 11, 12, 10]. Among the most promising ones is coherent lattice control to favor superconductivity, sometimes at temperatures significantly above the equilibrium T_c [7].
The root cause of these transient superconducting states is still debated. Most of the theories revolve around the role of the apical oxygen excitation in the bi-layered YBCO compound. One model directly involves non-linear phononics [18, 19]. Others demonstrate the dynamic enhancement of superconductivity as an effect of a parametric phonon driving acting on the BCS wave function [20]. Several authors attribute an enhancement of the superconducting phase as a consequence of stimulated competing orders [21, 22, 23]. Further ideas touch the topic of parametric cooling in different ways [24]. Furthermore, the effects of the excitation and temporal modulation on the spectrum of the phase fluctuations were considered, demonstrating a reduction of superconducting phase fluctuations in certain frequency ranges [25, 26]. Another effective theory directly derived the conductivity from the parametrically driven Josephson junction model [27, 28].
In a similar context this work develops a low-energy effective theory [14, 15] and

gains analytic insights into driven cuprate systems. Within the framework of the alternative Magnus expansion, a systematic expansion in the driving amplitude and the inverse of the driving frequency was developed [16]. Overall the method works for isolated and dissipative classical systems as well as for isolated quantum systems.

1.1 Normal and high T_c superconductors

The ongoing investigation of superconductivity started over hundred years ago in 1911. The Dutch physicist Heike Kammerlingh Onnes observed in his experiments with liquefied helium, that mercury cooled below 4.2K [29] exhibits „practically no resistance "[30][1]. Soon afterwards other metals were discovered to be superconducting and until the beginning of the 1930s the element niobium had the highest critical temperature at $T_c = 9.25$K. Then, alloys such as NbC and V_3Si were explored [31]. In the 1960s and 1970s niob-alloys still hold the record for the highest transition temperature, until Nb_3Ge was measured with critical temperature of about $T_c = 23$K [32].
The theoretical description of the superconducting effect was challenging. It was realized that the physical concept for superfluidity with a vanishing viscosity, and, therefore, the frictionless flow and superconductivity with vanishing resistance, is the same, namely the Bose-Einstein condensation (BEC). This quantum phenomenon occurs when a macroscopic number of bosonic particles condenses into the lowest energy state. In case for superfluid helium-4, these particles are electrical neutrally bosons. In the superconducting mercury, those particles are pairs of electrons with opposite spin and momentum which were bound together via a phonon-mediated interaction. While single electrons can not undergo the BEC phase transition, bosonic pairs of two electrons are able to condense into a charged superfluid. The underlying principle of electron pairing and a comprehensive microscopic description on superconductivity was revealed in 1957 by **B**ardeen, **C**ooper and **S**chrieffer, presenting their BCS theory [33].

1.1.1 Ginzburg-Landau theory

The Ginzburg-Landau (GL) theory [34] is a viable concept to characterize the superconducting phase transition by introducing an order parameter. It is nonzero in the ordered phase and equals zero in the disordered phase. The order parameter in a superconductor is a complex wave function Ψ describing the condensed electrons,

[1] Additionally it is was reported that at very same day he struggled with his cooling agent helium and witnessed the superfluid-transition of liquid helium-4 without realizing it [30].

also known as Cooper pairs. The Cooper pair wave function is

$$\Psi(\mathbf{r}) = |\Psi(\mathbf{r})|e^{i\theta(\mathbf{r})}. \tag{1.1}$$

The density of Cooper pairs is defined as $n_s(\mathbf{r}) = |\Psi(\mathbf{r})|^2$. The according GL free energy for charged particles coupled to an electromagnetic field is

$$F = F_n + \int d\mathbf{r} \left[\alpha|\Psi(\mathbf{r})|^2 + \frac{\beta}{2}|\Psi(\mathbf{r})|^4 + \frac{1}{2m^*}|(-i\hbar\nabla - q\mathbf{A})\Psi(\mathbf{r})|^2 + \frac{(\nabla \times \mathbf{A})^2}{2\mu_0} \right]. \tag{1.2}$$

μ_0 is the permeability. $\mathbf{A}$ is the gauge potential defining the magnetic flux density $\mathbf{B} = \nabla \times \mathbf{A}$ and F_n is the free energy of the normal state. m^* is the mass and q is the charge of a Cooper pair. Apriori in the GL theory α and β are material dependent phenomenological parameters which have to be determined experimentally.
The free energy in this form (1.2) requires a number of approximations, namely symmetry arguments and the expansion in terms of the spatially slowly varying order parameter [35]. It should be slowly varying as compared to the healing length, which does not always coincide with the Cooper pair radius. Furthermore, the momentum operator was replaced by the gauge invariant canonical momentum $-i\hbar\nabla \to -i\hbar\nabla - q\mathbf{A}$.
By minimizing the GL free energy (1.2) with respect to varations in the order parameter Ψ and the vector potential $\mathbf{A}$, one obtains the two GL equations

$$\alpha\Psi + \beta|\Psi|^2\Psi + \frac{1}{2m^*}(-i\hbar\nabla - q\mathbf{A})\Psi(\mathbf{r}) = 0, \tag{1.3}$$

$$\mathbf{J} = \frac{q}{m^*}|\Psi(\mathbf{r})|^2(\hbar\nabla\theta(\mathbf{r}) - q\mathbf{A}). \tag{1.4}$$

Ampére's law $\mu_0\mathbf{J} = \nabla \times \mathbf{B} = \nabla \times (\nabla \times \mathbf{A})$ and the complex phase representation (1.1) was used to obtain the structure of the second GL equation (1.4). Eq. (1.4) describes a supercurrent of particles with an effective charge q and mass m^* in the presence of a magnetic field. Initially, in their original work in 1950, Ginzburg and Landau identified q with the bare electron charge $-e$. In 1959, Gor'kov derived the GL equation from the BCS theory and established the correct form with $m^* = 2m$ and $q = -2e$. [36].
The mean-field form of the Cooper pair wave function $|\Psi| = \sqrt{-\alpha/\beta}$ [2] can be derived from (1.2) assuming the magnetic field is off, i.e $\mathbf{A} = 0$, and the density is spatially uniform.

[2]Conventionally one takes $\beta > 0$ and around the mean-field transition temperature $\alpha = \alpha_0(T - T_{0,c})$, hence α is positive above $T_{0,c}$ and negative below $T_{0,c}$ in superconducting phase

An electron travelling from the normal phase to the superconducting phase can not change its wave function abruptly, the change must take place over a finite distance [37]. Alternatively, the finite distance scale can be defined as the length over which the phase $\theta(\mathbf{r})$ of the order parameter has to bend such that the associated bending energy is equal to the superconducting condensation energy

$$\alpha|\Psi|^2 = \frac{\hbar^2}{2m^*}|\Psi|^2(\nabla\theta)^2 \tag{1.5}$$

$$\Leftrightarrow \alpha = \frac{\hbar^2}{2m^*}\xi^2 \tag{1.6}$$

$$\Leftrightarrow \xi = \sqrt{\frac{\hbar^2}{4m\alpha}}. \tag{1.7}$$

For the Cooper pairs the effective mass is $m^* = 2m$. ξ is called the coherence length or correlation length. This is basically the scale, over which the supercondcuting phase can recover from small perturbations. In the field of Bose-Einstein condensates, this length is called the healing length. There is an analogy between the GL equation (1.2) describing charged Bose-Einstein condensed Cooper pairs and the Gross-Pitaevski equation as the nonlinear Schrödinger-like equation for Bosons.
Using only θ and $\mathbf{A} = \mathbf{0}$, the free energy becomes

$$F = \frac{\rho_s}{2}\int d\mathbf{r}(\nabla\theta(\mathbf{r}))^2. \tag{1.8}$$

The superfluid stiffness is $\rho_s = \hbar^2 n_{0,s}/4m$ with the uniform superfluid density $n_{0,s} = |\Psi_0|^2$. Another characteristic quantity λ can be derived from the second GL equation (1.4) by replacing $\mathbf{J} = \mu_0^{-1}\nabla\times\mathbf{B}$ and taking the curl of (1.4),

$$\mu_0^{-1}\nabla\times\nabla\times\nabla\times\mathbf{A} = \nabla\times\frac{q}{m^*}|\Psi|^2\left[\hbar\nabla\theta(\mathbf{r}) - q\mathbf{A}\right] \tag{1.9}$$

$$-\mu_0^{-1}\Delta\mathbf{B} = -\frac{q^2}{m^*}|\Psi|^2\mathbf{B} \tag{1.10}$$

$$\Leftrightarrow \frac{1}{\lambda^2}B = \frac{q^2}{m^*}|\Psi|^2\mathbf{B} \tag{1.11}$$

$$\Leftrightarrow \lambda = \sqrt{\frac{2m}{(2e)^2 n_s}}. \tag{1.12}$$

The vector identities $\nabla\times\nabla\theta(\mathbf{r}) = 0$, $\nabla\times\nabla\times = \nabla(\nabla\cdot) - \Delta$ and the gauge $\nabla\cdot\mathbf{A} = 0$ were used to obtain eq. (1.12).
The London penetration depth λ [38] describes the length scale over which fluctuations in the magnetic field $\mathbf{B}$ occur. Exposed to an external magnetic field, a superconductor will expel or diminish the internal magnetic flux $\mathbf{B}$. This well-known Meissner effect was discovered in 1933 [39]. The London penetration depth is still

used to gain information on the superfluid density. The ratio of the penetration depth and the coherence length $\kappa = \lambda/\xi$ is the only free parameter required to characterize a superconductor within the GL framework. For a typical superconductor such as niobium, the penetration depth is $\lambda = 360$Å and one finds a coherence length of $\xi = 390$Å [40]. If one compares the coherence length to a typical crystal unit cell distance a of about $0.5 - 5$Å, one realizes that the Cooper pairs are delocalized over several lattice sites. So, a Cooper pair consists of a wave function over many other Cooper pairs, which can interfere and form a coherent ground state.

1.1.2 BCS theory

A key element of the BCS theory is the origin of the energy gap. To derive this, one starts with the quantum mechanical Schrödinger equation for two interacting electrons

$$\left[-\frac{\hbar\nabla_1^2}{2m} - \frac{\hbar\nabla_2^2}{2m} + V(\mathbf{r}_1 - \mathbf{r}_2)\right]\Psi(\mathbf{r}_1, \mathbf{r}_2) = E\Psi(\mathbf{r}_1, \mathbf{r}_2), \tag{1.13}$$

where $V(\mathbf{r}_1 - \mathbf{r}_2)$ is the interaction potential. A change to the center of mass coordinates $\mathbf{R} = (\mathbf{r}_1 + \mathbf{r}_2)/2$ and the relative coordinates $\mathbf{r} = \mathbf{r}_1 - \mathbf{r}_2$, and the respective Fourier transform of the introduced variables yields

$$\underbrace{\int \frac{d\mathbf{k}'}{(2\pi)^2} V(\mathbf{k} - \mathbf{k}')\Psi(\mathbf{k}')}_{\Delta(\mathbf{k})} = (E - 2\varepsilon_{\mathbf{k}})\Psi(\mathbf{k}), \tag{1.14}$$

assuming a vanishing center of mass momentum $\mathbf{K} = \mathbf{0}$ for the ground state. Furthermore, one defines the energy $\varepsilon_{\mathbf{k}} = \hbar^2 k^2/2m$. The kinetic energy of the relative coordinate has a minimum for electron pairs with opposite momentum $\mathbf{k} = \mathbf{k}_1 - \mathbf{k}_2$. By introducing the modified wave function $\Delta(\mathbf{k})$ one finds the following self-consistent equation

$$\Delta(\mathbf{k}) = -\int \frac{d\mathbf{k}'}{(2\pi)^2} \frac{V(\mathbf{k} - \mathbf{k}')}{2\varepsilon_{\mathbf{k}} - E}\Delta(\mathbf{k}'). \tag{1.15}$$

A first solution to equation (1.15) requires a few approximations. Taking a constant $\Delta(\mathbf{k}) = \Delta$ implies a symmetric wave function and anti-parallel aligned electron spins or a singlet state. Additionally, only the electrons close to the Fermi level are affected by the phonon-mediated attractive interaction. Furthermore, the interaction potential for unoccupied states above the Fermi level is described by $V(\mathbf{k} - \mathbf{k}') = -V_0$. Following these assumptions, the momentum integral in (1.15) can be replaced by an integral over a thin energy shell above the Fermi energy ε_{F} and equation (1.15)

yields

$$\Delta = V_0 \rho(\varepsilon_F) \Delta \int_{\varepsilon_\mathrm{F}}^{\varepsilon_F + \hbar\omega_\mathrm{D}} \frac{d\varepsilon}{2\varepsilon - E}. \tag{1.16}$$

ω_D is the Debye frequency of the material and $\rho(\varepsilon_F)$ is the density of states at the Fermi level. For the assumption $V_0\rho(\varepsilon_F) \ll 1$, the solution of (1.16) gives an estimate for the binding energy of the Cooper pairs

$$E_\mathrm{CP} = 2\varepsilon_\mathrm{F} - E = 2\hbar\omega_\mathrm{D} e^{-\frac{2}{V_0\rho(\varepsilon_F)}}. \tag{1.17}$$

Irrespective of the amplitude V_0 of the attractive interaction potential, the energy of the bound state of the electrons will be lower than the two electron energy at a fully occupied Fermi sea $E - 2\varepsilon_\mathrm{F} < 0$. The Fermi surface is required to clearly separate the unoccupied and the occupied electron states and to be spherically symmetric. It is important to point out that it is this assumption which does not hold for unconventional superconductors.

1.1.3 Unconventional supercondcutors

In 1986, Bednorz and Müller discovered that the ceramic copper-oxide materials become superconducting at unusual temperatures of about 35K or more [41]. This important break-through paved the way towards cuprate materials with critical temperatures at about 135K under standard conditions [42]. Additional classes of high temperature superconductors like fullerites [43] or iron-based ones [44] were discovered. However within the frame of this thesis, the focus is on the layered superconductors such as cuprates, ruthenates or bismuthates.

The search for a complete and comprehensive theory for high $\mathrm{T_c}$ superconductors is a vivid field of research [3]. With advances in experimental techniques, such as refined highly resolved photon emission spectroscopy [46] or improved crystal synthesis and progress from theoretical side, essential features for high $\mathrm{T_c}$ superconductivity were identified. The $\mathrm{CuO_2}$ planes play a key role for superconductivity in cuprates. These materials are highly anisotropic in a stark contrast to the pure metal superconductors or first superconducting alloys. The cuprates are regarded as quasi-two dimensional, with a weak interlayer coupling in the direction perpendicular to the planes [47]. The crystal structure motivates to involve Josephson junctions, yielding many macroscopic models which is elaborated in chapter 2.
Measurements of magnetic flux quanta and supercurrents yield particles with charge

[3] Even standard text books on superconductivity just report on established facts about high $\mathrm{T_c}$ materials and try to narrow down requirements and properties for a successful theory, because there is no satisfying theory available [35].

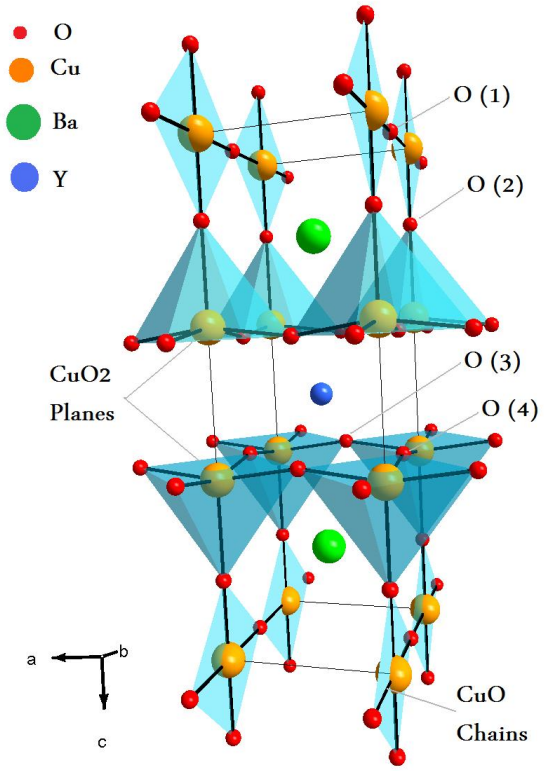

Figure 1.1: Anisotropic unit cell for the bilayered $YBCO$. The strongly correlated CuO_2 planes in ab-direction are separated by the intercalated spacer element Y in c-direction and a charge reservoir unit around the barium Ba and remaining copper oxide CuO components. The apical oxygen 0(2) is distorted along the c-axis via the excitation of the infra-active B_{1u} phonon mode, which leads to induced coherent transport above T_c for underdoped $YBCO$ [6, 7]. Modified from originial source [45].

$2e$. Hence, the origin of superconductivity has been traced back to the formation of Cooper pairs. However the pairing mechanism is not clear and the symmetry of the wave function may differ. Additionally, the typical coherence length is $\xi = 10 - 30\text{Å}$. Therefore, the spatial extension of coherently interfering Cooper pairs is smaller than the classical ones [48]. Obviously, fluctuations in the order parameter will play a more dominant role. According to Emery and Kivelson [49], there are two important energy scales for conventional superconductors. The first one is the BCS gap Δ, which is a measure for the strength of the mutual binding of electrons into Cooper pairs. The second one is the superfluid phase stiffness ρ_s, which measures the ability of the superconducting state to carry a supercurrent. In conventional superconductors Δ is much smaller than ρ_s. Hence, the destruction of superconductivity sets in with the breakup of electron pairs. In cuprates, the two energy scales are much more similar. Hence, for temperatures exceeding ρ_s, thermal agitation will destroy the superconductor's ability to carry a supercurrent, while the electron pairs still continue to exist. It has been concluded that superconductivity is reduced by phase fluctuations. However, quasiparticles to a certain extent modify the phase stiffness [13].
Another property of high-T_c superconductors is their high sensitivity to doping and stoichiometric changes as compared to classical superconductors.

1.2 Experiments on driven high-T_C-superconductors

So far, tunable material parameters, such as temperature, pressure, doping and stoichiometric changes were used to investigate the equilibrium properties of high T_c superconductors. However, advances allow to probe dynamic properties of these materials away from thermal and chemical equilibrium [50]. In this kind of experiments, an initial light pulse excites a nonequilibrium state with excess energy and a quasiparticle density. Then, a subsequent pulse, which is delayed relative to the pump, probes the transient state by detecting changes in the absorbance and the reflectivity. The analysis of the excitation and relaxation of quasiparticles interacting with the condensate yields information on, for example electron-phonon coupling, charge and spin order or the structure of the energy gap itself [51, 52, 53]. The high degree of control allows to alter the collective properties, such as the melting of an ordered phase [8], the light-induced transient superconductivity or transiently enhanced coherent transport [4, 5, 6, 7, 11, 10] . These experiments involved low-energy excitations, nonlinear driving of phonons, Josephson plasmons as well as elements of competing order.
A key finding is the phenomenon of light-induced coherent transport far above T_c in

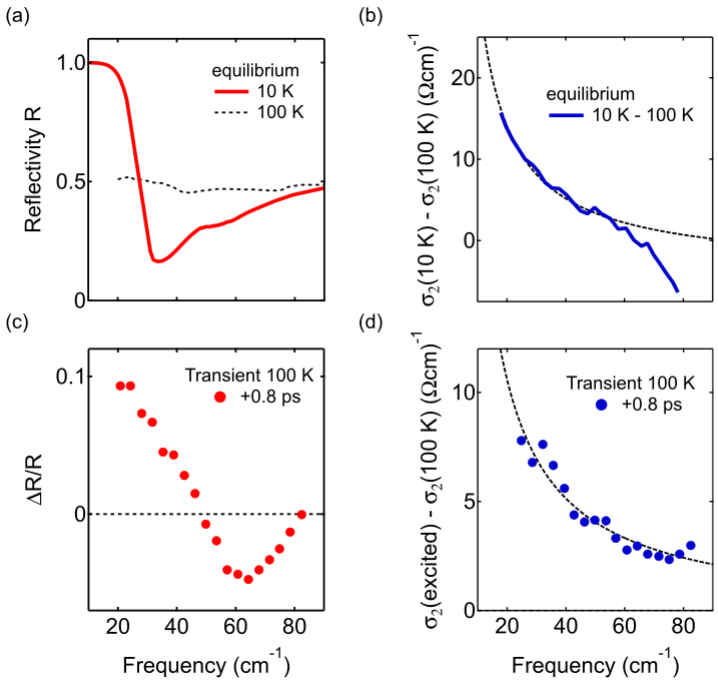

Figure 1.2: a) The equilibrium THz reflectivity of $YBa_2Cu_3O_{6.5}$ above (dashed line) and below the transition temperature of $T_C = 55$K(solid line)shows the appearance of a plasmon edge. (b) The temperature-driven change in the imaginary part of the optical conductivity σ_2 (solid line) across the metal-superconductor transition exhibits the typicall $1/\omega$ divergence for $\omega \to 0$ (dashed line). (c) and (d) The light-induced changes in these observables, 0.8ps after vibrational excitation of $YBa_2Cu_3O_{6.5}$ at 100K with $300-\text{fs}, 15\mu$m mid-infrared pulses, show signatures similar to the equilibrium superconducting state. The figure is taken from Ref. [10]

the underdoped YBCO [6, 7, 10]. A study of the underdoped cuprate $YBa_2Cu_3O_{6.5}$ after a vibrational excitation above T_c is shown in Figure 1.2.

The results are reminiscent of a transiently enhanced superconducting phase with a characteristic $1/\omega$ divergence in the imaginary part of the conductivity σ_2 and a typical reflectivity edge corresponding to the appearance of the Josephson plasmon in the superconducting state. The last point indicates a modification of the interlayer coupling during a pulse excitation.

The cuprate YBCO features a transverse Josephson plasmon which is strongly coupled to the mid-infrared active apical oxygen phononic mode. Via nonlinear phononics, this transverse Josephson plasmon affects the two longitudinal Josephson plasmon modes ω_w, ω_s. These two plasmons play a crucial role in the coherent interlayer transport and were studied in [6, 7, 10] The effect of the driven plasmons on the layered material is modelled theoretically in the next chapter. Accordingly a toy model will be derived, which serves for further analytic studies and still comprises

the key elements of these nonequilibrium experiments.

Chapter 2

Modeling driven high T_c superconductors

Based on the experiments with transient light-induced coherent interlayer transport [6, 7], a theoretical framework to study driven layered complex materials was developed which naturally encompasses the essentials of the layer structure of the material.
The thermally fluctuating state of a bi-layered cuprate superconductor, which is modulated and excited by an external time-dependent field, is analyzed. Highly anisotopic layered materials are often treated within the Lawrence-Doniach (LD) model or the related extended XY-model [54, 55, 56, 57, 49, 58, 59, 60, 61, 62]. This basically features a Ginzburg-Landau (GL) behavior in the superconducting layers, arising from the presence of the copper oxide planes, and a Josephson-junction like behavior in the direction perpendicular to these planes. So, cuprates and similar compounds are described as a Josephson stack of superconducting and insulating layers, schematically illustrated in figure 1.1.
Close to the critical equilibrium temperature T_c one assumes that the fluctuations of the condensate order parameter Ψ are predominant. Knowing that the phase ordering temperature T_θ determines T_c in the HTSC rather than the gap energy [63], the coexisting mechanism of pair breaking is less important and will be neglected in such a phenomenological model.
Several models were developed to theoretically analyse and explain these pump-probe experiments [18, 28]. Certain aspects have been published in [25, 16][1].
The purpose of this thesis is to establish a systematic analytic formalism to obtain a solution to the problem of a driven high-T_c superconductor around the critical

[1]Contribution to the publication in collaboration with the former colleagues Robert Höppner, Beilei Zhu and Professor Ludwig Mathey. Personal contributions will be marked, explained and embedded in the course of this thesis.

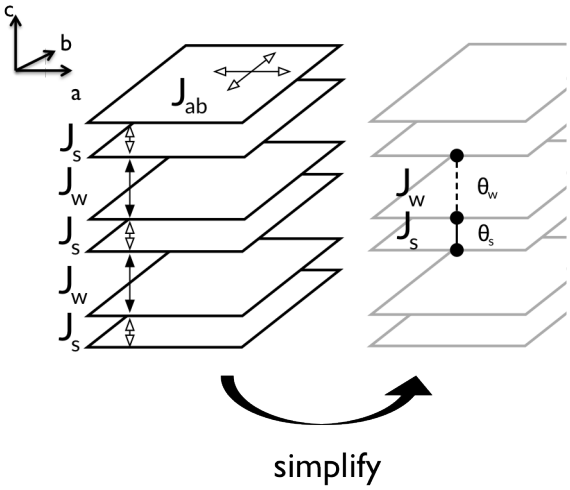

Figure 2.1: Phenomenological modelling of the driven YBCO material. Important here are the two different couplings in c-direction, composed of a weak J_{w} and strong hopping term J_{s}. Accordingly one assumes $J_{\mathrm{w}} < J_{\mathrm{s}}$. [3]

temperature. By means of the Magnus expansion, a low-energy effective theory is formulated which provides a systematic expansion in the ratio of the driving amplitude A and the driving frequency ω_{m}. Based on this theory, an effective stationary probability density of the driven state is derived and phase fluctuations can be computed. The presented theoretical model explains aspects of the observed transient superconductivity and the enhanced coherent transport in layered superconductors. Furthermore the elaborated theoretical framework provides a tool to deal with driven systems in the high-frequency regime $\omega_0 \ll \omega_{\mathrm{m}}$, where ω_0 denotes the natural frequency scale of the undriven system.

2.1 Phenomenological modelling of layered superconducting materials

Motivated by the microscopic structure of the cuprates with the superconducting *ab*-planes and the Josephson stacks in *c*-direction (figure 1.1), the LD model provides the basic features to analyze the driven high $\mathrm{T_c}$ compounds. The scheme of this setting is shown in figure 2.1.

Assuming a small nonzero BCS-pair density on each layer, the starting point is a bosonic pairing field, which is affected by the driving of the phononic modes

[3] The original shared figure for talks and presentations is from R. Höppner, I modified it for my purpose.

[64]. Around the critical temperature T_c, the fluctuations in the order parameter Ψ predominantly destroy the superconducting coherence, rather than a pair breaking mechanism. Thermal fluctuations in the pairing field will dominate at this temperatures, which allows for a classical treatment within the XY model [65].
The pairing field on each layer i and each site k in the phase-density representation is $\Psi_{i,k} = \sqrt{n_0 + n_{i,k}} \exp i\theta_{i,k}$ with the small mean-field density $n_0 = n_{0,i,k}$. The ab-plane is considered as isotropic, therefore the plane is reduced to one site and the site index k is dropped. Furthermore the in-plane tunneling J_{ab} is neglected. This model solely focusses on the driven Josephson junctions in c-direction and reduces to an anisotropic 1D chain along the c-axis. The corresponding undriven Hamiltonian expanded up to second order in n_i yields

$$H_0 = -\sum_{\langle ij \rangle} J_{ij} \cos\left(\theta_i - \theta_j\right) + \frac{E_c}{2} \sum_i n_i^2. \tag{2.1}$$

θ_i is the phase and n_i is the density fluctuation in the layer i. E_c is the charging energy, which is taken to be equal on each layer $E_c = E_{c,i} = E_{c,j}$. The summation index in the brackets $\langle ij \rangle$ indicates the sum over nearest neighboring layers throughout the thesis unless stated differently. The J_{ij} are the different tunneling matrix elements between the respective nearest neighboring layers. For a bilayered system like $YBCO$ the tunneling consists of a strong junction J_s and weak junction J_w in a staggered order, see also the right-hand side of figure 1.1.
By adding the conjugate term $\frac{E_c}{2} \sum_i n_i^2$ to the phase variable, one obtains a second derivative from the Hamilton equations of motion. This allows to investigate the full dynamics. The LD model contains a (quasi 2D) Ginzburg-Landau order parameter in the adjacent layers which are coupled by Josephson junctions. In the limit of zero spacing between the ab-planes, one recovers the standard Ginzburg-Landau model [66, 67].

2.1.1 Time-dependent driving

The resonant excitation of the apical oxygen distortions (see figure 1.1) periodicially alters the vibronic and electronic structure of the material [68, 18, 19]. As a consequence the two prominent Josephson plasmon frequencies associated with the apical oxygen phononic mode are modulated [6]. Neglecting the microscopic details, there are three practicable different ways to introduce modulations to the Josephson plasmon frequencies and the Josephson junctions via external driving. In order to discuss the couplings, it makes sense to derive the plasmon frequency first.
The plasmon frequency can be derived from the LD Hamiltonian and its equations

of motion. For a single undriven Josephson junction between two layers, these equations are

$$\dot{\theta}_1 = \partial_{n_1} H = E_c n_1 \tag{2.2}$$
$$\dot{\theta}_2 = \partial_{n_2} H = E_c n_2 \tag{2.3}$$
$$\dot{n}_1 = -\partial_{\theta_1} H = -J \sin(\theta_1 - \theta_2) \tag{2.4}$$
$$\dot{n}_2 = -\partial_{\theta_2} H = J \sin(\theta_1 - \theta_2). \tag{2.5}$$

Here the short hand notation for the first derivative with respect to time $\partial_t X = \dot{X}$ is introduced. Introducing the symmetrized relative coordinates $\theta = \theta_1 - \theta_2$ and $n = (n_1 - n_2)/2$ one obtains the two compact Josephson equations

$$\dot{\theta} = 2E_c n \tag{2.6}$$
$$\dot{n} = -J \sin\theta. \tag{2.7}$$

Taking the derivative with respect to time in (2.6) and subsequently plugging equation (2.7) into (2.6) yields the second-order differential equation

$$\ddot{\theta} = -\underbrace{2E_c J}_{:=\omega^2} \sin\theta. \tag{2.8}$$

¨denotes the second derivative with respect to time.
The associated frequency $\omega = \sqrt{2E_c J}$ is identified as the Josephson plasmon frequency of an undriven and undamped system.
The first extension is the linear (or dipole) coupling which directly couples the external driving field to the density n_i, yielding the Hamiltonian term

$$H_{dr,dip} = \sum_i A_i(t) n_i. \tag{2.9}$$

Deriving the equations of motion for a single junction with a staggered potential $A_i(t) = (-1)^i A(t)$, one finds

$$\dot{\theta} = 2E_c n + 2A(t), \tag{2.10}$$

which generates essentially a phase boost and leads to an externally driven Josephson junction. The second extension is the inductive coupling yielding a term

$$H_{dr,ind} = -\sum_{<ij>} J_{ij} A_{ij}(t) \cos(\theta_i - \theta_j). \tag{2.11}$$

Deriving the second order differential equation, this term leads to a parametrically driven Josephson junction and is motivated via the Peierls substitution, which yields an addtional time-dependent phase shift in the tunneling elements and therefore an effective $J_{ij}(t)$. The third coupling is the capacitive coupling

$$H_{dr,cap} = \frac{E_\mathrm{c}}{2} \sum_i A_{c,i}(t) n_i^2, \tag{2.12}$$

which leads to

$$\dot{\theta} = 2E_\mathrm{c}[1 + A(t)]n \tag{2.13}$$

in the single junction case. Again deriving the second order differential equation, this nonlinear coupling gives rise to a parametrically driven Josephson junction plus a phase-velocity-dependent term proportional to $\dot{A}n = \dot{A}(\dot{\theta}/E_\mathrm{c} - A)$. It could be interpreted as a time-dependent damping parameter.
The terminology of a capacitive and inductive coupling stems from the simplified analogy to the LC circuit for this layered superconductors. A change in the interlayer distance due the apical oxygen phonon modifies the capacitance on each layer and additionally alters the Josephson tunneling elements. The superconducting layers are described by the capacitive term and the Josephson junction part is associated as the inductive term.

2.1.2 Parameter ranges

The values of the parameters $J_\mathrm{w}, J_\mathrm{s}, E_\mathrm{c}$ in the Lawrence-Doniach model are constrained by the Josephson plasmon frequencies [6]. According to equation (2.8), the plasmon frequencies are approximated by $\omega_{\mathrm{s/w}} = \sqrt{2J_{\mathrm{s/w}}E_\mathrm{c}}$. The weak plasmon frequency scale is $\omega_\mathrm{w} = 1\mathrm{THz}$ and the strong one is $\omega_\mathrm{s} = 10\mathrm{THz}$. The respective LD parameters are summarized in table 2.1

2.1.3 Classical two-oscillator toy model

This section elaborates on a minimal model of a driven bilayered superconductor which ignores the in-plane tunneling J_ab. Around $T = T_\mathrm{c}$ thermal fluctuations dominate and a classical treatment is justified. Again, this minimal toy model amounts to a 1D chain along the c-direction comprising one strong and one weak junction, see figure 1.1. It requires three sites in the corresponding Hamiltonian to

	J_w	J_s	J_ab	E_c	A_0	γ
$E/k_\mathrm{B}(\mathrm{K})$	0.2	20	100	6250	$20-450$	10
$E/h(\mathrm{THz})$	0.0042	0.42	2.1	130.7	$0.42-9.4$	0.2
$E/h(\mathrm{meV})$	0.017	1.7	8.6	539.1	$1.7-38.8$	0.9

Table 2.1: Model parameters in $k_\mathrm{B}\times K, h\times\mathrm{THz}$ and meV. All parameters are given in energy units E. The parameters were chosen to roughly match the measured Josephson plasmon frequencies $\omega_{\mathrm{w/s}}=\sqrt{2J_{\mathrm{w/s}}E_\mathrm{c}}$. J_ab is similiar to the $\mathrm{T_c}$ of YBCO at about 100K which is the Kosterlitz-Thouless energy scale the for *ab*-plane. This the energy for a phase transition from an bound vortex-anitvortex state to unpaired and correlated vortices and antivortices. The presented XY model features this as a loss of phase coherence within the plane.

describe two Josephson junctions

$$H_0=-J_\mathrm{s}\cos\left(\theta_1-\theta_2\right)-J_\mathrm{w}\cos\left(\theta_2-\theta_3\right)+\frac{E_\mathrm{c}}{2}\left(n_1^2+n_2^2+n_3^2\right). \tag{2.14}$$

Initially, a linear coupling between the driving and the density is used. The time-dependent Hamiltonian with its staggered potential is, accordingly,

$$H_{dr}(t)=A(t)n_1-A(t)n_2+A(t)n_3. \tag{2.15}$$

$A(t)$ represents the externally applied time-dependent field. The driving protocol $A(t)$ is a priori arbitrary. It is sufficient to use a cosine driving $A(t)=A_0\cos\omega_m t$ with modulation frequency ω_m and a constant driving amplitude A_0 to cover the essential features.
The equations of motion (eom) derived from the Hamiltonian $H(t)=H_0+H_{dr}(t)$ are

$$\dot{\theta_1}=\partial_{n_1}H=E_\mathrm{c}n_1+A(t) \tag{2.16}$$
$$\dot{\theta_2}=\partial_{n_2}H=E_\mathrm{c}n_2-A(t) \tag{2.17}$$
$$\dot{\theta_3}=\partial_{n_3}H=E_\mathrm{c}n_3+A(t) \tag{2.18}$$
$$\dot{n_1}=-\partial_{\theta_1}H=-J_\mathrm{s}\sin\left(\theta_1-\theta_2\right) \tag{2.19}$$
$$\dot{n_2}=-\partial_{\theta_2}H=-J_\mathrm{w}\sin\left(\theta_2-\theta_3\right)+J_\mathrm{s}\sin\left(\theta_1-\theta_2\right) \tag{2.20}$$
$$\dot{n_3}=-\partial_{\theta_3}H=J_\mathrm{w}\sin\left(\theta_2-\theta_3\right). \tag{2.21}$$

To simplify the sin terms one combines the equations (2.16)-(2.21) and introduces the relative coordinates

$$\theta_\mathrm{s} = \theta_1 - \theta_2 \tag{2.22}$$

$$\theta_\mathrm{w} = \theta_2 - \theta_3 \tag{2.23}$$

$$n_\mathrm{s} = \frac{n_1 - n_2}{2} \tag{2.24}$$

$$n_\mathrm{w} = \frac{n_2 - n_3}{2}. \tag{2.25}$$

By this, one avoids trigonometric addition theorems and nonlinear couplings between the variables. The resulting equations are

$$\dot{\theta}_\mathrm{s} = 2E_\mathrm{c} n_\mathrm{s} + 2A(t) \tag{2.26}$$

$$\dot{\theta}_\mathrm{w} = 2E_\mathrm{c} n_\mathrm{w} - 2A(t) \tag{2.27}$$

$$\dot{n}_\mathrm{s} = -J_\mathrm{s} \sin\theta_\mathrm{s} - \frac{1}{2} J_\mathrm{w} \sin\theta_\mathrm{w} \tag{2.28}$$

$$\dot{n}_\mathrm{w} = -J_\mathrm{w} \sin\theta_\mathrm{w} - \frac{1}{2} J_\mathrm{s} \sin\theta_\mathrm{s}. \tag{2.29}$$

Taking the derivative of eq. (2.26) and eq. (2.27) with respect to time, the four first order differential equations (2.26)-(2.29) can be transformed into two second-order differential equations

$$\ddot{\theta}_\mathrm{s} = -\underbrace{2E_\mathrm{c} J_\mathrm{s}}_{\omega_\mathrm{s}^2} \sin\theta_\mathrm{s} - E_\mathrm{c} J_\mathrm{w} \sin\theta_\mathrm{w} + 2\dot{A}(t) \tag{2.30}$$

$$\ddot{\theta}_\mathrm{w} = -\underbrace{2E_\mathrm{c} J_\mathrm{w}}_{\omega_\mathrm{w}^2} \sin\theta_\mathrm{w} - E_\mathrm{c} J_\mathrm{s} \sin\theta_\mathrm{s} - 2\dot{A}(t). \tag{2.31}$$

Here, the two Josephon plasmon frequencies are $\omega_\mathrm{w}, \omega_\mathrm{s}$.
An anisotropic XY-model was employed to describe the fluctuating phase in a layered superconductor close to $\mathrm{T_c}$. A capacitive term $(E_\mathrm{c}/2)\sum_i n_i$ was added to allow for a complete description of the dynamics. The system was substantially reduced from a bulk model to a single pair of two Josephson junctions. Yet, the impact of the driving to the coherent transport along the c-axis has to be studied.

2.2 Langevin approach and Fokker-Planck equation

2.2.1 Langevin equation

The above system is an open system constantly gaining energy from the external laser field. To include the influence of the phonons, in the next step, one adds

a damping term and a Langevin noise term, which mimics, on the one hand, the Ohmic resistance in the material and, on the other hand, the excess degrees of freedom where the energy could be distributed to via phonon decay, for example.
The added damping and the noise term yield a classical description of two coupled oscillators which feature aspects of the driven YBCO compound with the following eom

$$\ddot{\theta}_{\mathrm{s}} = -\omega_{\mathrm{s}}^2 \sin\theta_{\mathrm{s}} - \frac{1}{2}\omega_{\mathrm{w}}^2 \sin\theta_{\mathrm{w}} + 2\dot{A}(t) - \gamma\dot{\theta}_{\mathrm{s}} + \xi_{\mathrm{s}} \tag{2.32}$$

$$\ddot{\theta}_{\mathrm{w}} = -\omega_{\mathrm{w}}^2 \sin\theta_{\mathrm{w}} - \frac{1}{2}\omega_{\mathrm{s}}^2 \sin\theta_{\mathrm{s}} - 2\dot{A}(t) - \gamma\dot{\theta}_{\mathrm{w}} + \xi_{\mathrm{w}}. \tag{2.33}$$

γ is the damping rate. The $\xi_{\mathrm{w/s}}$ are classical Langevin noise terms, which are assumed to be Gaussian white noise with the correlations

$$\langle \xi_{\mathrm{w/s}}(t_1)\xi_{\mathrm{w/s}}(t_2)\rangle = 4\gamma E_{\mathrm{c}} k_{\mathrm{B}} T \delta(t_1 - t_2). \tag{2.34}$$

k_{B} is the Boltzmann constant, which is usually set to 1, unless explicitly needed or given elsewhere. The ensemble average of the noise term $\langle \xi_{\mathrm{w/s}}(t)\rangle = 0$ vanishes. Furthermore, the average of the rapidly fluctuating force over a long time interval, as compared to the characteristic time $\tau = 1/\omega_0$ of the system, $\overline{\xi_i(t)} = 0$ averages out to zero. The temporal average is defined as $\overline{O} = \int_0^T O/T$. For a more realistic heat bath one should elaborate on the spectral density of the heat bath based on experimental results. It is assumed that the lattice environment with a broad phonon spectrum acts as an appropriate heat bath. The coupling to certain phonon modes is certainly not the same for the Josephson plasmon modes [6], hence one could introduce mode selective coupling to the heat bath γ_i. The specifics of the environment are sufficient to dissipate away the excess energy and to allow for steady states. This matter is further addressed after the derivation of the driven ensemble distributions at the end of Chapter 2.2.5 and in Chapter 3.
The differential equations (2.32),(2.33) can not be decoupled. Therefore, the strong junction in eq. (2.32) is considered as an externally driven oscillator, which is only negligbly affected by the presence of the weak junction. This treatment is justified by the separation of energy scales of the plasmon frequencies $\omega_{\mathrm{s}} \gg \omega_{\mathrm{w}}$. Further, this means the backaction effect is neglected. The backaction of the weak junction to the strong junction could lead to shifts or weak renormalization of the strong plasmon frequency. This is expected to be a rather minor effect as compared to the reverse case. However, the strong junction equation (2.32) is decoupled and its solution can be computed explicitly. A similar treatment was outlined in the contribution to Ref. [25]. There, the strong junction was considered as a driven harmonic oscillator.
The Langevin equation for the strong junction without backaction from the weak

junction is

$$\ddot{\theta}_\mathrm{s} = -\omega_\mathrm{s}^2 \sin\theta_\mathrm{s} + \underbrace{2\dot{A}(t)}_{F(t)} - \gamma\dot{\theta}_\mathrm{s} + \xi_\mathrm{s} + \mathcal{O}({\omega_\mathrm{w}}^2) \tag{2.35}$$

with $F(t) = F_0 \sin\omega_\mathrm{m} t = -2\omega_\mathrm{m} A_0 \sin\omega_\mathrm{m} t$. $\mathcal{O}({\omega_\mathrm{w}}^2)$ means the small contributions of the order $\sim E_\mathrm{c} J_\mathrm{w} \ll E_\mathrm{c} J_\mathrm{s}$ are omitted.
The full nonlinear problem is analytically hard to solve, so as a first approximation the system will be linearized for small phase differences $\theta_\mathrm{s} \approx 0$ between the layers. This is reasonable as long as the temperature is around the critical temperature $T \leq T_\mathrm{c}$.
Taylor expanding the nonlinear sine potential up to the first order in θ yields an equation for an externally driven harmonic oscillator coupled to a heat bath

$$\ddot{\theta}_\mathrm{s} = -\omega_\mathrm{s}^2 \theta_\mathrm{s} - \gamma\dot{\theta}_\mathrm{s} + F(t) + \xi_\mathrm{s}. \tag{2.36}$$

The external driving is composed of a deterministic periodic part $F(t)$ and a stochastic part ξ_s. The derivation of the solution for the driven harmonic oscillator equation of the strong junction can be found in the Appendix A. The driven harmonic oscillator solution is

$$\begin{aligned} \theta_\mathrm{s} &= \theta_{\mathrm{s},h} + \theta_{\mathrm{s},inh} && (2.37)\\ &= e^{-\frac{\gamma}{2}t}\left(B_1 \cos\left[\sqrt{\omega_\mathrm{s}^2 - \frac{\gamma^2}{4}}t\right] + B_2 \sin\left[\sqrt{\omega_\mathrm{s}^2 - \frac{\gamma^2}{4}}t\right]\right) \\ &\underbrace{-\frac{2\omega_\mathrm{m}^2\gamma A_0}{(\omega_\mathrm{s}^2 - \omega_\mathrm{m}^2)^2 + \omega_\mathrm{m}^2\gamma^2}}_{A_c}\cos\omega_\mathrm{m} t + \underbrace{\frac{2\omega_\mathrm{m}^2(\omega_\mathrm{s}^2 - \omega_\mathrm{m}^2)A_0}{(\omega_\mathrm{s}^2 - \omega_\mathrm{m}^2)^2 + \omega_\mathrm{m}^2\gamma^2}}_{A_s}\sin\omega_\mathrm{m} t, && (2.38) \end{aligned}$$

where B_1, B_2 are determined by the initial conditions. The solution can be used as a feedback response for the weak junction θ_w.

[5]The original shared figure for talks and presentations is from R. Höppner, I modified it for my purpose.

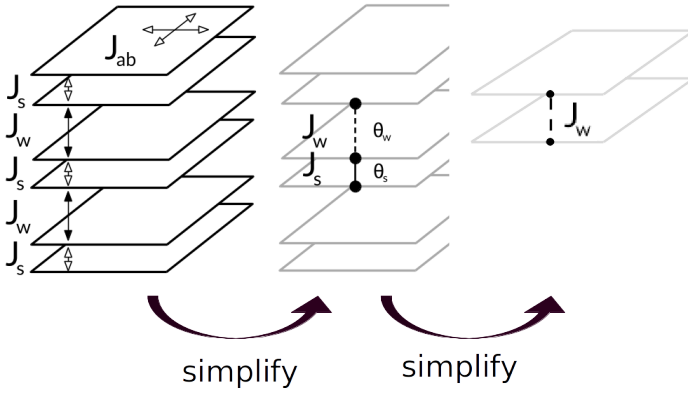

Figure 2.2: For $\omega_\mathrm{s} \gg \omega_\mathrm{w}$ the presence of the weak junction leaves the dynamics of the strong junction almost unaffected. Therefore, the equation of motion for the strong junction is decoupled and solved independently. The solution is fed back to renormalize the driving of the weak junction.[5]

2.2.2 Renormalized driving for the weak junction

The strong junction dynamics (2.38) renormalizes the driving of the weak junction according to

$$\ddot{\theta}_\mathrm{w} = -\omega_\mathrm{w}^2 \sin\theta_\mathrm{w} - \frac{1}{2}\omega_\mathrm{s}^2 \sin\theta_\mathrm{s} - 2\dot{A}(t) - \gamma\dot{\theta}_\mathrm{w} + \xi_\mathrm{w} \tag{2.39}$$

$$= -\omega_\mathrm{w}^2 \sin\theta_\mathrm{w} \underbrace{-\frac{1}{2}\omega_\mathrm{s}^2\theta_\mathrm{s} - 2\dot{A}(t)}_{=G(t)} - \gamma\dot{\theta}_\mathrm{w} + \xi_\mathrm{w}. \tag{2.40}$$

Here the equation (2.40) is linearized in θ_s. For the steady state of the strong junction response, the effective external driving term $G(t)$[6] becomes

$$G(t) = \underbrace{-\frac{{\omega_\mathrm{s}}^2 A_c}{2}}_{G_c}\cos\omega_\mathrm{m}t + \underbrace{\left(2\omega_\mathrm{m}A_0 - \frac{{\omega_\mathrm{s}}^2 A_s}{2}\right)}_{G_s}\sin\omega_\mathrm{m}t \tag{2.41}$$

This driving term can be cast into the form $G(t) = G_0\sin(\omega_\mathrm{m}t + \phi_0)$. The renormalized amplitude is $G_0 = \sqrt{G_c^2 + G_s^2}$ and the shifted relative initial phase is defined as $\phi_0 = \arctan(G_c/G_s)$. A global shift on the time axis $t \to t - \phi_0/\omega_\mathrm{m}$ eliminates the initial phase and one obtains $G(t) = G_0\sin\omega_\mathrm{m}t$.

[6] Technically the damping term $-\gamma\dot{\theta}$ was added after the derivation of the second order differential equation. This slightly changes the form of the driving coefficients G_c and G_s.

To summarize, equation (2.40) describes the dynamics of a driven bilayered superconductor by using a toy model. The dynamics in the *ab*-plane was neglected and the anisotropy along the *c*-direction was kept. After a separation of the strong junction dynamics, its solution was fed back as a response to the weak junction resulting in equation (2.40) with a significantly renormalized driving.

2.2.3 Non-linear feedback for the weak junction

From the numerical simulation for the anisotropic 1D chain, the response of the strong junction phase θ_s exhibited a skewed behavior as reported in Ref. [25] [7]. This indicates that one might consider the first anharmonicities also in an analytically treatment. By expanding eq. (2.32) up to the cubic term one obtanins the forced Duffing oscillator equation, which describes the non-linear response of the strong junction. The solution to the forced Duffing oscillator equation

$$\ddot{\theta}_\mathrm{s} = -\omega_\mathrm{s}^2 \left(\theta_\mathrm{s} - \frac{\theta_\mathrm{s}^3}{6}\right) - \gamma\dot{\theta}_\mathrm{s} + \underbrace{2\dot{A}(t)}_{F(t)} + \xi_\mathrm{s} \tag{2.42}$$

is developed in Appendix B, see also Ref.[69].
Taking into account the nonlinearity, in the form of the cubic term, the amplitude of θ_s can bifurcate, meaning for a certain given frequency ω_b it has a high and low amplitude solution. This is a direct result from the Cardano method which includes three cube roots. Depending on the parameters more of these roots become real and thus physical solutions, see also Appendix B. The analytic expression for the solutions of (2.42) are lengthy and not of practical use for further calculations as feedback for the weak junction. However, the Duffing response is shown numerically and implicitly analytically in figure (2.3). Details for the analytical computation of the second moment $\langle {\theta_\mathrm{s}}^2 \rangle$ are presented in the following sections.

2.2.4 Overdamped regime and Fokker-Planck equation

In a first approach the differential equation for the weak junction (2.40) is solved in the overdamped limit $\gamma \gg \omega_\mathrm{w}, J_\mathrm{w}$. Hence the dynamics of the $\ddot{\theta}_\mathrm{w}$ term is neglected and the according first order equation is

$$\dot{\theta}_\mathrm{w} = -\frac{\omega_\mathrm{w}^2}{\gamma}\sin(\theta_\mathrm{w}) + \frac{G(t)}{\gamma} + \frac{\xi_\mathrm{w}}{\gamma}. \tag{2.43}$$

[7] For this paper the bulk simulation was performed by Robert Höppner and single junction simulation was done by Beilei Zhu.I only contributed to the analytical part.

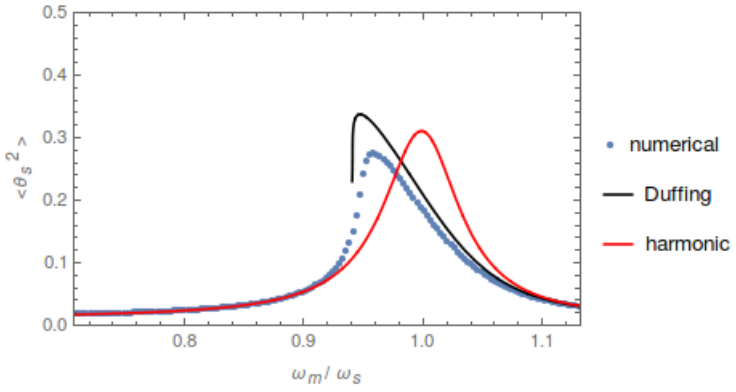

Figure 2.3: Time averaged variances of the strong junction computed numerically (blue), analytically with the linear oscillator model (red) and with the Duffing oscillator model (black). The Duffing model also features the skewness of the variance peak arising from the non-linearity in the eom (2.42). The parameters in the numerics given temperature units K are $J_\mathrm{s} = 50, J_\mathrm{w} = 0.5, A_0 = 0.06, E_\mathrm{c} = 5000, T = 0.5, \gamma = 50$. The numerical data for this plot was provided by Beilei Zhu.

The goal is to determine the non-equilibrium distribution $P_{dr}[\theta_\mathrm{w}, t]$ for the driven system at a finite temperature which allows to compute variances and phase fluctuations. To this end, the Smoluchowski equation is derived from the overdamped Langevin equation (2.43), which is the overdamped special case for the Fokker-Planck equation. This can be done without the explicit knowledge of the underlying probability density or microscopic mechanism. Only the macroscopic equation of motion (2.43) and the knowledge on the thermal equilibrium state for the undriven system are required to construct the equation of motion for the probability density [70].
The Fokker-Planck equation takes into account the first two terms of the Kramers-Moyal expansion and has the following generic structure

$$\partial_t P[\theta, t] = -\frac{\partial}{\partial_\theta}\left(A[\theta, t]P\right) + \frac{1}{2}\frac{\partial^2}{\partial_\theta^2}\left(B[\theta, t]P\right). \tag{2.44}$$

The coefficient $A[\theta, t]$ is derived from the macroscopic equation of motion $\dot{\theta}_\mathrm{w} = \cdots$. For the Smoluchowski equation, in the overdamped case, this eom is often approximated by the macroscopic force term acting on the system, renormalized by the mass of the particle m and the damping γ, e.g $A[x, t] = F[x, t]/(m\gamma)$. The Smoluchowski equation for the overdamped and externally driven Josephson Junction (2.43) is

$$\partial_t P[\theta_\mathrm{w}, t] = \frac{2E_\mathrm{c}J_\mathrm{w}}{\gamma}\frac{\partial}{\partial\theta_\mathrm{w}}\left(\sin\theta_\mathrm{w}\ P[\theta_\mathrm{w}, t]\right) + \frac{G(t)}{\gamma}\frac{\partial}{\partial\theta_\mathrm{w}}P[\theta_\mathrm{w}, t] + \frac{2E_\mathrm{c}k_\mathrm{B}T}{\gamma}\frac{\partial^2}{\partial{\theta_\mathrm{w}}^2}P[\theta_\mathrm{w}, t]. \tag{2.45}$$

The expression $2E_{\mathrm{c}}J_{\mathrm{w}} = {\omega_{\mathrm{w}}}^2$ is associated to the weak plasmon fequency in a bi-layered system. The analog inverse mass term for the Josephson junction is E_{c}. $P[\theta_{\mathrm{w}}, t]$ is defined as the time-dependent probability distribution of θ_{w} on the interval $(-\pi, \pi]$. Without external driving $G(t) = 0$ the thermal equilibrium solution of the Fokker-Planck equation (2.45) is

$$P_{eq} = Ne^{\left[\frac{J_{\mathrm{w}}}{k_{\mathrm{B}}T}\cos\theta_{\mathrm{w}}\right]}. \tag{2.46}$$

N is the standard normalization. For $G(t) \neq 0$ the following exponential ansatz for the non-equilibrium distribution [8] is proposed

$$P[\theta_{\mathrm{w}}, t] = N\exp(f[\theta_{\mathrm{w}}, t]) \tag{2.47}$$

with f being the formal solution to the driven Josephson junction problem at finite temperature. By inserting the ansatz eq. (2.47) into eq. (2.45) one obtains the following differential equation for f

$$\partial_t f = \frac{2E_{\mathrm{c}}}{\gamma}\left(T\left[\partial_{\theta_{\mathrm{w}}\theta_{\mathrm{w}}}f + (\partial_{\theta_{\mathrm{w}}}f)^2\right] + J_{\mathrm{w}}\left[\cos\theta_{\mathrm{w}} + \sin\theta_{\mathrm{w}}\partial_{\theta_{\mathrm{w}}}f\right]\right) + \frac{G(t)}{\gamma}\partial_{\theta_{\mathrm{w}}}f. \tag{2.48}$$

From (2.48) one deduces that f has to be periodic in θ_{w} and its according Fourier expansion is $f = \sum_n \exp[in\theta_{\mathrm{w}}]a_n(t)$. Principally this Fourier ansatz contains all higher harmonics. However, for practical purpose the expansion is limited to the first harmonics $n = \pm 1$. This is a valid approximation in the weak driving $|F| \leq \gamma J_{\mathrm{w}}$ and in the high temperature regime $T \gg J_{\mathrm{w}}$. Correspondingly, the real ansatz is

$$f[\theta_{\mathrm{w}}, t] = \frac{J_{\mathrm{w}}}{T}\left[(1 + a_{\mathrm{c}}(t))\cos\theta_{\mathrm{w}} + a_{\mathrm{s}}(t)\sin\theta_{\mathrm{w}}\right]. \tag{2.49}$$

This "base set" covers the first harmonics, explicitly ignoring the higher harmonic contributions arising from the particular terms $\propto (\partial_{\theta_{\mathrm{w}}}f)^2$ and $\propto \sin\theta_{\mathrm{w}}\partial_{\theta_{\mathrm{w}}}f$. By construction, the time-dependent dimensionless Fourier coefficients $a_{\mathrm{c}}, a_{\mathrm{s}}$ take into account the nonequilibrium admixture. Applying the ansatz (2.49) to eq.(2.48), a subsequent projection onto $\cos\theta_{\mathrm{w}}$ and $\sin\theta_{\mathrm{w}}$ yields the equations of motion for the Fourier coefficients $a_{\mathrm{c}}(t)$ and $a_{\mathrm{s}}(t)$in the form

$$\dot{a}_{\mathrm{s}}(t) = -\frac{2E_cT}{\gamma}a_{\mathrm{s}}(t) - \frac{G_0\sin\omega_{\mathrm{m}}t}{\gamma} \tag{2.50}$$

$$\dot{a}_{\mathrm{c}}(t) = -\frac{2E_cT}{\gamma}a_{\mathrm{c}}(t) + \frac{G_0\sin\omega_{\mathrm{m}}t}{\gamma}a_{\mathrm{s}}(t), \tag{2.51}$$

[8] The ansatz was proposed by my former supervisor Prof. Ludwig Mathey [25].

after a linearization of the equations assuming $a_\mathrm{c}, a_\mathrm{s} \ll 1$ and keeping terms up to the order G_0^2. Setting the equilibrium initial condition $a_\mathrm{c}[0] = a_\mathrm{s}[0] = 0$ the solutions to (2.50) and (2.51) are

$$a_\mathrm{s}(t) = C_1 \exp(-t/t_r) - C_1 \cos\omega_\mathrm{m} t + C_2 \sin\omega_\mathrm{m} t \tag{2.52}$$

$$a_\mathrm{c}(t) = \exp(-t/t_r)\,(C_3 + C_4 \cos\omega_\mathrm{m} t) - \frac{C_4}{2} + C_5 \cos 2\omega_\mathrm{m} t + C_6 \sin 2\omega_\mathrm{m} t, \tag{2.53}$$

with the coefficients

$$C_1 = -\frac{G_0 \gamma \omega_\mathrm{m}}{\gamma^2 {\omega_\mathrm{m}}^2 + 4E_\mathrm{c}^2 T^2} \tag{2.54}$$

$$C_2 = -\frac{G_0 2E_\mathrm{c} T}{\gamma^2 {\omega_\mathrm{m}}^2 + 4E_\mathrm{c}^2 T^2} \tag{2.55}$$

$$C_3 = -\frac{G_0^2(\gamma^2 {\omega_\mathrm{m}}^2 + 4E_\mathrm{c}^2 T^2)}{4\left((\gamma^2 {\omega_\mathrm{m}}^2 + 2E_\mathrm{c}^2 T^2)^2 + \gamma^2 {\omega_\mathrm{m}}^2 E_\mathrm{c}^2 T^2\right)} \tag{2.56}$$

$$C_4 = \frac{G_0^2(\gamma^2 {\omega_\mathrm{m}}^2 + E_\mathrm{c}^2 T^2)}{(\gamma^2 {\omega_\mathrm{m}}^2 + 2E_\mathrm{c}^2 T^2)^2 + \gamma^2 {\omega_\mathrm{m}}^2 E_\mathrm{c}^2 T^2} \tag{2.57}$$

$$C_5 = \frac{G_0^2(-\gamma^2 {\omega_\mathrm{m}}^2 + 2E_\mathrm{c}^2 T^2)}{4\left((\gamma^2 {\omega_\mathrm{m}}^2 + 2E_\mathrm{c}^2 T^2)^2 + \gamma^2 {\omega_\mathrm{m}}^2 E_\mathrm{c}^2 T^2\right)} \tag{2.58}$$

$$C_6 = \frac{G_0^2(3E_\mathrm{c}\gamma\omega_\mathrm{m} T)}{4\left((\gamma^2 {\omega_\mathrm{m}}^2 + 2E_\mathrm{c}^2 T^2)^2 + \gamma^2 {\omega_\mathrm{m}}^2 E_\mathrm{c}^2 T^2\right)}. \tag{2.59}$$

A transient time scale $t_{tr} = \gamma/(2TE_\mathrm{c})$ was introduced in (2.53). The driving amplitude F_0 should be always compared to either the scale of TE_c or $\gamma\omega_\mathrm{m}$ to quantify the magnitude of the nonequilibrium Fourier coefficients $a_\mathrm{c}, a_\mathrm{s}$. By means of these coefficients one constructs the nonequilibrium distribution for the driven system in the form

$$P_{dr}[\theta_\mathrm{w}, t] = N(t) \exp\left(\frac{J_\mathrm{w}}{T}\left[(1 + a_\mathrm{c}(t))\cos\theta_\mathrm{w} + a_\mathrm{s}(t)\sin\theta_\mathrm{w}\right]\right). \tag{2.60}$$

The probability density must be normalized to 1 at every time t, therefore the normalization constant is explicitly time-dependent. This subsection provided the idea of an exponential ansatz to solve the Smoluchowski equation, which will be further extended and formalized in the next chapters. In the following a first application of the exponential solution is presented, namely the analytical access to nonequilibrium variance.

2.2.4.1 Variance of the currents across the weak and the strong Josephson Junctions

The Josephson current is defined as $j_{\mathrm{s,w}} = J_{\mathrm{s,w}} \sin\theta_{\mathrm{s,w}}$. Accordingly, the variance of the current for a thermal ensemble of a single Josephson junction is

$$V_{\mathrm{s,w},eq} = \langle \sin^2\theta_{\mathrm{s,w}} \rangle_{eq} - \langle \sin\theta_{\mathrm{s,w}} \rangle_{eq}^2 \tag{2.61}$$

$$= \int_{-\pi}^{\pi} d\theta_{\mathrm{s,w}} \sin^2\theta_{\mathrm{s,w}} P_{eq}[\theta_{\mathrm{s,w}}] - \cancelto{0 \text{ in eq.}}{\left(\int_{-\pi}^{\pi} d\theta_{\mathrm{s,w}} \sin\theta_{\mathrm{s,w}} P_{eq}[\theta_{\mathrm{s,w}}] \right)^2} \tag{2.62}$$

$$= \frac{T}{J_{\mathrm{s,w}}} \frac{I_1[J_{\mathrm{s,w}}/T]}{I_0[J_{\mathrm{s,w}}/T]}. \tag{2.63}$$

Here, $I_n[x]$ is the modified Bessel function of n^{th} order. The equilibrium (eq.) expectation value of the current $\langle \sin\theta_{\mathrm{s,w}} \rangle_{eq}$ vanishes, because the second integral in (2.62) yields an even function in $\theta_{\mathrm{s,w}}$ which is zero in the boundaries from $(-\pi, \pi)$. The equilibrium distribution P_{eq} is symmetric in $\theta_{\mathrm{s,w}}$ and the current $\sim \sin\theta_{\mathrm{s,w}}$ is an uneven function. The result for the variance (2.63) is the analog to the equipartition theorem for the non-linear cos potential. The expectation values were computed with respect to the equilibrium probability distribution

$$P_{eq} = N \exp\left[(J_{\mathrm{s,w}}/T) \cos\theta_{\mathrm{s,w}} \right]. \tag{2.64}$$

The normalization constant N is defined as

$$N^{-1} = \int_{-\pi}^{\pi} d\theta_{\mathrm{s,w}} \exp\left[(J_{\mathrm{s,w}}/T) \cos\theta_{\mathrm{s,w}} \right] \tag{2.65}$$

$$= 2\pi I_0[J_{\mathrm{s,w}}/T], \tag{2.66}$$

to normalize the probability distribution to 1. In the high temperature limit $T \gg J$ the analytical exact result (2.63) is approximated by

$$V_{\mathrm{s,w},eq} \approx \frac{1}{2} - \frac{J_{\mathrm{s,w}}^2}{16T^2} + \frac{J_{\mathrm{s,w}}^4}{96T^4}. \tag{2.67}$$

The infinite temperature limit for the expectation value of the bounded function $\sin\theta_{\mathrm{s,w}}^2$ is consistently 1/2. This result applies for both, the decoupled undriven weak and strong junction.
For the driven system, the variance of the weak junction is obtained analogously

$$V_{\mathrm{w},dr} = \langle \sin^2\theta_{\mathrm{w}} \rangle_{dr} - \langle \sin\theta_{\mathrm{w}} \rangle_{dr}^2, \tag{2.68}$$

by using the constructed non-equilibrium probability distribution (2.60) for the weak junction. Again, within the high-temperature expansion and in leading order of the coefficients $a_\mathrm{c}, a_\mathrm{s}$ the time-dependent variance follows as

$$V_{\mathrm{w},dr}(t) \approx \frac{1}{2} - \frac{J_\mathrm{w}^2}{16T}\left(1 + 2a_\mathrm{c}(t) + 3a_\mathrm{s}^2(t)\right). \tag{2.69}$$

The contribution of the coefficients is proportional to G_0^2, as a_s scales with G_0 and a_c with G_0^2 (2.54)-(2.59). The exponential ansatz covers the transient behavior [25]. After averaging the coefficients over time, e.g. over a driving period $T_m = 2\pi/\omega_\mathrm{m}$ in the steady state, the effective variance of the current is

$$\overline{V}_{\mathrm{w},dr} = \overline{\langle \sin^2\theta_\mathrm{w}\rangle_{dr}(t)} - \overline{\langle \sin\theta_\mathrm{w}\rangle_{dr}(t)}^2 \tag{2.70}$$

$$\approx \frac{1}{2} - \frac{J_\mathrm{w}^2}{16T^2}\left(1 - \frac{F_0^2}{\gamma^2{\omega_\mathrm{m}}^2 + 4T^2E_\mathrm{c}^2}\right). \tag{2.71}$$

This is consistent with the full numeric results reported in Ref. [25]. The presence of the driving leads to a suppression of the fluctuations in the Josephson current $J \sim J_\mathrm{w}\sin\theta_\mathrm{w}$.

2.2.5 Generalization to Kramers equation (KE)

The Smoluchowski equation is a valid equation of motion for an ensemble of overdamped driven Josephson junctions, provided the Josephson potential $J_\mathrm{w}\sin\theta_\mathrm{w}$ is practically constant over the distance in which the conjugate variable n_w is damped out, namely when $\gamma \gg J_\mathrm{w}, \omega_\mathrm{w}$. This leads to a single equation of motion for θ_w, required to construct the usual Smoluchowski equation.
If the overdamped condition $\gamma \gg J_\mathrm{w}, \omega_\mathrm{w}$ does not hold, one has to construct a joint probability distribution for $P[\theta_\mathrm{w}, n_\mathrm{w}, t]$. For further convenience, the index w is dropped, since only the weak junction is considered in the following.
The corresponding equation of motion for $P[\theta, n, t]$ is a bivariate FP equation. It was derived and used by Kramers [71] to describe reaction kinetics [71], as it describes the Brownian motion in a potential. The so called Kramers equation (KE) is also used in other fields for example for relaxation of dipoles or also for Josephson tunneling [72]

$$\frac{\partial}{\partial t}P(\theta, n, t) = L_K\ P(\theta, n, t) = \tag{2.72}$$

$$-\frac{\partial}{\partial\theta}\underbrace{\left(E_\mathrm{c}n - A(t)\right)}_{\dot{\theta}}P + \frac{\partial}{\partial n}\underbrace{\left(J\sin\theta + \gamma n\right)}_{-\dot{n}}P + \frac{\gamma T}{E_\mathrm{c}}\frac{\partial^2}{\partial n^2}P. \tag{2.73}$$

The solution of the Kramers equation (2.73) is not constrained in γ and is allowed to explore the entire phase space during the time evolution.
The Smoluchowski equation, the Fokker-Planck equation in the overdamped limit, has been solved via an exponential ansatz $P = \exp[f(\theta, t)]$ and perturbation theory in the coefficients for f. However, an ansatz for the bivariate equation

$$f(\theta, n, t) = \frac{J}{T}\left((1 + a_{\mathrm{c1,n0}}(t))\cos\theta + a_{\mathrm{s1,n0}}(t)\sin\theta + a_{\mathrm{s1,n1}}(t)\sin\theta\ n + a_{\mathrm{c1,n1}}(t))\cos\theta\ n\right) + \frac{E_{\mathrm{c}}}{2T}(1 + a_{n2}(t))n^2 \tag{2.74}$$

leads to equations for the coefficients $a_{\mathrm{c1,n0}}(t), \ldots$ which can not be linearized meaningfully and solved analytically. Furthermore, it is not clear a priori that the nonequilibrium bivariate distribution is of exponential form. In principal the probability distribution can assume any random shape set by the initial conditions, acting forces and couplings. Though by performing cumulant expansion for example, one assumes an exponential shape.
Therefore, a universal strategy to obtain a nonequilibrium probability distribution $P_{dr}[\theta, n, t]$ is developed in Chapters 3 and 4. Chapter 3 recaps the basics of the underlying Floquet theory and the Magnus expansion. Chapter 4 demonstrates how to derive effective Floquet Hamiltonians via the alternative Magnus expansion approach.

Chapter 3

Fundamentals of driven systems

3.1 Time-dependent driving

A common feature of pump-probe experiments is the high-frequency external driving to control the low-frequency behavior. Therefore, the high-frequency regime was studied and a low-energy effective theory was established. This allows to construct time-independent effective Hamiltonians. By means of these static Hamiltonians one is able to estimate and analytically compute observables such as fluctuations, variances and currents away from equilibrium. This low-energy effective theory misses to describe some resonances, which one usually can capture in the extended Floquet space picture. However, within the framework of this thesis, the focus was to develop a theory for the low-frequency dynamics away from the resonances.
In Section 3.2 of this chapter, essential parts of the Floquet theory are reviewed and the concept of the stroboscopic Floquet Hamiltonian is introduced. Afterwards, the high-frequency regime is discussed to make a connection between the stroboscopic and the effective Floquet Hamiltonian. Subsequently, a Magnus scheme is developped to perturbatively approximate an effective Floquet Hamiltonian in the high-frequency limit. The limitations and the validity of this low-energy effective Hamiltonian approach is discussed, such as the convergence properties of the Magnus series or sufficient conditions for the average Hamiltonian theory. Furthermore, the advantages and disadvantages of having a time-independent Hamiltonian within the exponential perturbation theory will be outlined.

3.2 Floquet theory and Magnus expansion

Periodically driven systems occur in various experimental setups. Typical situations aim to probe processes which involve mechanical shaking or deformation or the application of a periodic probing current or the irradiation of material by electromagnetic waves. Even a priori non-driven systems can become periodically time-dependent by transforming them for example into the interaction picture [73] or into the rotating frame, which is a common technique in laser physics.
In the simplest system case, one considers systems subject to a monochromatic periodic driving with a dimensionless coupling strength A and a driving frequency ω_{m}. The dynamics of periodically driven systems can be highly complex. Usually the analysis is restrained to the two extreme regimes of slow and fast driving. In the first regime, the system practically adiabatically follows the instantaneous Hamiltonian $H(t)$ at any time t. Hence, the system adapts sufficiently fast to changes of the time-dependent Hamiltonian. This adiabatic regime is set by the condition $\omega_{\mathrm{m}} \ll \omega_0$, where ω_0 represents the natural frequency scale of the nondriven system. In the fast driving regime $\omega_{\mathrm{m}} \gg \omega_0$, the driving does not couple resonantly to slow degrees of freedom in the system. Rather it can renormalize or "dress" the low-energy Hamiltonian with an effective static potential, which depends on the driving amplitude and the driving frequency. The well-known Kapitza pendulum [74, 75] is such an example. This is a classical pendulum whose pivot is vibrating fastly. For certain parameters the rather counter-intuitive unstable inverted pendulum position can be dynamically stabilized. The effect of dynamical stabilization is also used in Paul traps [76] where ions are localized in field minima produced by time-dependent electromagnetic fields. Further examples are the reduced ionization rates in atomic systems irradiated by high-frequency and high-intensity electromagnetic fields [77]. By increasing the field strength the ionization rate is also increased up to a critical radiation field intensity A_{crit}. Beyond A_{crit} the ionization rate drops due to an effective deformation of the atomic binding potential for the electrons.
In the following, effective Floquet Hamiltonians in the high-frequency limit are derived by means of the Magnus expansion. To this end, it is mandatory to recap the essentials of the Floquet theory and the related Floquet Hamiltonian. Introducing exponential perturbation theory, one can identify and extract Floquet Hamiltonians. By comparing the exponential perturbative solution to the exponential of the time evolution operator or the thermal density matrix $\sim \exp[-\beta H]$, where $\beta = 1/(k_{\mathrm{B}}T)$, it is possible to deduce effective Hamiltonians.

3.2.1 Floquet Hamiltonian

This section introduces the basic concepts of Floquet theory and the stroboscopic time evolution of periodically driven systems. The starting point is the Schrödinger equation for the unitary time evolution operator $U(t, t_0)$, although the concepts presented here can as well be applied to classical systems. In general, the Floquet theory is applicable to a system of linear differential equations with periodic coefficients $\dot{x} = A(t)x$, where the periodic coefficient matrix is $A(t) = A(t + T)$ and T denotes the driving period of the system.
For a given periodic Hamiltonian $H(t + T) = H(t)$, one deals with the following non-autonomous linear differential equation

$$i\hbar \frac{\partial U(t, t_0)}{\partial t} = H(t)U(t, t_0), \tag{3.1}$$

where the initial condition is $U(t_0, t_0) = \mathrm{I}$ with the identity operator I. $\hbar$ is the Planck constant, which is set to $\hbar = 1$ or will given explicitly when needed.
The periodic driving has consequences for the solution of the time evolution operator (3.1). $U(t, t_0)$ is invariant under discrete translations in time $(t_1, t_2) \to (t_1 + nT, t_2 + nT)$ for integer n. Combined with the factorization group property of the time evolution operator

$$U(t_2, t_1) = U(t_2, t)U(t, t_1), \tag{3.2}$$

for arbitrary t, one deduces for the periodic case with a fixed time intervall $(t_0, t_0 + 2T)$

$$U(t_0 + 2T, t_0) = U(t_0 + 2T, t_0 + T)U(t_0 + T, t_0). \tag{3.3}$$

This can be generalized to

$$U(t_0 + nT, t_0) = U(t_0 + T, t_0)^n. \tag{3.4}$$

The one-cycle evolution operator can be defined with the time-independent stroboscopic Floquet Hamiltonian H_{sF} [1]

$$U(t_0 + T, t_0) = \exp\left(-iH_{\mathrm{sF}}[t_0]T\right). \tag{3.5}$$

In this definition, the stroboscopic Floquet Hamiltonian H_{sF} depends on the choice of the initial reference time t_0 defining the stroboscopic periodic driving. Following

[1] The required unitary gauge transformation and the detailed construction can be found in e.g. Refs. [15],[78],[79]

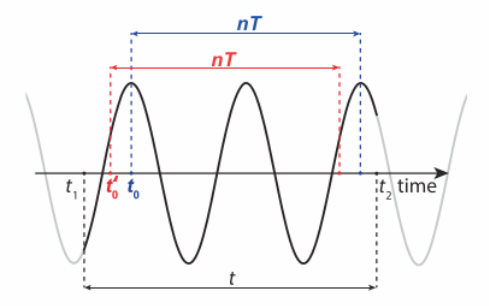

Figure 3.1: Time evolution of a system from time t_1 to time t_2. The stroboscopic time window starts at a time t_0, which can be chosen anywhere in the first period $[t_1, t_1+T)$. This gauge choice t_0 generally affects the form of the stroboscopic Floquet Hamiltonian $H_{\mathrm{sF}}[t_0]$. Figure taken from Ref. [14].

Bukov et al. [14] it is also called a Floquet gauge. The parametric gauge dependence is indicated by $[t_0]$. The actual time-dependence is distinguished by (t). As long as there are no experimental restrictions, such as driving protocols with random intial conditions or a fixed trigger point for the measurement, one often chooses a Floquet gauge such that H_{sF} gets the most convenient form. For example, by fixing t_0 one eliminates the relative initial phase of the periodic driving φ_0, e.g., $\cos[\omega_{\mathrm{m}}(t-t_0)+\varphi_0] \to \cos\omega_{\mathrm{m}}t$. Or one simply chooses $t_0 = 0$ for a symmetric driving $f(t) = \cos\omega_{\mathrm{m}}t$.

In the derviation of the Floquet Hamiltonians, the ambiguity of having a whole set of equivalent $H_{\mathrm{sF}}[t_0]$ was extensively discussed [15, 79, 14] and solved by the introduction of an effective Hamiltonian H_{eff}. There is a similar idea in the concept of the average Hamiltonian theory (AHT). In the field multi-pulse nuclear magnetic resonance (NMR) spectroscopy damping factors and perturbation series contributions are dependent on t_0, leading to an incorrect theoretical treatment [80]. By fixing t_0, one chooses a representation or rather a coordinate system in which one performs the average Hamiltonian (AH) calculation. However, it is shown that the different AHs are equivalent to a t_0-independent Hamiltonian and to each other.
A priori this choice is arbitrary, but there are formulations such that the family of Floquet Hamiltonians $H_{\mathrm{sF}}[t_0]$ become independent from the initial time t_0. This will be further explained in a subsequent section [15, 14, 81].
For exactly one cycle T, the time evolution of the system can be described by a constant operator $H_{\mathrm{sF}}[t_0]$ [2]. For times $t = nT$ with n integer, the stroboscopic time

[2]The precise requirement is that H_{F} must be a local physical Hamiltonian. For macroscopic systems there is no guarantee that this is the case. In some generic interacting systems, local H_{F} might even not exist [82].

evolution according to Eq. (3.4) is

$$U(t_0 + nT, t_0) = \exp\left(-iH_{\mathrm{sF}}[t_0]nT\right). \tag{3.6}$$

The stroboscopic time evolution might be deceptive, since there is always a trade-off between the simplicity of the stroboscopic Floquet Hamiltonian and the loss of information on the dynamics within one period $t < T$ or for $t \neq nT$. However, precisely the information obtained or exchanged during the cycle leads to additional effects, such as line broadening in NMR spectra [83]. For $t < T$ or $t \neq nT$, the concept of the stroboscopic Floquet Hamiltonian can be generalized. It includes the introduction of the stroboscopic kick operators K_{s} [79], which propagate from the initial time $t_1 \in [-T, 0]$ to the reference time of the periodic evolution t_0 and after the last full period to the final time $t_2 \in [0, T]$,

$$U(t_2, t_1) = e^{-iK_{\mathrm{s}}[t_0](t_2)} e^{-iH_{\mathrm{sF}}[t_0](t_1 - t_2)} e^{iK_{\mathrm{s}}[t_0](t_1)}. \tag{3.7}$$

$K_{\mathrm{s}}[t_0](t)$ is a function of t and parametrically dependent on t_0.
The stroboscopic kick operators take into account the deviations on time scales $t < T$, the dynamics of the fast varying contributions or the so called micromotion. They allow to describe the time evolution (3.1) with a time-independent Floquet Hamiltonian H_{sF}. The respective operators $K_{\mathrm{s}}, H_{\mathrm{sF}}$ are dependent on the Floquet gauge, which fixes the reference point t_0 of the stroboscopic evolution in between the times t_1 and t_2, see Figure 3.1. A brief discussion and the implicit definition of the kick operator is given in the Appendix C. Setting the initial time t_1 to coincide with Floquet gauge t_0 one gets the common Floquet form of the propagator

$$U(t, t_0) = e^{-iK_{\mathrm{s}}[t_0](t)} e^{-iH_{\mathrm{sF}}[t_0](t_0 - t)} \tag{3.8}$$

$$= P(t, t_0) e^{-iH_{\mathrm{sF}}[t_0](t_0 - t)}. \tag{3.9}$$

The micromotion operator is defined by

$$P(t, t_0) = U(t, t_0) e^{iH_{\mathrm{sF}}[t_0](t_0 - t)}, \tag{3.10}$$

which links the P-operator to the Floquet Hamiltonian. By definition, the P operator is also periodic in time.
Fixing the Floquet gauge t_0 means that the stroboscopic Floquet Hamiltonian $H_{\mathrm{sF}}[t_0]$ is ultimately linked to the initial time of the experiment or measurement. Strongly fluctuating and not well controllable starting or measurement times cause the Floquet Hamiltonian to change accordingly. In particular involving fastly driven experiments are prone to this effect. However, in numerical simulations one has full

control over initial conditions and time intervals.
For a quantum particle in a periodic lattice the Bloch theorem [84] yields the formally analog result to (3.9), but in space. In the lattice case, one rewrites the eigenfunctions as $\varphi(x) = \sum_k u_k(x)e^{ikx}$ with periodic Bloch functions $u_k(x)$ and an exponential whose "Floquet exponents" are the eigenvalues of the lattice Hamiltonian.
There is a family of equivalent operators for P and H_{F}, which depends on the gauge choice t_0. By means of the Hermitean kick operator K one can perform a similarity transformation on H_{sF}. This leads to a fixed Floquet Hamiltonian, which is independent from t_0 [14, 81],

$$H_{\mathrm{F}} = e^{iK(t_0)} H_{\mathrm{sF}}[t_0] e^{-iK(t_0)}. \tag{3.11}$$

This transformation shifts the t_0-dependence entirely to the kick operators $K[t_0]$ and allows for an unambiguous definition of a time-independent H_{F}. For finite systems, the existence of such a time-independent frame with a constant H_{F} is guaranteed by the Floquet-Lyapunov theorem REF[85]. Namely, for a linear system of ordinary differential equations with periodic coefficients, there exists a linear periodic transformation of coordinates, which turns this system into a system with constant coefficients. This transformation is in general difficult to find.
Therefore, a workaround is developed to obtain the Floquet Hamiltonian. In the high frequency limit, the stroboscopic Floquet Hamiltonian H_{sF} is often given by the time-averaged Hamiltonian

$$H_{\mathrm{av}} = \frac{1}{T} \int_0^T H(t) dt. \tag{3.12}$$

However, there are important exceptions when H_{F} is not simply given by H_{av} (3.12), even in the infinite frequency limit $T \to 0$ [3]. These particular situations often give rise to remarkable behavior such as dynamical stabilization referring to the classcial Kapitza pendulum with a fastly varying pivot and a stable solution in the upward position [86]. The presence and the additional information on the micromotion part within one period are often a key to obtain nontrivial stroboscopic Floquet Hamiltonians [83]. Another prerequisite for nontrivial dynamics is that for $t_1 \neq t_2$ the Hamiltonian should not commute with itself $[H(t_1), H(t_2)] \neq 0$. Even for $\int H_{\mathrm{dr}}(t)dt = 0$ there can still be contributions to the stroboscopic Floquet Hamiltonian from $H_{\mathrm{dr}}(t)$ in higher orders of the approximation schemes, e.g.,$H_{\mathrm{dr}}(t)^2$.
The naive statement to say the shorter the driving period $T = 2\pi/\omega_{\mathrm{m}}$, the better the

[3] This happens, for example, if the driving term scales with $\omega_{\mathrm{m}} \sim 1/T$. More details are given in Ref. [14]

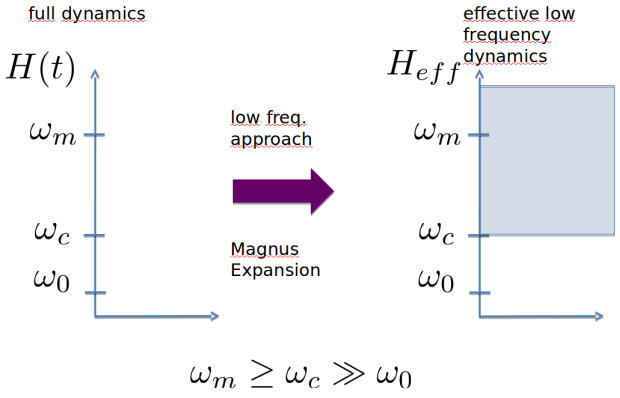

Figure 3.2: This scheme illustrates the hierarchy of frequencies. Usually one takes a frequency cut-off ω_c which is way above the low-energy dynamics one wants to describe. The shaded area is averaged out information on the high-energy scale of the system which may resulted into a low-energy effective contribution.

stroboscopic Floquet Hamiltonian approximates the complete time-evolution operator $U(t, t_0)$ is strictly not correct.

In practice, one introduces a frequency cut-off $\omega_0 < \omega_c \leq \omega_m$ to exclude or include certain energy regimes, see Fig. 3.2. This, in turn, implies a hierarchy of the Floquet Hamiltonian in the high frequency limit with corrections of the order $1/\omega_c$ [87]. The focus of this thesis is compute the corrections in terms of $1/\omega_c$ and the driving amplitude A for a systematic construction of low-energy effective Hamiltonians.

3.2.2 High frequency expansion and Magnus series

Generally it is not possible to determine H_{sF} in a closed form, so one has to rely on approximation schemes [83, 88, 89, 90, 91, 92, 93, 94, 79]. An efficient tool to compute the Floquet Hamiltonian in the high frequency limit is the Magnus expansion (ME) [88]. It is a perturbative scheme in the driving period T, which can be interpreted as an inverse frequency expansion via $T = 2\pi/\omega$. Hence, the series is especially suitable in the short-time limit $T = t - t_0 \ll 2\pi/\omega_0$ or for high frequencies with $\omega \gg \omega_0$, where ω_0 is the natural characteristic frequency scale of the undriven system.

To derive the Magnus scheme, one starts again with the Schrödinger equation

$$i\hbar \frac{\partial U(t,t_0)}{\partial t} = \lambda H(t) U(t,t_0). \tag{3.13}$$

The initial condition is $U(t_0,t_0) = \mathrm{I}$ and $H(t)$ is an arbitrary time-dependent Hamiltonian. λ is a dimensionless bookkeeping parameter, which can be taken as $\lambda = 1$ in the end. Without loss of generality, one sets $t_0 = 0$ in the following.

Integrating the above equation (3.13) and applying it iteratively, one obtains the formal solution

$$U(t,0) = \mathbf{1} - \frac{i\lambda}{\hbar}\int_0^t dt_1 H(t_1) U(t_1,0) \tag{3.14}$$

$$\vdots$$

$$= \mathbf{1} - \frac{i\lambda}{\hbar}\int_0^t H(t_1) + \left(-\frac{i\lambda}{\hbar}\right)^2 \int_0^t dt_1 \int_0^{t_1} dt_2 H(t_1)H(t_2) + \cdots \tag{3.15}$$

$$+ \left(-\frac{i\lambda}{\hbar}\right)^n \int_0^t dt_1 \cdots \int_0^{t_{n-1}} dt_n H(t_1)\cdots H(t_n), \tag{3.16}$$

where the times are ordered according to $t \geq t_1 \geq \cdots \geq t_n$. The so called Dyson series iteratively represents the full unitary solution. This scheme is equivalent to the time-dependent perturbation theory (TDPT).

The whole series encompasses an unitary operator, however in practice one truncates the series at a certain order of λ and the result is no longer unitary [95] [96]. Similiarly, the Taylor series of the periodic sin function ceases to be periodic when truncated. The non-unitary character might be a problem, especially for quasi-stationary states.

The formal solution to (3.13) can be trivially written as

$$U(t,0) = \exp\left[-\frac{i\lambda}{\hbar}\int_0^t ds H(s)\right]. \tag{3.17}$$

However, this is invalid for a time-dependent Hamiltonian, where a priori the commutator at different times t, t' may not vanish $[H(t), H(t')] \neq 0$. Indeed, interesting dynamics and physics in driven systemes originate from the non-vanishing commutator $[H(t), H(t')]$. The commutator of two elements A, B of an associative algebra is defined as $[A, B] = AB - BA$.
Introducing the time-ordering operator

$$\mathcal{T}(A(t_1)B(t_2)) = \begin{cases} A(t_1)B(t_2), & if \quad t_1 > t_2 \\ B(t_2)A(t_1), & if \quad t_2 > t_1 \end{cases} , \tag{3.18}$$

the symbolic representation of the infinite series (3.16) is written as

$$U(t,0) = \mathcal{T}\left(\exp\left[-\frac{i\lambda}{\hbar}\int_0^t dsH(s)\right]\right). \tag{3.19}$$

It is unknown, whether equation (3.16) amounts to an exponential representation for the operator $U(t,0)$. The same applies to (3.19). However, it is a formal solution of the Schrödinger equation with a time-dependent Hamiltonian.
The conventional series expansion of the exponential in (3.17) includes the n^{th} power of the single integral, but from (3.16) one gets some multiple nested integrals.
The Magnus expansion (ME) [88] approximates an exponential solution to (3.13), see also Ref. [87] for a clear recent review. Hence, one writes the propagator as

$$U(t,t_0) = \exp\Omega(t,t_0) = I + \sum_{n=1}^{\infty}\frac{1}{n!}\Omega^n \tag{3.20}$$

with the intial condition $\Omega(t_0,t_0) = 0$. The Magnus expansion is referred to as exponential perturbation theory (EPT). By changing the unknown from U to Ω, one actually looks for the logarithm of the time evolution operator.
Since U has to fulfill the Schrödinger equation (3.13), Ω is constraint to solve an associated equation.
Following the reasoning of the insightful papers [97, 78], one needs two important features to derive the equation for Ω. The first feature is the group property: The time-evolution operator fulfills

$$U(t_2,t_0) = U(t_2,t_1)U(t_1,t_0). \tag{3.21}$$

The second one is a lemma from the famous Baker-Campbell-Hausdorff (BCH) formula, sometimes known as the Zassenhaus formula, which helps to express the product of two operator valued exponentials. For any two non-commuting operators X

and Y, the product is

$$\exp X \exp Y = \exp\left(X + Y + \frac{1}{2}[X,Y] + \frac{1}{12}[X,[X,Y]] + \frac{1}{12}[Y,[Y,X]] + \cdots\right). \tag{3.22}$$

The exponent on the right-hand side is an infinite series and the terms are nested commutators of increasing order. The explicit form of the series is not known, although there exist algorithms to compute it to finite order [98]. The number of terms in the order m grows as $\mathcal{O}\left(2^m/m\right)$. Despite the complexity, a compact formula gives one part of the BCH series to all orders in one of the two involved operators [99]. The complete expansion in Y yields

$$\exp X \exp Y = \exp\left(X + Y + \sum_{k=1}^{\infty}(-1)^k \frac{B_k}{k!} \underbrace{[Y,[\cdots[Y}_{k-times},X]] + \mathcal{O}(X^2)\right). \tag{3.23}$$

Here, B_k are the Bernoulli numbers.
Considering the infinitesimal interval δt, the time evolution operator is decomposed into a short term evolution $U(t+\delta t, t)$ and the standard evolution $U(t, t_0)$, i.e.,

$$U(t+\delta t, t_0) = U(t+\delta t, t)U(t, t_0) \tag{3.24}$$

$$\overset{(3.20)}{\Leftrightarrow} \exp[\Omega(t+\delta t, t_0)] = \exp[\Omega(t+\delta t, t)]\exp[\Omega(t, t_0)]. \tag{3.25}$$

Here, the time evolution operator was replaced by an exponential solution (3.20). During the short time intervall $(t, t+\delta t)$ the Hamiltonian takes a constant value $H(t)$. Hence, the Schrödinger equation for the short term evolution $U(t+\delta t, t)$ frozen at time t yields

$$U(t+\delta t, t) - \underbrace{U(t,t)}_{\mathbf{1}} \approx -\frac{i\lambda}{\hbar} H(t)\delta t \underbrace{U(t,t)}_{\mathbf{1}}. \tag{3.26}$$

Substituting $U(t+\delta t, t) = \mathbf{1} + \sum_{n=1}^{\infty} \frac{1}{n!}\Omega^n(t+\delta t, t)$, the first order in Ω and δt is

$$\Omega(t+\delta t, t) \approx -\frac{i\lambda}{\hbar} H(t)\delta t \tag{3.27}$$

$$\Leftrightarrow \exp[\Omega(t+\delta t, t)] = \exp\left(-\frac{i\lambda}{\hbar} H(t)\delta t\right) \tag{3.28}$$

$$\Leftrightarrow U(t+\delta t, t) = \exp\left(-\frac{i\lambda}{\hbar} H(t)\delta t\right), \tag{3.29}$$

which leads to

$$\exp[\Omega(t+\delta t,t_0)] \approx \exp\left(-\frac{i\lambda}{\hbar}H(t)\delta t\right)\exp(\Omega(t,t_0)). \tag{3.30}$$

Unifying the exponents in (3.30) via formula (3.23) one keeps track of the first order in δt

$$\begin{aligned}\Omega(t+\delta t,t_0) &= \Omega(t,t_0) \\ &\quad -\frac{i\lambda}{\hbar}\delta t\left\{H(t)+\sum_{k=1}^{\infty}(-1)^k\frac{B_k}{k!}\underbrace{[\Omega(t,t_0),[\cdots[\Omega(t,t_0)}_{k-times},H]]\right\}+\mathcal{O}(\delta t^2).\end{aligned} \tag{3.31}$$

Dividing by δt, substracting $\Omega(t,t_0)$ and taking the limit $\delta t \to 0$ yields the exact result

$$\frac{\partial\Omega(t,t_0)}{\partial t} = -\frac{i\lambda}{\hbar}H - \frac{i\lambda}{\hbar}\sum_{k=1}^{\infty}(-1)^k\frac{B_k}{k!}\underbrace{[\Omega(t,t_0),[\cdots[\Omega(t,t_0)}_{k-times},H]]. \tag{3.32}$$

The convenience of the time-evolution operator in the exponential representation is revealed after an expansion of Ω in terms of the parameter λ. Substituting the Magnus series

$$\Omega = \sum_{k=1}^{\infty}\lambda^k\Omega_k \tag{3.33}$$

into equation (3.32), one sorts the terms according to their order in λ and derives an infinite set of trivally integrable equations for each Ω_k. There is a recursive hierarchy in the equations. To get the equation for Ω_n, the previous order Ω_{n-1} is required. Hence there are $n-1$ equations to solve up to Ω_1. The literature provides various recursive algorithms to obtain the Magnus terms [100], [101],[102]. For the purpose of this thesis, it suffices to explicitly give the first four Magnus terms. After some tedious algebra and accounting for the nested commutators in equation (3.32) one

gets

$$\Omega_1 = \frac{1}{i\hbar}\int_{t_0}^{t} dt_1 H(t_1) \tag{3.34}$$

$$\Omega_2 = \frac{1}{2(i\hbar)^2}\int_{t_0}^{t} dt_1 \int_{t_0}^{t_1} dt_2 [H(t_1), H(t_2)] \tag{3.35}$$

$$\begin{aligned}\Omega_3 = \frac{1}{6(i\hbar)^3}&\int_{t_0}^{t} dt_1 \int_{t_0}^{t_1} dt_2 \int_{t_0}^{t_2} dt_3 \\ &([H(t_1), [H(t_2), H(t_3)]] + [H(t_3), [H(t_2), H(t_1)]])\end{aligned} \tag{3.36}$$

$$\begin{aligned}\Omega_4 = \frac{1}{12(i\hbar)^4}&\int_{t_0}^{t} dt_1 \int_{t_0}^{t_1} dt_2 \int_{t_0}^{t_2} dt_3 \int_{t_0}^{t_3} dt_4 \\ &([H(t_1), [H(t_2), [H(t_3), H(t_4)]]] + [H(t_2), [H(t_3), [H(t_4), H(t_1)]]] \\ &+[H(t_1), [H(t_4), [H(t_3), H(t_2)]]] + [H(t_4), [H(t_3), [H(t_1), H(t_2)]]])\,.\end{aligned} \tag{3.37}$$

These are the commonly derived Magnus terms, which are also found in the literature such as in Refs. [103, 104, 105].
The series was derived in the short-time limit for the time evolution operator. Each temporal integral in the equations (3.34) - (3.37) yields one additional order in the time window $T = t - t_0$ or $T = 2\pi/\omega$ in terms of the inverse frequency. In this case, the scale is set either by a cut-off frequency ω_c or by a driving frequency ω_m. Accordingly, the Magnus terms Ω_k with subscript k are ordered in powers of the short time window T^k or $1/\omega^k$ in inverse frequencies.
With these Magnus terms, the solution $U(t, t_0)$ to the Schrödinger equation with the time-dependent Hamiltonian,

$$i\hbar\frac{\partial U(t, t_0)}{\partial t} = H(t)U(t, t_0), \tag{3.38}$$

has a true exponential representation written in the form

$$U(t, t_0) = \exp\left[\sum_{k=1}^{\infty}\Omega_k(t, t_0)\right] = \mathcal{T}\exp\left[-\frac{i}{\hbar}\int_{t_0}^{t} H(t')dt'\right]. \tag{3.39}$$

In general, it is not always guaranteed that the ME converges, a brief discussion on this issue is provided in Section 3.2.4. However, often the first few orders provide useful physical insights, such as the narrowing of absorption lines in nuclear magnetic resonance spectroscopy [106, 107].
If the system is subject to a periodic driving, one can employ the stroboscopic Floquet Hamiltonian concept and the ME becomes a versatile tool to approximate effective Floquet Hamiltonians.

Applying the Floquet theorem to the full time evolution operator (3.9) and finally evaluating it within the stroboscopic time window (t_0+T, t_0) yields

$$U(t_0+T,t_0) = \underbrace{P(t_0+T,t_0)}_{=\mathbf{1}} \exp\left[-\frac{i}{\hbar}H_{\mathrm{sF}}(t_0+T-t_0)\right] \tag{3.40}$$

$$= \exp\left[-\frac{i}{\hbar}H_{\mathrm{sF}}T\right]. \tag{3.41}$$

Additionally, one expands the stroboscopic Floquet Hamiltonian H_{sF} into orders of the inverse frequency $1/\omega^k$

$$H_{\mathrm{sF}} = \sum_{k=0} H_{\mathrm{sF,k}}. \tag{3.42}$$

The Magnus expanded time evolution operator within the stroboscopic time window $U(t_0+T,t_0) = \exp[\Omega(t_0+T,t_0)] = \exp\left[-\frac{i}{\hbar}H_{\mathrm{sF}}T\right]$ can be compared order by order with H_{sF}. Dividing the Magnus solution in the exponent (3.39) by the period T, the contributions to H_{sF} are

$$H_{\mathrm{sF},0} = \frac{i\hbar}{T}\Omega_1(t_0+T,t_0), \tag{3.43}$$

$$H_{\mathrm{sF},1} = \frac{i\hbar}{T}\Omega_2(t_0+T,t_0), \tag{3.44}$$

$$H_{\mathrm{sF},2} = \frac{i\hbar}{T}\Omega_3(t_0+T,t_0), \tag{3.45}$$

$$H_{\mathrm{sF},3} = \frac{i\hbar}{T}\Omega_4(t_0+T,t_0). \tag{3.46}$$

A priori, the right-hand sides of (3.43)-(3.46) comprises the information from **all** frequency components within the perturbative $1/\omega$ Magnus scheme. In contrast, the micromotion operator separates the fast-varying degrees of freedom from the Floquet Hamiltonian.

For a detailed study of this matter, one decomposes the original Hamiltonian $H(t)$ into its Fourier harmonics with a certain expansion frequency ω, being given by the driving, the transition or eigenfrequency,i.e

$$H(t) = \sum_{l\in\mathbb{Z}} e^{il\omega t}H_l, \tag{3.47}$$

where the $H_l = (1/T)\int_0^T H(t)e^{-il\omega t}dt$ are the respective Fourier coefficients. This allows to exactly distingiush the low-frequency or constant contributions of the Magnus terms from the stroboscopic Floquet Hamiltonian. Furthermore, the contributions dependent on the initial time t_0 can be identified. After applying the expres-

sions to the Magnus terms (3.34)-(3.37), the stroboscopic Floquet Hamiltonian has the following specific form

$$H_{\mathrm{sF},0} = \frac{1}{T}\int_{t_0}^{t_0+T} dt_1 H(t_1) \tag{3.48}$$

$$= H_0 \tag{3.49}$$

$$H_{\mathrm{sF},1} = \frac{1}{2(i\hbar)T}\int_{t_0}^{t_0+T} dt_1 \int_{t_0}^{t_1} dt_2 [H(t_1), H(t_2)] \tag{3.50}$$

$$\overset{(3.47)}{=} \underbrace{\frac{1}{2(i\hbar)T}\int_{t_0}^{t_0+T} dt_1 \int_{t_0}^{t_1} dt_2 \sum_{k,l} e^{ik\omega t_1} e^{il\omega t_2}}_{\sum_{k,l} c_{kl}} [H_k, H_l] \tag{3.51}$$

$$= \frac{1}{\hbar\omega}\sum_{l=1}^{\infty}\frac{1}{l}\left([H_l, H_{-l}] + e^{il\omega t_0}[H_0, H_l] - e^{-il\omega t_0}[H_0, H_{-l}]\right), \tag{3.52}$$

where the spectral factor c_{kl} is defined as

$$c_{kl} = \frac{1}{2(i\hbar)T}\int_{t_0}^{t_0+T} dt_1 \int_{t_0}^{t_1} dt_2 e^{ik\omega t_1} e^{il\omega t_2}. \tag{3.53}$$

For time periodic problems, these are the analog of the structure factors from condensend matter physics in periodic lattices, which again confirms the strong analogy between Floquet theory and Bloch theory.
Theoretically, all higher harmonics with label l contribute to the constant stroboscopic Floquet Hamiltonian, though their contributions fall off as $\omega_0/(l\omega)$, where ω_0 is the natural frequency scale of the Hamiltonian H. This is exactly the common condition for which the application of the Magnus expansion is useful and where the characteristic frequency ω of the time-dependent part in the Hamiltonian $H(t)$ (3.47) should be much larger than the natural frequency scale, $\omega \gg \omega_0$.
Equation (3.52) highlights the t_0-dependent terms in the first order of the stroboscopic Floquet Hamiltonian $H_{\mathrm{sF},1}[t_0]$. These gauge-dependent terms lead to ambiguous expressions for the stroboscopic Floquet Hamiltonians $H_{\mathrm{sF}}[t_0]$. However, by applying a unitary gauge transformation one obtains a genuinely time- and t_0-independent effective Floquet Hamiltonian H_{F} [15, 80, 81, 90]. The action of the unitary transformation to the effective Floquet Hamiltonian,

$$H_{\mathrm{F}} = e^{iK[t_0](t)} H_{\mathrm{sF}}[t_0] e^{-iK[t_0](t)}, \tag{3.54}$$

is just a rearrangement of the t_0-expressions between the kick operator K and the stroboscopic Floquet Hamiltonian such that the effective Floquet Hamiltonian H_{F} becomes t_0 independent.

Even without the konwoledge of the required unitary transformation into the co-rotating frame, one can specify the condition for the construction of the effective Floquet Hamiltonian. The contribution of the Fourier decomposition with the spectral factor (3.53) must be a constant expression before performing the outermost integral over t_1. Therefore, the exponents have to cancel each other out which enforces $k + l = 0$. Applying this rule to equation (3.51), the effective Floquet Hamiltonian H_{F} is approximated by

$$H_{\mathrm{F},1} = \frac{1}{\hbar\omega} \sum_{l=1} \frac{1}{l} \left[H_l, H_{-l}\right]. \tag{3.55}$$

This first order expression coincides with the one of Ref. [15]. The next order of the stroboscopic Floquet Hamiltonian from the Magnus expansion is

$$\begin{aligned} H_{\mathrm{sF},2} =& \frac{1}{3!(i\hbar)^2 T} \int_{t_0}^{t_0+T} dt_1 \int_{t_0}^{t_1} dt_2 \int_{t_0}^{t_2} dt_3 \\ & \left([H(t_1), [H(t_2), H(t_3)]] + [H(t_3), [H(t_2), H(t_1)]]\right). \end{aligned} \tag{3.56}$$

Explicitly evaluating $H_{\mathrm{sF},2}$ in the spectral decomposition yields the following combinatoric expression

$$\begin{aligned} H_{\mathrm{sF},2} =& \underbrace{\frac{1}{3!(i\hbar)^2 T} \int_{t_0}^{t_0+T} dt_1 \int_{t_0}^{t_1} dt_2 \int_{t_0}^{t_2} dt_3 \sum_{k,l,m} e^{ik\omega t_1} e^{il\omega t_2} e^{im\omega t_3}}_{\sum_{k,l,m} c'_{klm}} \times \\ & \left([H_k, [H_l, H_m]] + [H_m, [H_l, H_k]]\right), \end{aligned} \tag{3.57}$$

with the second order spectral factor

$$c'_{klm} = \frac{1}{3!(i\hbar)^2 T} \int_{t_0}^{t_0+T} dt_1 \int_{t_0}^{t_1} dt_2 \int_{t_0}^{t_2} dt_3 e^{ik\omega t_1} e^{il\omega t_2} e^{im\omega t_3}. \tag{3.58}$$

Rearranging the Fourier indices for different temporal arguments (3.57), one obtains an expression with just one nested commutator in the form

$$\begin{aligned} H_{\mathrm{sF},2} =& \frac{1}{3!(i\hbar)^2 T} \int_{t_0}^{t_0+T} dt_1 \int_{t_0}^{t_1} dt_2 \int_{t_0}^{t_2} dt_3 \sum_{k,l,m} [H_k, [H_l, H_m]] \times \\ & \left(e^{ik\omega t_1} e^{il\omega t_2} e^{im\omega t_3} + e^{ik\omega t_3} e^{il\omega t_2} e^{im\omega t_1}\right). \end{aligned} \tag{3.59}$$

The redefined spectral factor is, accordingly,

$$c_{klm} = \frac{1}{3!(i\hbar)^2 T} \int_{t_0}^{t_0+T} dt_1 \int_{t_0}^{t_1} dt_2 \int_{t_0}^{t_2} dt_3 \left(e^{ik\omega t_1} e^{il\omega t_2} e^{im\omega t_3} + e^{ik\omega t_3} e^{il\omega t_2} e^{im\omega t_1} \right). \tag{3.60}$$

It is always more convenient to deal with a more complex scalar factor than to manipulate and compare the sum over the nested commutators (3.57), especially in higher orders.
Under the condition $k + l + m = 0$, one sums up all possible configurations, which of course require different commutators, such as the combinations involving a zero index

$$c_{0,-k,k} \to [H_0, [H_{-k}, H_k]] = \qquad [H_{-k}, [H_0, H_k]] - [H_k, [H_0, H_{-k}]] \tag{3.61}$$

$$c_{-k,0,k} \to [H_{-k}, [H_0, H_k]] \tag{3.62}$$

$$c_{-k,k,0} \to [H_{-k}, [H_k, H_0]] = \qquad -[H_{-k}, [H_0, H_k]]. \tag{3.63}$$

In equation (3.61)-(3.63) the Jacobi identity for the commutator $[A, [B, C]] + [B, [C, A]] + [C, [A, B]] = 0$ was applied to obtain the standard order.
Similiarly, the spectral factors with two running indices demand the following commutators

$$c_{k-m,-k,m} \to [H_{k-m}, [H_{-k}, H_m]] = [H_{-k}, [H_{k-m}, H_m]] - [H_m, [H_{k-m}, H_{-k}]] \tag{3.64}$$

$$c_{-k,k-m,m} \to [H_{-k}, [H_{k-m}, H_m]] \tag{3.65}$$

$$c_{-k,m,k-m} \to [H_{-k}, [H_m, H_{k-m}]] = [H_{-k}, [H_{k-m}, H_m]]. \tag{3.66}$$

After some index manipulation and the evaluation of the spectral factors, this totals up to the effective second order Floquet Hamiltonian

$$H_{\mathrm{F},2} = \sum_{k \neq 0} \left(\frac{[H_{-k}, [H_0, H_k]]}{(k\hbar\omega)^2} + \sum_{m \neq 0,k} \frac{[H_{-k}, [H_{k-m}, H_m]]}{k(m-k)(\hbar\omega)^2} \right). \tag{3.67}$$

The prefactors of this expression differ from the ones found in [15, 14], however structurewise the expressions coincide. The origin of the different numerical prefactors are the different approximation schemes to the Floquet Hamiltonian and its t_0-independent terms. From the Floquet perspective, a tripartite ansatz for the

unitary time evolution operator yields

$$U(t,t_0) = U_K(t,t_0)e^{-\frac{i}{\hbar}H_\mathrm{F}(t-t_0)}U_K^\dagger(t,t_0) \tag{3.68}$$

$$= e^{iK(t,t_0)}e^{-i\frac{i}{\hbar}H_\mathrm{F}(t-t_0)}e^{-iK(t,t_0)}, \tag{3.69}$$

where U_K is a transformation into the co-rotating frame with no micromotion present and the phase evolution is governed by the time-independent Floquet Hamiltonian. After a perturbative expansion in $1/\omega$ of either U_K or K and H_F, one finds different prefactors than for the standard bipartite Floquet ansatz with the micromotion operator

$$U(t,t_0) = P(t,t_0)e^{-\frac{i}{\hbar}H_\mathrm{F}(t-t_0)} \tag{3.70}$$

$$= (\mathbf{1} + P_1 + P_2 + \dots)\sum_n \left(\frac{(t-t_0)}{i\hbar}\right)^n \frac{(H_{\mathrm{F},1} + H_{\mathrm{F},2} + \dots)^n}{n!}. \tag{3.71}$$

The high-frequency Magnus approximation for a short stroboscopic time window is a single exponential approximation

$$U(T+t_0,t_0) = e^{-i\frac{T}{\hbar}(H_{\mathrm{F},1}+H_{\mathrm{F},2}+\dots)}. \tag{3.72}$$

In contrast to the tripartite ansatz the latter two approaches still carry residual information from the micromotion operator in form of a t_0-dependence. This issue and the order by order terms of the kick operators K and H_F are discussed in [79, 15, 81, 14]. The method of taking the Magnus expansion and sorting out the constant constribution is just a further approach to construct an effective Hamiltonian, without having the admixtures of the t_0-dependent terms from the micromotion.
The third order stroboscopic Floquet Hamiltonian in spectral decomposition accordingly follows as

$$H_{\mathrm{sF},3} = \sum_{klmn} c_{klmn}[H_k,[H_l,[H_m,H_n]]], \tag{3.73}$$

with the spectral factor

$$\begin{aligned} c_{klmn} =& \frac{1}{12(i\hbar)^3}\int_{t_0}^{t} dt_1 \int_{t_0}^{t_1} dt_2 \int_{t_0}^{t_2} dt_3 \int_{t_0}^{t_3} dt_4 \left(e^{ik\omega t_1 + il\omega t_2 + im\omega t_3 + in\omega t_4}\right. \\ &\left. + e^{ik\omega t_2 + il\omega t_3 + im\omega t_4 + in\omega t_1} + e^{ik\omega t_1 + il\omega t_4 + im\omega t_3 + in\omega t_2} + e^{ik\omega t_4 + il\omega t_3 + im\omega t_1 + in\omega t_2}\right). \end{aligned} \tag{3.74}$$

The third-order effective Floquet Hamiltonian again requires $k+l+m+n=0$. It is a huge computational effort to perform the manipulation of the fourfold commutators.

Hence, one formally notes

$$H_{\mathrm{F},3} = \sum_{klmn,\, k+l+m+n=0} c_{klmn}[H_k, [H_l, [H_m, H_n]]], \tag{3.75}$$

In the present case of a cosine or sine driving, one only deals with the first harmonics $(k, l, m, n) = \pm 1$, which is justified since higher harmonics are stronger suppressed by the factor of the order $1/k^3$. Of course, for more elaborated driving protocols one may require higher harmonics or even polychromatic driving, Ref. [108]. Some fourth order terms will be explicitly computed in Chapter 5 on behalf of some solvable reference examples.

3.2.3 Generalization to closed and open classical systems

The Magnus expansion is generally suitable to describe the short time dynamics and provides a solution to linear non-autonomous differential equations of the type

$$\partial_t P = L(t)P. \tag{3.76}$$

The method is applicable to isolated and open classical systems, and to closed quantum systems, which means the approach works for time-dependent Lagrangians and Hamiltonians as well as for classical master equations like the Fokker-Planck equation.
The exponential form of the Magnus solution is analogous to either the thermal distribution $\rho_{th} \sim \exp[-\beta H]$ or time evolution operator $U = \exp[-iHt]$, which enables us to compare the approximated effective Hamiltonians with the ones of the undriven systems. In the classical case, one uses the Poisson brackets $\{O_1, O_2\} = \partial_x O_1 \partial_p O_2 - \partial_p O_1 \partial_x O_2$ instead of the commutator.

3.2.4 Validity and limitations of the low-energy effective theory

In general, it is not known whether the ME is asymptotic or has a finite radius of convergence [109]. The Floquet-Magnus expansion is guaranteed to converge, if

$$\int_0^T \|H(t)\| dt \leq \xi_F, \tag{3.77}$$

where ξ_F is a constant of the order of 1. Many mathematical papers try to refine the number on the right-hand side [110, 111]. Criteria are often given in the context of solvable models like the quantum two-level system [112]. The ME is a

tool to compute the Floquet Hamiltonian in the high-frequency limit, hence the setting is $\omega_{\mathrm{m}} \gg \omega_0$, which automatically satisfies (3.77). Physically, the existence of resonances leads to fast efficient heating in the system. Thus, one either avoids heating by coupling to a sufficiently large low-temperature heat bath. Or the systems are studied far off-resonance, which implies that the Magnus-Floquet theory is not suitable to cover the dynamics around resonances [4] [113]. However, for a low-energy effective theory driven at high frequencies $\omega_{\mathrm{m}} \gg \omega_0$, the method can be safely used. Even if the perturbative expansion for the effective Hamiltonian is asymptotic, it can be still physically useful. That means the first few orders can give a physical intuition and can be fairly accurate. Generally, for short or finite times, the Magnus expansion can be mostly safely used. For long term approximations or quasi-stationary behavior, one needs to be more cautious with the Magnus results. Another criterion for the convergence of a solvable system is

$$\omega > \sqrt{{\omega_0}^2 + \omega_{\mathrm{A}}^2} \tag{3.78}$$

where the natural frequency ω_0 has been rescaled by a driving term $\omega_{\mathrm{A}} = \omega_0 A$ with a dimensionless driving amplitude A [114]. ω represents the cut-off, the driving frequency or the expansion frequency. Hence, the statement is again, the system has to be considered off-resonant.

This chapter introduced the Floquet-Magnus theory. The concept and the usability of the Magnus expansion was explained. An alternative approach to derive gauge-invariant effective Floquet Hamiltonians was developped. By introducing the concept of the spectral factors c_{ijk} with certain "Bragg"-conditions one obtains the respective Magnus contributions for each order without any further required gauge transformations in a straight forward manner. In the subsequent Chapter 4 the Magnus expansion is extended to provide a systematical expansion in the ratio of the driving amplitude A and the driving frequency $1/\omega_{\mathrm{m}}$. Explicit formulas up to fourth order in A are derived.

[4] For large times $t \gg T$, it was shown that in a spin systems an n-spin resonance energy transfer heats up the system, though it is not very likely to happen and can be neglected for the short-time dynamics.

Chapter 4

Alternative Magnus expansion

In this Chapter, an alternative Magnus formalism for periodically driven systems is developed such that it provides a systematical expansion in the driving amplitude A and the inverse of the driving frequency ω_{m}. Motivated by the experiments, the high-frequency limit $\omega_{\mathrm{m}} \gg \omega_0$ is studied assuming that the system is tractable and the corresponding Floquet Hamiltonians do exist. Naturally, infinite heating of the driven system is prevented by coupling it to a heat bath which guarantees that the presumable steady state is reached. As for isolated systems heating in the low-frequency regime is often reduced if the energy spectra are well separated. In the present configuration, the high energy plasmon has a frequency of 10THz and the low energy ones is about 1THz.
Parts of this derivation have been published in Section 3 of the paper Ref.[16], though the line of arguing and the range of validity have been reconsidered and considerably extended. The perturbative parameter always appears in powers of $(\omega_0/\omega_{\mathrm{m}})^m A^2 n$, which allows to study fairly large amplitudes in the high frequency regime $\omega_{\mathrm{m}} \gg \omega_0$. The example in Ref.[16] studied the parameteric oscillator. For strong driving, e.g. $(\omega_0/\omega_{\mathrm{m}})^m A^2 n > 1$, the perturbative treatment becomes invalid , an effective parameteric resonance was observed. Especially the dependence on the relative initial driving phase $\phi_0 = \omega_m t_0$ [1] has been rederived and eliminated, see Sec. 3.2.2, and the prefactors in the higher orders of the Magnus expansion have been corrected.

4.1 Effective low-energy theory

The reduction of the full dynamics to an effectively static low-frequency description allows to apply standard techniques, such as dressing of quantum states, which are

[1] The Magnus expansion creates a dependence on the driving phase, which can lead to artificial symmetry breaking (Floquet gauge)[15] and ambiguous effective Hamiltonians.

usually only available for time-independent systems [78]. Hence, the construction of such dressed or effectively static Hamiltonians facilitates analytical approaches, as for example a non-autonomous differential equation becomes autonomous again. Furthermore, in the short time limit $T_m = 2\pi/\omega_\mathrm{m} \ll T_0 = 2\pi/\omega_0$ one can approximate the non-equilibrium distribution by $P_\mathrm{dr} \sim \exp[-\beta H_\mathrm{eff}]$, where $\beta = 1/(k_\mathrm{B}T)$ with a given system temperature T. Ideally, this approximation holds in the weak coupling and weak driving regime with a heat bath.
The equilibrium distribution of a thermally destributed undriven system is $P_\mathrm{th} \sim \exp[-\beta H_0]$. Given a driven Hamiltonian $H(t)$, one cannot directly deduce a time-independent Hamiltonian or a steady state distribution. One either has to solve the master equation or determine the Floquet states, or use, as demonstrated in Section 2.2.4, an elobarated ansatz (2.49). The alternative Magnus formalism provides effectively static solutions in exponential form to linear differential equations like the Schrödinger equation, the Fokker-Planck or Kramers equation without any computation of Floquet states or the nececssity of an ansatz. It suffices to know the equilibrium term L_0 and the driven term $L_{dr}(t)$. The computational effort is shifted to the evaluation of nested commutators and nested time integrals over driving protocols $f(t)$.

4.2 Systematic expansion in the driving field strength and the inverse driving frequency

4.2.1 Interaction picture and back transformation

The Hamiltonian is decomposed into a free undriven Hamiltonian part H_0 and a perturbed driven part H_1 with the dimensionless perturbation parameter A

$$H(t) = H_0 + AH_1(t). \tag{4.1}$$

The structure of the Magnus terms (3.37) with their nested commutators combines different orders in A in every order of the Magnus expansion. Conceptionally, the n^{th} order Magnus term contributes to all the other orders up to n in A [115] [2]. Hence it is impossible to get complete systematical access to the individual orders of A. This problem is avoided by transforming the problem into the interaction picture

[2] Looking at the series expansion of $\exp[X+Y] = \sum_{k=0}^{\infty} \frac{(X+Y)^k}{k!}$, one has to expand the product $(X+Y)^k$ into a sum and find admixtures of Y in every order of k.

according to

$$H_{0,I}(t) = \exp[iH_0 t/\hbar] H_0 \exp[-iH_0 t/\hbar] = H_0 \tag{4.2}$$

$$AH_{1,I}(t) = \exp[iH_0 t/\hbar] AH_1(t) \exp[-iH_0 t/\hbar]. \tag{4.3}$$

The according differential equation for the time evolution operator in the interaction picture is

$$i\hbar \frac{\partial U_I}{\partial t} = AH_{1,I}(t) U_I. \tag{4.4}$$

Applying the Magnus expansion to (4.4), the resulting nested commutators contain the bare orders of A. Therefore, the order of the Magnus expansion conincides with order of the driving term A.
Generalizing to linear differential operators $L(t)$, one assumes $L(t)$ can be decomposed into an undriven part L_0 and a time-dependent driven part $L_{\mathrm{dr}}(t)$

$$L(t) = L_0 + L_{\mathrm{dr}}(t). \tag{4.5}$$

For the Schrödinger equation the respective operators are $L_0 = H_0/(i\hbar)$ and $L_{\mathrm{dr}}(t) = AH_1(t)/(i\hbar)$. Analogously, one introduces an auxiliary interaction picture for the operator L to handle the orders in the driving amplitude, i.e.,

$$L_I(t,s) = \exp[-L_0 s] L(t) \exp[L_0 s], \tag{4.6}$$

$$\rho_I(t,s) = \exp[-L_0 s] \rho(t) \exp[L_0 s], \tag{4.7}$$

which amounts to the standard interaction picture term for $L_I(t,t) = L_I(t)$ and $\rho_I(t,t) = \rho_I(t)$. The additionally introduced variable s is useful for the back transformation into the Schrödinger picture, because it allows to distingiush between temporal arguments arising from the transformation into the interaction picture and the argument used for the driving term $L_{\mathrm{dr}}(t)$.
The respective equation of motion for an abritrary linear operator L is

$$\partial_t \rho_I = L_{\mathrm{dr,I}}(t) \rho_I, \tag{4.8}$$

with $L_{\mathrm{dr,I}}(t) = \exp[-L_0 t] L_{\mathrm{dr}}(t) \exp[L_0 t]$. The formal solution is

$$\rho_I(t) = \mathcal{T} \left(\exp \left[\int_{t_0}^{t} ds L_{\mathrm{dr,I}}(s) \right] \right) \rho_I(t_0). \tag{4.9}$$

$\rho_I(t_0)$ is the initial state at t_0 in the interaction picture, which is set to $\rho_I(t_0) = \mathbf{1}$. The true exponential representation of equation (4.9) is given by the Magnus

expansion

$$\rho_I(t) \overset{Magnus}{=} \exp[\Omega_I(t,t_0)] = \exp\left[\sum_k \Omega_{k,I}(t,t_0)\right]. \tag{4.10}$$

Analoguosly to the time evolution operator, the Magnus terms $\sum_k \Omega_{k,I}$ approximate the integral of the operator $L_{\mathrm{dr,I}}(t)$ in the exponential $\Omega_I(t,t_0) = \int_{t_0}^{t} dt' L_{\mathrm{dr,I}}(t')$. Hence the derivative is $\dot{\Omega}_I = \sum_k \dot{\Omega}_{k,I} = L_{\mathrm{dr,I}}(t)$.
The first-order Magnus term for the solution of (4.8) is

$$\Omega_{1,I}(t,t_0) = \int_{t_0}^{t} dt_1 \exp[-L_0 t_1] L_{\mathrm{dr}}(t_1) \exp[L_0 t_1] \tag{4.11}$$

$$\Rightarrow \quad \dot{\Omega}_{1,I} = L_{1,\mathrm{dr,I}}(t) \tag{4.12}$$

$$= \exp[-L_0 t] L_{\mathrm{dr}}(t) \exp[L_0 t]. \tag{4.13}$$

The reduction by one time integral to construct the Magnus term for $L_{\mathrm{dr,I}}(t)$ is a performance boost, especially in the case of the higher Magnus expressions with their nested temporal integrals.
$\dot{\Omega}_{1,I}(t)$ is the first Magnus contribution to the operator in the interaction picture $L_{\mathrm{dr,I}}(t)$. After the time-dependent back transformation into the Schrödinger picture, one obtains the first-order Magnus correction

$$L_1(t) = \exp[L_0 t] \dot{\Omega}_{1,I}(t) \exp[-L_0 t] \tag{4.14}$$

$$= \exp[L_0 t] L_{1,\mathrm{dr,I}}(t) \exp[-L_0 t] \tag{4.15}$$

$$= L_{\mathrm{dr}}(t), \tag{4.16}$$

which is by construction of first order in A.
The second-order Magnus term is

$$L_2(t) = \exp[L_0 t] \dot{\Omega}_{2,I}(t) \exp[-L_0 t] \tag{4.17}$$

$$= \frac{1}{2} \exp[L_0 t] \frac{d}{dt} \left(\int_{t_0}^{t} dt_1 \int_{t_0}^{t_1} dt_2 [L_{\mathrm{dr,I}}(t_1), L_{\mathrm{dr,I}}(t_2)] \right) \exp[-L_0 t] \tag{4.18}$$

$$= \frac{1}{2} \exp[L_0 t] \int_{t_0}^{t} dt_2 [L_{\mathrm{dr,I}}(t), L_{\mathrm{dr,I}}(t_2)] \exp[-L_0 t] \tag{4.19}$$

$$= \frac{1}{2} \int_{t_0}^{t} dt_2 [L_{\mathrm{dr}}(t), \exp[L_0(t-t_2)] L_{\mathrm{dr}}(t_2) \exp[-L_0(t-t_2)]]. \tag{4.20}$$

The temporal arguments in (4.20) resemble the definition of the transformation of the 'shifted' interaction picture (4.6).
To evaluate (4.20), another important lemma of the BCH-formula is needed. For

non-commuting operators X, Y, the following formula holds

$$e^{sX}Ye^{-sX} = Y + s[X,Y] + \frac{s^2}{2!}[X,[X,Y]] + \cdots + \frac{s^n}{n!}\underbrace{[X,[\cdots,[X}_{n-times},Y]\cdots]] + \cdots \tag{4.21}$$

$$= \sum_n \frac{s^n}{n!}\mathrm{ad}_{\mathrm{X}}^{\mathrm{n}}\mathrm{Y}, \tag{4.22}$$

with the definition of the n^{th} adjoint action of X on Y

$$\mathrm{ad}_{\mathrm{X}}^{\mathrm{n}}\mathrm{Y} = \underbrace{[X,[\cdots,[X}_{\mathrm{n-times}},\mathrm{Y}]\cdots]]. \tag{4.23}$$

For the final computation of (4.20), one assumes that the original driving term has the decomposition $L_{\mathrm{dr}}(t) = L_{\mathrm{dr},0}f(t)$. $f(t)$ is the driving protocol modifying the driving amplitude in time. $L_{\mathrm{dr},0}$ is a time-independent operator representing any kind of coupling between the system and the driving. Its structure does not change in time, however, the amplitude is modulated via the scalar function $f(t)$.
A prerequisite for the applicability of the Floquet-Magnus theory to derive stroboscopic Floquet Hamiltonians is the periodicity $f(t) = f(t+T)$. Nonetheless, if this does not strictly hold, e.g., the driving protocol is not periodic with a Gaussian envelope, one can still approximate the transient effective Hamiltonian. In this case, one has to be careful with the stroboscopic averaging time window $T_c = 2\pi/\omega_{\mathrm{c}}$. Furthermore, the Floquet gauge t_0 and the associated kick operators K become more relevant. However, this work focuses on a quasi steady-state approximation derived exclusively for periodic drivings. Hence, there is no need for the kick operators.
Applying (4.22) to (4.20) with $s = t - t_2$, $X = L_0$ and $Y = L_{\mathrm{dr}}(t_2) = L_{\mathrm{dr},0}f(t_2)$ one obtains the following expression for the perturbative expansion in s

$$\begin{aligned} L_2(t) = \frac{1}{2}\int_{t_0}^{t} dt_2 f(t)f(t_2)\,\{&[L_{\mathrm{dr},0},L_{\mathrm{dr},0}] \\ &+[L_{\mathrm{dr},0},[L_0,L_{\mathrm{dr},0}]](t-t_2) + [L_{\mathrm{dr},0},[L_0,[L_0,L_{\mathrm{dr},0}]]]\frac{(t-t_2)^2}{2!} + \cdots\Big\} \end{aligned} \tag{4.24}$$

$$\begin{aligned} = \frac{1}{2}\int_{t_0}^{t} dt_2 f(t)f(t_2)\,\{&[[L_0,L_{\mathrm{dr},0}],L_{\mathrm{dr},0}](t_2-t) \\ &-[[L_0,[L_0,L_{\mathrm{dr},0}]],L_{\mathrm{dr},0}]\frac{(t-t_2)^2}{2!} + \cdots\Big\} \end{aligned} \tag{4.25}$$

Introducing the short hand notation for the n^{th} adjoint action

$$ {L_{\mathrm{dr},0}}^{n} = \underbrace{[L_0, [\ldots, [L_0}_{n-times}, L_{\mathrm{dr},0}]\ldots]] = \mathrm{ad}^{\mathrm{n}}_{\mathrm{L}_0}\mathrm{L}_{\mathrm{dr},0}, \tag{4.26} $$

the second order Magnus term (4.25) of $L_{\mathrm{dr}}(t)$ is compactly written as

$$ \begin{aligned} L_2(t) = -\frac{1}{2}\int_{t_0}^{t} dt_2 f(t)f(t_2)\left\{[{L_{\mathrm{dr},0}}^{1}, L_{\mathrm{dr},0}](t-t_2)\right. \\ \left. +[{L_{\mathrm{dr},0}}^{2}, L_{\mathrm{dr},0}]\frac{(t-t_2)^2}{2!} + \cdots \right\}. \end{aligned} \tag{4.27} $$

In the above Eq. (4.27) the commutators with the same arguments, namely $[L_{\mathrm{dr},0}, L_{\mathrm{dr},0}]$ and $[{L_{\mathrm{dr},0}}^{1}, {L_{\mathrm{dr},0}}^{1}]$, were dropped, because of the 'factorization' assumption $L_{\mathrm{dr}}(t) = L_{\mathrm{dr},0}f(t)$ with constant $L_{\mathrm{dr},0}$. If the operator $L_{\mathrm{dr},0}$ itself changed in time, one would find $[L_{\mathrm{dr},0}(t_i), L_{\mathrm{dr},0}(t_j)] \neq 0$. It requires some combinatorics to find the non-zero commutators, but the algebraic prefactors of $(t-t_i)^n$ are straightforward since they correspond to the adjoint action superscript n. This allows to rewrite Eq. (4.27) as

$$ L_2(t) = C_{10}(t)[{L_{\mathrm{dr},0}}^{1}, L_{\mathrm{dr},0}] + C_{20}(t)[{L_{\mathrm{dr},0}}^{2}, L_{\mathrm{dr},0}] + C_{30}(t)[{L_{\mathrm{dr},0}}^{3}, L_{\mathrm{dr},0}], \tag{4.28} $$

where the time-dependent coefficients are just read-off from equation (4.27), i.e.,

$$ C_{10}(t) = -\frac{A^2}{2}\int_{t_0}^{t} dt_2 f(t)f(t_2)(t-t_2), \tag{4.29} $$

$$ C_{20}(t) = -\frac{A^2}{2}\int_{t_0}^{t} dt_2 f(t)f(t_2)\frac{(t-t_2)^2}{2!}, \tag{4.30} $$

$$ C_{30}(t) = -\frac{A^2}{2}\int_{t_0}^{t} dt_2 f(t)f(t_2)\frac{(t-t_2)^3}{3!}. \tag{4.31} $$

The first entry of the commutator has the temporal argument t which cancels the algebraic prefactor $(t-t_i)^n$. Therefore, the mixed terms proportional to $[{L_{\mathrm{dr},0}}^{2}, {L_{\mathrm{dr},0}}^{1}]$ do not appear here.

4.2.1.1 Third and fourth order Magnus terms

After the perturbative back transformation to the Schödinger picture, the leading four orders of the Magnus expansion are derived. These are the necessary orders to construct effective Hamiltonians or operators.

The first order Magnus contribution to the operator $L_{\mathrm{dr}}(t)$ was

$$L_1(t) = \exp[L_0 t]\dot{\Omega}_{1,I}(t)\exp[-L_0 t] \tag{4.32}$$
$$= L_{\mathrm{dr},0} f(t) \tag{4.33}$$
$$= C_0(t) L_{\mathrm{dr},0}. \tag{4.34}$$

The first order correction is proportional to the bare driving term $C_0(t) = f(t)$. For the construction of the time-independent effective Hamiltonian, this term will be considered in a stroboscopic averaged time window $(t_0, t_0 + T_c)$, with the time defined via the cut-off frequency $T_c = 2\pi/\omega_{\mathrm{c}}$. Ultimately, this time window determines how coarse-grained the frequency resolution is. The higher the considered frequencies the shorter the time window should be. Vice versa if the averaging windows is larger than the period of the undriven system $T_c > T_0$ the dynamics is no longer covered accurately. The respective Magnus orders Ω_k converge with the order of the stroboscopic time window T_c^{k+n}, where n is the index of the polynomial contributions $(t - t_i)^n$ from the perturbative back transformation.
The stroboscopic evaluation of (4.34) finally yields the first effective time-independent contribution

$$L_{\mathrm{eff},1} = [L_1(t)]_{\omega<\omega_{\mathrm{c}},\cancel{t_0}} = \sum_n L_{\mathrm{eff},1}^{(1,n)}. \tag{4.35}$$

The bracket $[\cdot]_{\omega<\omega_{\mathrm{c}},\cancel{t_0}}$ indicates the projection onto the non-oscillating and low-frequency contributions and the expressions being independent of t_0. This is demonstrated along the example of a simple cos-driving. The according first order coefficient would be

$$[\cos\omega_{\mathrm{m}} t]_{\omega<\omega_{\mathrm{c}},\cancel{t_0}} = \frac{1}{T_c}\int_{t_0}^{t_0+T_c} dt\cos\omega_{\mathrm{m}} t \tag{4.36}$$
$$= \mathcal{O}\left(\frac{\sin[\omega_{\mathrm{m}}(T_c+t_0)] - \sin[\omega_{\mathrm{m}} t_0]}{\omega_{\mathrm{m}} T_c}\right) \tag{4.37}$$
$$= 0. \tag{4.38}$$

For $T_c = T_m = 2\pi/\omega_{\mathrm{m}}$ this is exactly zero. For $T_c \gg T_m$ the fastly oscillating integrals in the coefficients are approximately zero, because the denominator $\omega_{\mathrm{m}} T_c$ suppresses the contribution. Furthermore, they contain t_0 terms.

In contrast a second order contribution proportional to a $\cos^2 \omega_{\mathrm{m}} t$ expression yields

$$[(\cos \omega_{\mathrm{m}} t)^2]_{\omega<\omega_{\mathrm{c}},\not{t_0}} = \frac{1}{T_c} \int_0^{T_c} dt \cos^2 \omega_{\mathrm{m}} t \tag{4.39}$$

$$= \frac{1}{T_c} \int_{t_0}^{t_0+T_c} dt \left(\frac{1}{2} + \frac{\cos 2\omega_{\mathrm{m}} t}{2} \right) \tag{4.40}$$

$$= \frac{1}{2} + \mathcal{O}\left(\frac{\sin[\omega_{\mathrm{m}}(T_c + t_0)] - \sin[2\omega_{\mathrm{m}} t_0]}{4\omega_{\mathrm{m}} T_c} \right) \tag{4.41}$$

$$= \frac{1}{2}. \tag{4.42}$$

If there is just one driving term, only the non-oscillating part of $f(t)$ and contributions from the perturbative expansion $\sim (t - t_i)^n \sim T_c^n$ can appear under these conditions. It is mandatory for higher orders of the Magnus terms that the contributions from the oscillating terms cancel each other in the exponent to avoid a t_0 dependence (4.42). This 'zero phase' condition most likely enforces constant contributions. Other fastly oscillating contributions from the coefficients are averaged out.

The analytic evaluation of the projection $[\cdot]_{\omega<\omega_{\mathrm{c}},\not{t_0}}$, in particular the ones for higher orders, is performed via the programm Mathematica, which suppresses all t_0 dependent terms. The formally correct way is shown in the previous chapter and makes use of Fourier components to determine the constant contributions. However, it is also advantageous to circumvent the Fourier expansion of $L_{\mathrm{dr}}(t)$ und work directly with the driving protocols which results in a straightforward prescription for the coefficients, such as the second order coefficients in (4.29) - (4.31).

The second order was deduced to be

$$L_2(t) = C_{10}(t)[{L_{\mathrm{dr},0}}^1, L_{\mathrm{dr},0}] + C_{20}(t)[{L_{\mathrm{dr},0}}^2, L_{\mathrm{dr},0}] + C_{30}(t)[{L_{\mathrm{dr},0}}^3, L_{\mathrm{dr},0}] \tag{4.43}$$

with the coefficients given in Eqs. (4.29) - (4.31). To approximate the contribution to the stroboscopic effective operator L_{eff}, the stroboscopic averaging over the time intervall T_c is performed and furthermore the condition for the t_0 terms is applied. This leads to the second order contribution

$$L_{\mathrm{eff},2} = [L_2(t)]_{\omega<\omega_{\mathrm{c}},\not{t_0}} = \sum_i L_{\mathrm{eff},2}^{(2,i)}. \tag{4.44}$$

The next two orders are derived in a similar way. The third order correction is

$$L_3 = \exp[L_0 t]\dot{\Omega}_{3,I}(t)\exp[-L_0 t] \tag{4.45}$$

$$= \frac{1}{6}\exp[L_0 t]\int_{t_0}^{t} dt_2 \int_{t_0}^{t_2} dt_3 \left\{[L_{\mathrm{dr,I}}(t),[L_{\mathrm{dr,I}}(t_2),L_{\mathrm{dr,I}}(t_3)]]\right.$$
$$\left.-[L_{\mathrm{dr,I}}(t_3),[L_{\mathrm{dr,I}}(t),L_{\mathrm{dr,I}}(t_2)]]\right\}\exp[-L_0 t]. \tag{4.46}$$

Each individual $L_{\mathrm{dr,I}}(t_i)$ in the Schrödinger picture has intercalated terms of the structure $\exp[(t-t_0)L_0]L_{\mathrm{dr},0}\exp[-(t-t_0)L_0]$. Using (4.22) to expand these terms leads algebraic prefactors for the different occuring time arguments, i.e.,

$$L_3 = \frac{1}{6}\int_{t_0}^{t} dt_2 \int_{t_0}^{t_2} dt_3 f(t)f(t_2)f(t_3)\left\{[L_{\mathrm{dr},0},[{L_{\mathrm{dr},0}}^1,L_{\mathrm{dr},0}]](t-2t_2+t_3)\right.$$
$$+[{L_{\mathrm{dr},0}}^1,[{L_{\mathrm{dr},0}}^1,L_{\mathrm{dr},0}]]((t-t_3)(t-t_2))$$
$$\left.+[L_{\mathrm{dr},0},[{L_{\mathrm{dr},0}}^2,L_{\mathrm{dr},0}]]\frac{1}{2}(2(t-t_2)^2-(t-t_3)^2)+\cdots\right\}. \tag{4.47}$$

By construction the involved expressions are of third order in the driving protocol $f(t)$.
Introducing the third order coefficients, (4.47) is compactly rewritten as

$$L_3 = C_{010}(t)[L_{\mathrm{dr},0},[{L_{\mathrm{dr},0}}^1,L_{\mathrm{dr},0}]] + C_{110}(t)[{L_{\mathrm{dr},0}}^1,[{L_{\mathrm{dr},0}}^1,L_{\mathrm{dr},0}]]$$
$$+ C_{020}(t)[L_{\mathrm{dr},0},[{L_{\mathrm{dr},0}}^2,L_{\mathrm{dr},0}]]. \tag{4.48}$$

The temporal integrals for the coefficients c_{klm} contain the three-fold product of the modulation function $1/6\int_{t_0}^{t}dt_2\int_{t_0}^{t_2}dt_3 f(t)f(t_2)f(t_3)$ times the polynomial in the times arising from perturbation theory of the backtransformation into the Schrödinger picture. The subscript klm indicates the order in perturbation theory of the backtransformation in the nested commutator structure. Hence the subscript 110 labels the prefactor of the commutator $[{L_{\mathrm{dr},0}}^1,[{L_{\mathrm{dr},0}}^1,L_{\mathrm{dr},0}]]$ and so on. The coefficients for an arbitrary driving $f(t)$ from equation (4.47) are

$$C_{010}(t) = \frac{1}{6}\int_{t_0}^{t} dt_2 \int_{t_0}^{t_2} dt_3 f(t)f(t_2)f(t_3)(t-2t_2+t_3)$$
$$C_{110}(t) = \frac{1}{6}\int_{t_0}^{t} dt_2 \int_{t_0}^{t_2} dt_3 f(t)f(t_2)f(t_3)(t-t_2)(t-t_3)$$
$$C_{020}(t) = \frac{1}{6}\int_{t_0}^{t} dt_2 \int_{t_0}^{t_2} dt_3 f(t)f(t_2)f(t_3)\frac{1}{2}\left[2(t-t_2)^2-(t-t_3)^2\right]. \tag{4.49}$$

The effective third-order Magnus correction to the original operator $L_{\rm dr}(t)$ is

$$L_{\rm eff,3} = [L_3]_{\omega<\omega_{\rm c}} = \sum_i L^{(3,i)}_{\rm eff,3}. \tag{4.50}$$

The fourth Magnus term in the Schrödinger picture is

$$\begin{aligned} L_4 &= \exp[L_0 t]\dot{\Omega}_{4,I}(t)\exp[-L_0 t] \qquad (4.51)\\ &= \frac{1}{12}\exp[L_0 t]\int_{t_0}^{t} dt_2 \int_{t_0}^{t_2} dt_3 \int_{t_0}^{t_3} dt_4 \times \\ &([L_{\rm dr,I}(t),[L_{\rm dr,I}(t_2),[L_{\rm dr,I}(t_3),L_{\rm dr,I}(t_4)]]] \\ &+[L_{\rm dr,I}(t_2),[L_{\rm dr,I}(t_3),[L_{\rm dr,I}(t_4),L_{\rm dr,I}(t)]]] \\ &+[L_{\rm dr,I}(t),[L_{\rm dr,I}(t_4),[L_{\rm dr,I}(t_3),L_{\rm dr,I}(t_2)]]] \\ &+[L_{\rm dr,I}(t_4),[L_{\rm dr,I}(t_3),[L_{\rm dr,I}(t),L_{\rm dr,I}(t_2)]]])\exp[-L_0 t]. \qquad (4.52)\end{aligned}$$

Again, the perturbative transformation of $L_{\rm dr,I}(t_i)$ into the Schrödinger picture is performed by applying (4.22). Similar to the third-order coefficients, one introduces the fourth-order coefficients with a common integral prefactor

$$\frac{1}{12}\int_{t_0}^{t} dt_2 \int_{t_0}^{t_2} dt_3 \int_{t_0}^{t_3} dt_4 f(t_1)f(t_2)f(t_3)f(t_4)\cdot, \tag{4.53}$$

times some polynomials in the time arguments which can be explicitly found in the Appendix E. In a concise form one obtains

$$\begin{aligned} L_4 = {} & C_{0010}(t)[L_{\rm dr,0},[L_{\rm dr,0},[{L_{\rm dr,0}}^1,L_{\rm dr,0}]]] + C_{0110}(t)[L_{\rm dr,0},[{L_{\rm dr,0}}^1,[{L_{\rm dr,0}}^1,L_{\rm dr,0}]]] \\ & + C_{1010}(t)[{L_{\rm dr,0}}^1,[L_{\rm dr,0},[{L_{\rm dr,0}}^1,L_{\rm dr,0}]]] + C_{0020}(t)[L_{\rm dr,0},[L_{\rm dr,0},[{L_{\rm dr,0}}^2,L_{\rm dr,0}]]] \\ & + C_{0021}(t)[L_{\rm dr,0},[L_{\rm dr,0},[{L_{\rm dr,0}}^2,{L_{\rm dr,0}}^1]]] + C_{0120}(t)[L_{\rm dr,0},[{L_{\rm dr,0}}^1,[{L_{\rm dr,0}}^2,L_{\rm dr,0}]]] \\ & + C_{1020}(t)[{L_{\rm dr,0}}^1,[L_{\rm dr,0},[{L_{\rm dr,0}}^2,L_{\rm dr,0}]]] + C_{0210}(t)[L_{\rm dr,0},[{L_{\rm dr,0}}^2,[{L_{\rm dr,0}}^1,L_{\rm dr,0}]]] \\ & + C_{2010}(t)[{L_{\rm dr,0}}^2,[L_{\rm dr,0},[{L_{\rm dr,0}}^1,L_{\rm dr,0}]]] + C_{0030}(t)[L_{\rm dr,0},[L_{\rm dr,0},[{L_{\rm dr,0}}^3,L_{\rm dr,0}]]]. \end{aligned}$$

Applying the defined projection $[\cdot]_{\omega<\omega_{\rm c},\not 0}$ the effective fourth order Magnus correction to the original operator $L_{\rm dr}(t)$ is

$$L_{\rm eff,4} = [L_4]_{\omega<\omega_{\rm c},\not 0} = \sum_i L^{(4,i)}_{\rm eff,4}. \tag{4.54}$$

The higher-order Magnus terms approximate the time-independent effective operator $L_{\rm eff}$ which was derived from $L(t) = L_0 + L_{\rm dr}(t)$. The basic idea is to start off with an undriven system operator L_0 and a driving term which couples to the system $L_{\rm dr}(t) = L_{\rm dr,0}f(t)$. Provided these three ingredients $(L_0, f(t), L_{\rm dr,0},)$, one

can construct an effective time-independent operator L_{eff}

$$L(t) = L_0 + L_{\text{dr},0} f(t) \quad \Rightarrow \quad L_{\text{eff}} = L_0 + L_{\text{eff},1} + L_{\text{eff},2} + L_{\text{eff},3} + L_{\text{eff},4}. \tag{4.55}$$

The procedure is applicable to open and isolated classical systems as well as to isolated driven quantum systems. A rigorous derivation of the classical limit for ME is found in the appendix A of [116] and in Ref. [117]. In the limit $\hbar \to 0$ the quantum commutator has to be replaced by the Poisson bracket $\frac{1}{i\hbar}[\dots] \to \{\dots\}$. For case of an open system, $L(t)$ would be the master equation operator, like the Fokker-Planck or Kramers operator. For case of an isolated system the equations of motion are derived from the Poisson bracket.

4.3 Summary

This section provides a short summary on how to construct an effective Hamiltonian. The first step is to apply the Magnus expansion in the interaction picture to get a systematic expansion in the driving amplitude $f(t) \propto A$. The result is that the order in A coincides with the order of the Magnus expansion. The second and third steps are to set the stroboscopic window for the Magnus terms and the according projection onto the low-frequency components to obtain L_{eff}. The perturbative back transformation into the Schrödinger picture and the subsequent low-frequency projection give access to the inverse frequency series. The complete schematical work flow is as follows:

1. Interaction-picture for $L(t) = L_0 + L_{\text{dr}}(t)$
   with $L_{\text{dr,I}}(t) = \exp[-L_0 t] L_{\text{dr}}(t) \exp[L_0 t]$

$$\partial_t \rho = L(t)\rho \tag{4.56}$$

$$\Leftrightarrow \partial_t \rho_I = L_{\text{dr,I}}(t)\rho_I \tag{4.57}$$

$$\Leftrightarrow \rho_I(t) = \mathcal{T}\left(\exp\left[\int_{t_0}^{t} ds L_{\text{dr,I}}(s)\right]\right)\rho_I(t_0) \tag{4.58}$$

2. Magnus expansion with $\int_{t_0}^{t} ds L_{\mathrm{dr,I}}(s) = \Omega_I = \sum_k \Omega_{k,I}$

$$\Omega_{1,I} = \int_{t_0}^{t} dt_1 L_{\mathrm{dr,I}}(t_1) \tag{4.59}$$

$$\Omega_{2,I} = \frac{1}{2}\int_{t_0}^{t} dt_1 \int_{t_0}^{t_1} dt_2 [L_{\mathrm{dr,I}}(t_1), L_{\mathrm{dr,I}}(t_2)] \tag{4.60}$$

$$\Omega_{3,I} = \frac{1}{6}\int_{t_0}^{t} dt_1 \int_{t_0}^{t_1} dt_2 \int_{t_0}^{t_2} dt_3 \\ ([L_{\mathrm{dr,I}}(t_1), [L_{\mathrm{dr,I}}(t_2), L_{\mathrm{dr,I}}(t_3)]] - [L_{\mathrm{dr,I}}(t_3), [L_{\mathrm{dr,I}}(t_1), L_{\mathrm{dr,I}}(t_2)]]) \tag{4.61}$$

$$\vdots$$

3. Perturbative back transformation to Schödinger picture using the BCH formula to get the Magnus corrections to $L_{\mathrm{dr}}(t)$

$$\begin{aligned} L_1(t) &= \exp[L_0 t]\dot{\Omega}_{1,I}(t)\exp[-L_0 t] \\ &= f(t)L_{\mathrm{dr},0} \\ L_2(t) &= \exp[L_0 t]\dot{\Omega}_{2,I}(t)\exp[-L_0 t] \\ &= \cdots \\ L_3(t) &= \cdots \\ &\vdots \end{aligned} \tag{4.62}$$

4. Represent $L(t) \approx L_0 + \sum_i L_i(t)$ in Magnus terms with t_0, t

5. Stroboscopic window T_c and low-frequency cut-off $\omega_0 \ll \omega_{\mathrm{c}}$

$$L_{\mathrm{eff}} = L_0 + \left[\sum_i L_i(t)\right]_{\omega<\omega_{\mathrm{c}},f_0} \tag{4.63}$$

In summary, this approach establishes a scheme to systematically derive an effective time-independent operator L_{eff}, given an undriven system operator L_0 and driven system part in the form of $L_{\mathrm{dr}}(t) = f(t)L_{\mathrm{dr},0}$. This alternative Magnus formalism provides a systematic expansion in the driving amplitude and the inverse driving frequency. The expressions for $L_{\mathrm{eff},1}$-$L_{\mathrm{eff},4}$ have been explicitly computed and compact formulas have been derived. In the next chapter this alternative Magnus expansion shall be applied reference examples like the parametric oscillator to benchmark the method. And finally it will be applied a driven Josephson junction.

Chapter 5

Applications of the alternative Magnus expansion

In this Chapter, the alternative Magnus expansion shall be applied to important problems of driven condensed-matter systems. As a first example, the developed method is applied to the steady state of a classiscal parametric oscillator with and without coupling to a heat bath. Additionally, the isolated quantum parametric oscillator is considered. The obtained results are compared to numerical results and to some standard solutions. The common solution provides a recurrence relation for the characteristic values and coefficients of the Mathieu equation in the form of a continued fraction [118]. In particular the characteristic values can be compared and systematized to the Magnus approach via the Mathieu parameters a, q. The lower-energy effective theory also covers the effect of dynamical stabilization, which occurs in the second order of the Magnus expansion. Beyond this, higher order effects further renormalize the oscillator frequency and additionally create a weakly renormalized temperature [1], when applied to open systems with a thermal environment [16].

Due to the systematic expansion in the inverse driving frequency $1/\omega_{\mathrm{m}}$ and the amplitude A in a combined dimensionless perturbation parameter $(\omega_0/\omega_{\mathrm{m}})^n A^m < 1$, the amplitude A is allowed to become large while the frequency ratio is sufficiently small. Whereas the standard Magnus expansion just relies on the high-frequency regime $\omega_0/\omega_{\mathrm{m}} \ll 1$.

The extra robustness and control of the alternative Magnus expansion is also re-

[1] The thermodynamically considered concept of temperature does not strictly hold for nonequilibrium systems, for an overview and a further discussion on this issue, check Ref.[119] and related references therein, but this is beyond the scope of this thesis. However, in the present case it was observed that after the application of the alternative Magnus approach on a linear master equations, like the Fokker-Planck equation, the temperature dependent diffusion coefficient, e.g. the prefactor of ∂_{pp}, was renormalized.

flected in the frequency renormalization of the parametric oscillator. It is quantitatively accurate even for large $A > 1$ or close to the parametric instability. Around the instability, the separation of time scales between the driving and renormalized eigenfrequency breaks down and the Magnus expansion begins to become inaccurate and invalid, as expected [2].
As a more involved example, the system of a driven Josephson junction coupled to a heat bath is examined. Motivated by recent pump-probe experiments, different driving scenarios can be tested theoretically. By deducing effective descriptions one can investigate which scenario has the most prominent features. The analytical results are also compared to numerical results.

5.1 The classical and quantum parametric oscillator

A system which already exhibits non-trivial features due to presence of the external driving is the classical parametric oscillator. This instructional system allows to estimate certain system parameters within a straightforward Floquet approach. With this reference case, one is able to compare the extensions and deviations to the results of the developed theory and the numerical exact results.

The parametric oscillator is a harmonic oscillator system with a time-dependent frequency $\omega^2(t) = {\omega_0}^2(1 + A\cos\omega_{\mathrm{m}}t)$. Its Hamiltonian has the form

$$H = H_0 + H_{dr} \tag{5.1}$$

$$H_0 = \frac{m{\omega_0}^2}{2}x^2 + \frac{1}{2m}p^2 \tag{5.2}$$

$$H_{dr} = \frac{m{\omega_0}^2}{2}A\cos\left(\omega_{\mathrm{m}}t\right)x^2. \tag{5.3}$$

p and x denote the momentum and the spatial coordinate of the classical oscillator, m the mass and ω_0 the bare oscillator frequency. A is the dimensionless amplitude of the parametric driving term and ω_{m} the driving frequency. In the following sections the system will be solved by different approaches and methods. The results are then compared and classified among each other to make a connection between the standard methods and the Magnus approach.

[2] Irrespective of other conditions, the Magnus expansion is a high-frequency and short-to-intermediate time expansion. However, for strong driving $A > (\omega_{\mathrm{m}}/\omega_0)^{n/m}$ the series becomes inaccurate and the renormalized frequency eventually matches the first parametric resonance, more details follow in Sec. 5.1

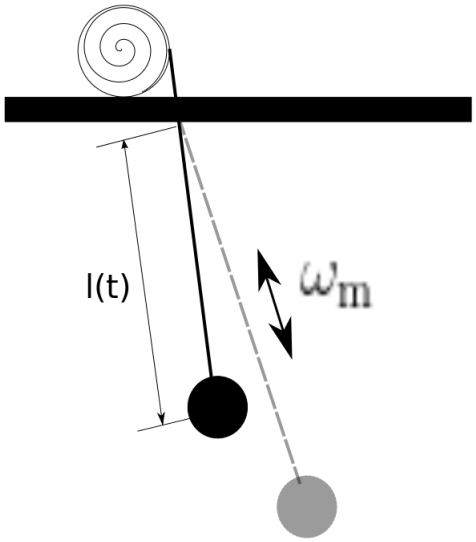

Figure 5.1: This is a scheme of a mechanical realization of the parametric oscillator. The pendulum is suspended to a motor through a hole in the ceiling which varies the length of the pendulum by Δl with frequency ω_m. The undriven eigenfrequency of the pendulum is $\omega_0 = \sqrt{g/l}$. Hence, the square of the driven pendulum frequency can be approximated by $\omega^2(t) \approx {\omega_0}^2(1 + \Delta l(t))$.

5.1.1 Floquet approach

In this section the renormalization of the eigenfrequency due to the presence of the driving is derived within a Floquet approach.
The Hamiltonian equations of motion of the isolated parametric oscillator (5.1) are

$$\dot{x} = \frac{p}{m} \tag{5.4}$$

$$\dot{p} = -m\omega_0^2(1 + A\cos[\omega_m t])x. \tag{5.5}$$

After combining the two first order differential equations and the substitution $\tau = \omega_\mathrm{m} t/2$, one derives the canonical form of the Mathieu equation

$$\frac{\partial^2 x}{\partial \tau^2} + \underbrace{(a - 2q\cos[2\tau])}_{\omega^2(\tau)} x = 0. \tag{5.6}$$

Furthermore, the standard Mathieu equation parameters a and q for the parametric oscillator are $a = 4{\omega_0}^2/{\omega_\mathrm{m}}^2$ and $q = -2{\omega_0}^2 A/{\omega_\mathrm{m}}^2$. By introducing the dimensionless variable τ, the two Mathieu parameter a and q already obtain the structure proportional to $1/\omega_\mathrm{m}$. In particular q is identified as the purturbative expansion parameter.
The Mathieu equation is the special case of the Hill equation comprising only a single harmonic mode. The general Hill equation reads $\ddot{x} + f(\tau)x = 0$ where $f(\tau)$ is a periodic function, which can be rewritten in a Fourier series $f(\tau) = \sum_n a_n \exp[in\tau]$. The coefficient in the second order differential equation (5.6) is periodic in time, so according to the Floquet theorem [120], the two independent solutions are written as

$$x_1(\tau) = e^{i\lambda\tau} z_1(\tau) \tag{5.7}$$

$$x_2(\tau) = e^{-i\lambda\tau} z_2(\tau). \tag{5.8}$$

λ is the unknown and to be determined Floquet exponent, which is conveniently written as $i\lambda$. Hence in a subsequent stability analysis, the unstable regions are identified by the condition $Im[\lambda(a,q)] \neq 0$. $z_{1/2}(\tau)$ are periodic functions matching the period of the coefficient in equation (5.6) with the parity condition $z_2(\tau) =$

$z_1(-\tau)$. After Fourier expanding $z_{1/2}$, the general periodic solution is

$$x(\tau) = A' \sum_{n=-\infty}^{\infty} C_{2n} e^{i(2n+\lambda)\tau} + B' \sum_{n=-\infty}^{\infty} C_{2n} e^{-i(2n+\lambda)\tau} \tag{5.9}$$

$$= A \sum_{n=-\infty}^{\infty} C_{2n} \cos[(2n+\lambda)\tau] + iB \sum_{n=-\infty}^{\infty} C_{2n} \sin[(2n+\lambda)\tau]. \tag{5.10}$$

The index n labels the Floquet bands. $A = (A' + B')/2$ and $B = (A' - B')/2$ are constants, which are set by the initial and the boundary conditions. Further initial conditions and the parity discussions are omitted and after applying (5.10) to (5.6) the resulting coefficient equation for the cosine part of the Mathieu equation is

$$\begin{aligned} &- A \sum_{n=-\infty}^{\infty} (2n+\lambda)^2 C_{2n} \cos[(2n+\lambda)\tau] \\ &+ A \sum_{n=-\infty}^{\infty} a C_{2n} \cos[(2n+\lambda)\tau] \\ &- A \sum_{n=-\infty}^{\infty} 2q C_{2n} \cos[(2n+\lambda)\tau] \cos 2\tau = 0. \end{aligned} \tag{5.11}$$

With the trignometric identity $2\cos\phi\cos\theta = \cos(\phi-\theta) + \cos(\phi+\theta)$, Eq. (5.11) can be compactly written as

$$A \sum_{n=-\infty}^{\infty} \left\{ \left[a - (2n+\lambda)^2\right] C_{2n} - qC_{2n-2} - qC_{2n+2} \right\} \cos[(2n+\lambda)\tau] = 0. \tag{5.12}$$

The sum in the inner bracket of Eq. (5.12) can be understood as a recursion relation for the coefficient C_{2n}

$$qC_{2n} = a - (2n+\lambda)^2 \left(C_{2n-2} + C_{2n+2}\right). \tag{5.13}$$

Recursively substituting the coefficients $C_{2n\pm2}$, the recursion may be solved with respect to the Floquet exponent $\lambda(a,q)$. The continued fraction method (CFM) is also equivalent to the recursive substitution of the C_{2n-x} in Eq. (5.13).
After a projection onto the $\cos[(2n+\lambda)\tau]$ basis, the sum connecting the precedent and the subsequent coefficients Eq.(5.12) can be mapped onto an infinite matrix for

the coefficients C_{2n} as

$$R - a\mathrm{I} = \begin{pmatrix} \ddots & & & & & & \\ & q & (2n-2+\lambda)^2 - a & q & & & \\ & & q & (2n+\lambda)^2 - a & q & & \\ & & & q & (2n+2+\lambda)^2 - a & q & \\ & & & & & & \ddots \end{pmatrix}. \tag{5.14}$$

The R matrix is the remainder after separation of the diagonal element $-aC_{2n}$. This linear system of equations has non-trivial solutions if $\det(\mathrm{R} - \mathrm{aI}) = 0$. This formally looks like an eigenvalue problem for the Mathieu parameter a. Since a is given, the characteristic polynomial of (5.14) can be solved for the unknown Floquet exponent $\lambda(a, q)$. For non-linear oscillators like the Duffing oscillator with its x^3 potential this kind of solution does not work, because the coefficient equations for the C_n also become non-linear.

The more Floquet bands or coefficients C_n one takes into account, the higher the order in the driving parameter q becomes. For $n = 0$ and neglecting the coefficients C_{-4} and C_4, the characteristic polynomial for the remaining 3×3 matrix of (5.14) is

$$-\lambda^6 + (8 + 3a)\lambda^4 - (16 + 3a^2 - 2q^2)\lambda^2 - (a - 4)(2q^2 - a^2 + 4a) = 0. \tag{5.15}$$

In order to get an overview on the result for λ, one switches back from the Mathieu parameters a, q to the former parameters $\omega_0, \omega_\mathrm{m}, A$. Already by substituting to $\tau = 2\omega_\mathrm{m} t$ one obtained the natural $1/\omega_\mathrm{m}$ structure, which fits into the perturbative picture for the low-energy effective theory for $\omega_\mathrm{m} \gg \omega_0$.

The solution for the Floquet exponent λ in Eq. (5.15) is plotted in terms of A and $\omega_0/\omega_\mathrm{m}$ in Fig. 5.2. In the high-frequency limit $\omega_\mathrm{m} \gg \omega_0$ the effective eigenfrequency reads

$$\omega_\mathrm{eff}{}^2 = \left(\frac{\omega_\mathrm{m}}{2}\right)^2 \lambda^2 = \omega_0{}^2 \left(1 + \frac{A^2 \omega_0{}^2}{2\omega_\mathrm{m}{}^2} + \frac{2A^2 \omega_0{}^4}{\omega_\mathrm{m}{}^4} + \frac{8A^2 \omega_0{}^6}{\omega_\mathrm{m}{}^6} + \frac{3A^4 \omega_0{}^6}{4\omega_\mathrm{m}{}^6}\right). \tag{5.16}$$

Clearly, ω_eff is the effective renormalized eigenfrequency, which is stiffened by the presence of the driving as compared the bare frequency ω_0. The renormalization is given in polynomials of $(\omega_0/\omega_\mathrm{m})^l A^n$. An analogue structure will be obtained by the low-energy effective theory via the alternative Magnus expansion in the next section without any Fourier base ansatz and without any recursive formula.

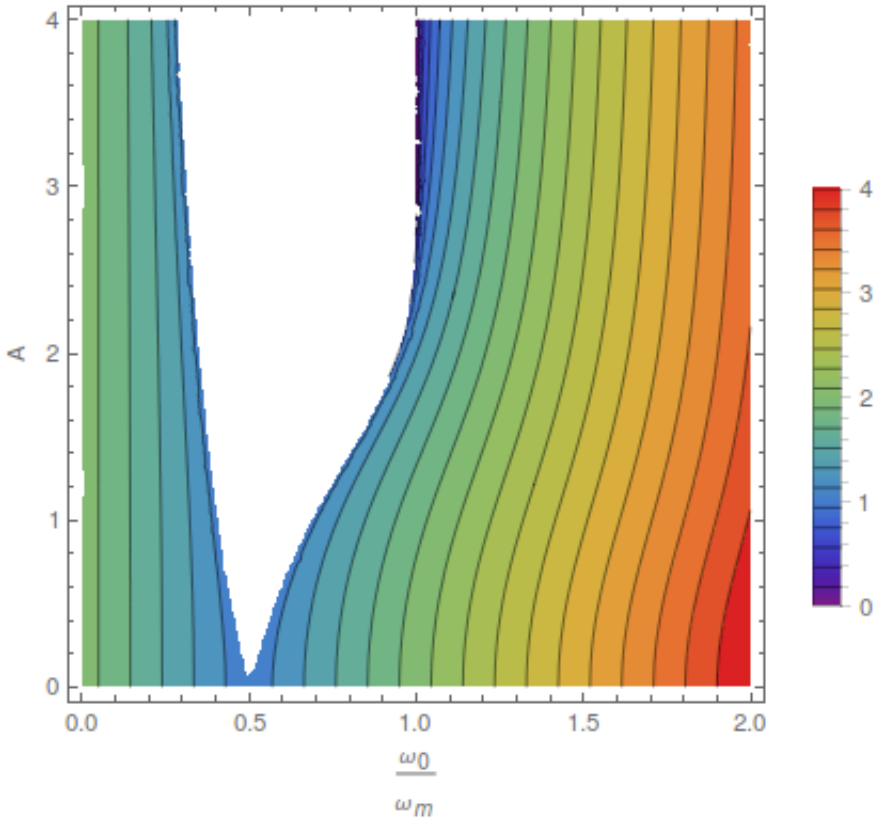

Figure 5.2: Stability map for the Floquet exponent λ, plotted as a function of the driving amplitude A and the dimensionless oscillator parameter $\omega_0/\omega_\mathrm{m}$. The resonance at $\omega_0/\omega_\mathrm{m} = 0.5$ is the standard parametric resonance for $\omega_\mathrm{m} = 2\omega_0$. The unstable region with $Im[\lambda] \neq 0$ is marked white. The instability region grows with driving amplitude, also known as power broadening. The low-energy effective theory works away from the resonances in the regime of $\omega_0/\omega_\mathrm{m} \ll 1$. For large amplitudes $A_\mathrm{crit} \gg 1$, the power broadened resonance also affects the high-frequency regime $\omega_0/\omega_\mathrm{m} \ll 1$, which is usually away from any resonances. The observation that the effective eigenfrequency becomes resonant with the driving will be further discussed at the end of this section.

5.1.2 Alternative Magnus approach to the isolated quantum parametric oscillator

Next, the parametric oscillator is treated quantum mechanically within the alternative Magnus expansion. The system setup is given by the Hamiltonian

$$H = H_0 + H_d \tag{5.17}$$

$$H_0 = \frac{m\omega_0^2}{2}x^2 + \frac{1}{2m}p^2 = \hbar\omega_0 a^\dagger a \tag{5.18}$$

$$H_d = \frac{m\omega_0^2}{2}A\cos(\omega_m t)\,x^2 = \frac{\hbar\omega_0}{4}A\cos(\omega_m t)\,(aa + a^\dagger a^\dagger + 2a^\dagger a + 1), \tag{5.19}$$

where ω_0 is the bare frequency of the undriven oscilllator, ω_m the driving frequency, A the driving amplitude and m the respective mass of the oscillator. The conjugate variables are represented in terms of the creation and annihilation operator

$$x = \sqrt{\frac{\hbar}{2\omega_0 m}}\left(a + a^\dagger\right) \tag{5.20}$$

$$p = -i\sqrt{\frac{\hbar\omega_0 m}{2}}\left(a - a^\dagger\right) \tag{5.21}$$

obeying the commutation relation $[x, p] = i\hbar$ or respectively $[a, a^\dagger] = 1$. To apply the formulas of the effective Magnus corrections, one identifies

$$H_0 = \hbar\omega_0 a^\dagger a \tag{5.22}$$

$$H_{dr} = \frac{\hbar\omega_0}{4}(aa + a^\dagger a^\dagger + 2a^\dagger a + 1) \tag{5.23}$$

$$f(t) = A\cos(\omega_m t)\,. \tag{5.24}$$

The first order Magnus term (4.34) of H_eff is

$$H_1 = \frac{1}{i\hbar}A\cos(\omega_\mathrm{m} t)H_{dr}. \tag{5.25}$$

The first low-frequency Magnus correction to the unperturbed Hamiltonian H_0 is the projection onto the low-frequency sector

$$H_{\mathrm{eff},1} = i\hbar\left[H_1\right]_{\omega<\omega_\mathrm{c},f_0} = 0. \tag{5.26}$$

The Magnus series is a formal solution for the exponential of the Schrödinger equation $i\hbar\dot{U} = H(t)U$ which means $U = \exp[\Omega] \approx \exp[H_\mathrm{eff}t/(i\hbar)]$. There is no low-frequency contribution in first order of the Magnus expansion for the standard driving protocol of the parametric oscillator (5.24).

The second order correction given in Eq. (4.43) is in this case given by

$$H_2 = C_{10}(t)[H^1_{dr}, H_{dr}] + C_{20}(t)[H^2_{dr}, H_{dr}] + \cdots . \tag{5.27}$$

With the useful relations $[a^\dagger a, aa] = -2aa$, $[a^\dagger a, a^\dagger a^\dagger] = 2a^\dagger a^\dagger$, $[aa, a^\dagger a^\dagger] = 4a^\dagger a + 2$, one determines the adjoint actions of H_0 on H_{dr} as

$$H^1_{dr} = [H_0, H_{dr}] = \frac{\hbar^2\omega_0^2}{4}(2a^\dagger a^\dagger - 2aa) \tag{5.28}$$

$$H^2_{dr} = [H_0, [H_0, H_{dr}]] = \frac{\hbar^3\omega_0^3}{4}(4a^\dagger a^\dagger + 4aa) \tag{5.29}$$

$$H^3_{dr} = [H_0, [H_0, [H_0, H_{dr}]]] = \frac{\hbar^4\omega_0^4}{4}(8a^\dagger a^\dagger - 8aa). \tag{5.30}$$

The evaluation of the nested commutators yields then

$$[H^1_{dr}, H_{dr}] = -\frac{\hbar^3\omega_0^3}{2}(a^\dagger a^\dagger + aa + 2a^\dagger a + 1) \tag{5.31}$$

$$[H^2_{dr}, H_{dr}] = -\hbar^4\omega_0^4(a^\dagger a^\dagger - aa) \tag{5.32}$$

$$[H^3_{dr}, H_{dr}] = -\hbar^5\omega_0^5 2(a^\dagger a^\dagger + aa + 2a^\dagger a + 1). \tag{5.33}$$

$$\tag{5.34}$$

The low frequency components of the coefficients (4.29)-(4.31) with $f(t) = A\cos\omega_{\mathrm{m}}t$ are

$$[C_{10}(t)]_{\omega<\omega_{\mathrm{c}},\not\omega_0} = -\frac{1}{i\hbar}\frac{A^2}{4\hbar^2{\omega_{\mathrm{m}}}^2} \tag{5.35}$$

$$[C_{20}(t)]_{\omega<\omega_{\mathrm{c}},\not\omega_0} = 0 \tag{5.36}$$

$$[C_{30}(t)]_{\omega<\omega_{\mathrm{c}},\not\omega_0} = -\frac{1}{i\hbar}\frac{A^2}{4\hbar^2{\omega_{\mathrm{m}}}^2}. \tag{5.37}$$

Therefore, the effective second-order Magnus term of equation (5.27) for the parametric oscillator is

$$H_{\mathrm{eff},2} = i\hbar\,[H_2]_{\omega<\omega_{\mathrm{c}},\not\omega_0} = \frac{\hbar\omega_0}{4}(a^\dagger a^\dagger + aa + 2a^\dagger a + 1)\left(\frac{A^2{\omega_0}^2}{2{\omega_{\mathrm{m}}}^2} + \frac{2A^2{\omega_0}^4}{{\omega_{\mathrm{m}}}^4}\right). \tag{5.38}$$

The third-order Magnus term has the shape

$$\begin{aligned} H_3 = {} & C_{010}(t)[H_{dr}, [H^1_{dr}, H_{dr}]] + C_{110}(t)[H^1_{dr}, [H^1_{dr}, H_{dr}]] \\ & + C_{020}(t)[H_{dr}, [H^2_{dr}, H_{dr}]]. \end{aligned} \tag{5.39}$$

Due to the symmetry of the nested integrals in the coefficients C_{ijk} (4.49) and $f(t) = A\cos\omega_{\mathrm{m}}t$, the low-frequency projection immediately yields

$$[C_{010}(t)]_{\omega<\omega_{\mathrm{c}},\not{f}_0} = 0 \tag{5.40}$$
$$[C_{110}(t)]_{\omega<\omega_{\mathrm{c}},\not{f}_0} = 0 \tag{5.41}$$
$$[C_{020}(t)]_{\omega<\omega_{\mathrm{c}},\not{f}_0} = 0. \tag{5.42}$$

Hence, there is no third-order contribution to the effective low-frequency Hamiltonian H_{eff}. Straightforward to the fourth-order Magnus term, one finds

$$H_4 = C_{0010}(t)[H_{dr},[H_{dr},[H^1_{dr},H_{dr}]]] + C_{0110}(t)[H_{dr},[H^1_{dr},[H^1_{dr},H_{dr}]]] \tag{5.43}$$
$$+ C_{1010}(t)[H^1_{dr},[H_{dr},[H^1_{dr},H_{dr}]]] + C_{0020}(t)[H_{dr},[H_{dr},[H^2_{dr},H_{dr}]]] \tag{5.44}$$
$$+ C_{0021}(t)[H_{dr},[H_{dr},[H^2_{dr},H^1_{dr}]]] + C_{0120}(t)[H_{dr},[H^1_{dr},[H^2_{dr},H_{dr}]]] \tag{5.45}$$
$$+ C_{1020}(t)[H^1_{dr},[H_{dr},[H^2_{dr},H_{dr}]]] + C_{0210}(t)[H_{dr},[H^2_{dr},[H^1_{dr},H_{dr}]]] \tag{5.46}$$
$$+ C_{2010}(t)[H^2_{dr},[H_{dr},[H^1_{dr},H_{dr}]]] + C_{0030}(t)[H_{dr},[H_{dr},[H^3_{dr},H_{dr}]]]. \tag{5.47}$$

The projection of the coefficients C_{ijkl} (E.19)-(E.28) with $f(t) = A\cos\omega_{\mathrm{m}}t$ results in

$$[C_{0010}(t)]_{\omega<\omega_{\mathrm{c}},\not{f}_0} = \frac{1}{i\hbar}\frac{A^4}{12(i\hbar)^4}\frac{9}{16{\omega_{\mathrm{m}}}^4} \tag{5.48}$$
$$[C_{0110}(t)]_{\omega<\omega_{\mathrm{c}},\not{f}_0} = 0 \tag{5.49}$$
$$[C_{1010}(t)]_{\omega<\omega_{\mathrm{c}},\not{f}_0} = 0 \tag{5.50}$$
$$[C_{0020}(t)]_{\omega<\omega_{\mathrm{c}},\not{f}_0} = 0 \tag{5.51}$$
$$[C_{0021}(t)]_{\omega<\omega_{\mathrm{c}},\not{f}_0} = \frac{1}{i\hbar}\frac{A^4}{12(i\hbar)^6}\frac{5}{32{\omega_{\mathrm{m}}}^6} \tag{5.52}$$
$$[C_{0120}(t)]_{\omega<\omega_{\mathrm{c}},\not{f}_0} = -\frac{1}{i\hbar}\frac{A^4}{12(i\hbar)^6}\frac{37}{32{\omega_{\mathrm{m}}}^6} \tag{5.53}$$
$$[C_{1020}(t)]_{\omega<\omega_{\mathrm{c}},\not{f}_0} = \frac{1}{i\hbar}\frac{A^4}{12(i\hbar)^6}\frac{1}{32{\omega_{\mathrm{m}}}^6} \tag{5.54}$$
$$[C_{0210}(t)]_{\omega<\omega_{\mathrm{c}},\not{f}_0} = -\frac{1}{i\hbar}\frac{A^4}{12(i\hbar)^6}\frac{25}{16{\omega_{\mathrm{m}}}^6} \tag{5.55}$$
$$[C_{2010}(t)]_{\omega<\omega_{\mathrm{c}},\not{f}_0} = -\frac{1}{i\hbar}\frac{A^4}{12(i\hbar)^6}\frac{1}{32{\omega_{\mathrm{m}}}^6} \tag{5.56}$$
$$[C_{0030}(t)]_{\omega<\omega_{\mathrm{c}},\not{f}_0} = -\frac{1}{i\hbar}\frac{A^4}{12(i\hbar)^6}\frac{39}{64{\omega_{\mathrm{m}}}^6}. \tag{5.57}$$

The needed nested commutators are

$$[H_{dr},[H_{dr},[H^1_{dr},H_{dr}]]] = 0 \tag{5.58}$$
$$[H_{dr},[H_{dr},[H^2_{dr},H^1_{dr}]]] = -2(\hbar\omega_0)^7(a^\dagger a^\dagger + aa + 2a^\dagger a + 1) \tag{5.59}$$
$$[H_{dr},[H^1_{dr},[H^2_{dr},H_{dr}]]] = 0 \tag{5.60}$$
$$[H^1_{dr},[H_{dr},[H^2_{dr},H_{dr}]]] = 2(\hbar\omega_0)^7(a^\dagger a^\dagger + aa + 2a^\dagger a + 1) \tag{5.61}$$
$$[H_{dr},[H^2_{dr},[H^1_{dr},H_{dr}]]] = 2(\hbar\omega_0)^7(a^\dagger a^\dagger + aa + 2a^\dagger a + 1) \tag{5.62}$$
$$[H^2_{dr},[H_{dr},[H^1_{dr},H_{dr}]]] = 0 \tag{5.63}$$
$$[H_{dr},[H_{dr},[H^3_{dr},H_{dr}]]] = 0. \tag{5.64}$$

Hence the fourth-order Magnus term for the parametric oscillator is

$$H_{\mathrm{eff},4} = i\hbar[H_4]_{\omega<\omega_c,f_0} = \frac{\hbar\omega_0}{4}(a^\dagger a^\dagger + aa + 2a^\dagger a + 1)\frac{9A^4{\omega_0}^6}{8{\omega_\mathrm{m}}^6}. \tag{5.65}$$

Rearranging all of the Magnus contributions finally yields

$$H_\mathrm{eff} = H_0 + H_{\mathrm{eff},2} + H_{\mathrm{eff},4} \tag{5.66}$$
$$= \hbar\omega_0 a^\dagger a + \frac{\hbar\omega_0}{4}(a^\dagger a^\dagger + aa + 2a^\dagger a + 1)\left(\frac{A^2{\omega_0}^2}{2{\omega_\mathrm{m}}^2} + \frac{2A^2{\omega_0}^4}{{\omega_\mathrm{m}}^4} + \frac{9A^4{\omega_0}^6}{8{\omega_\mathrm{m}}^6}\right) \tag{5.67}$$
$$= \frac{p^2}{2m} + \frac{m{\omega_0}^2x^2}{2}\left(1 + \frac{A^2{\omega_0}^2}{2{\omega_\mathrm{m}}^2} + \frac{2A^2{\omega_0}^4}{{\omega_\mathrm{m}}^4} + \frac{9A^4{\omega_0}^6}{8{\omega_\mathrm{m}}^6}\right). \tag{5.68}$$

The effective constructed Hamiltonian resembles a renormalized harmonic oscillator system with the renormalized frequency

$${\omega_\mathrm{eff}}^2 = {\omega_0}^2\left\{1 + \frac{A^2{\omega_0}^2}{2{\omega_\mathrm{m}}^2} + \frac{2A^2{\omega_0}^4}{{\omega_\mathrm{m}}^4} + \frac{9A^4{\omega_0}^6}{8{\omega_\mathrm{m}}^6}\right\}. \tag{5.69}$$

The result indicates an enhancement of the effective eigenfrequency as compared to the undriven case. This is in agreement with the effective frequency extracted from the Floquet exponent given in Eq. (5.16) up to the order $(\omega_0/\omega_\mathrm{m})^4A^4$. However, there is a deviation in the order $(\omega_0/\omega_\mathrm{m})^4A^6$. The alternative Magnus expansion yields $C_{46,mag} = 9/8$, while the determinant method predicts $C_{46,det} = 3/4$, see Eq. (5.16).

This sixth order coefficient from the determinant method was derived via a truncation down to a 3×3 matrix. It is possible that for higher orders one needs to extend the matrix and then solve the characteristic polynomial for the effective eigenfrequency. Table 5.1 shows the solutions of the characteristic polynomials in

	$altMag$	2×2	3×3	5×5	7×7	9×9
C_{22}	1/2	1/4	1/2	1/2	1/2	1/2
C_{24}	2	0	2	2	2	2
C_{26}	8	0	8	8	8	8
C_{42}	0	0	0	0	0	0
C_{44}	0	0	0	0	0	0
C_{46}	9/8	−1/16	3/4	25/32	25/32	25/32

Table 5.1: Dependence of coefficients C_{lm} on the matrix size for the determinant method. For matrices smaller than 5×5 the sixth-order coefficients differ. Solving the characteristic polynomial, one expands for $\omega_0/\omega_\mathrm{m} \ll 1$ and $A \ll 1$, it is likely that via some combinations lower-order terms contribute to higher-order terms or one has to consider an infinite matrix to obtain an exact result. The coefficient C_{46} stabilizes for larger matrices$> 5\times 5$, at that point it is hard to conclude whether the result is converged to a stable value or the computation of the Magnus term was incorrect. Up to the fourth order in $(\omega_0/\omega_\mathrm{m})^4 A^4$ the results coincide.

the form

$$\omega_\mathrm{eff}{}^2 = \omega_0{}^2 \left\{ 1 + C_{22}\frac{A^2\omega_0{}^2}{\omega_\mathrm{m}{}^2} + C_{24}\frac{A^2\omega_0{}^4}{\omega_\mathrm{m}{}^4} + C_{26}\frac{A^2\omega_0{}^6}{\omega_\mathrm{m}{}^6} \right. \tag{5.70}$$

$$\left. + C_{42}\frac{A^4\omega_0{}^2}{\omega_\mathrm{m}{}^2} + C_{44}\frac{A^4\omega_0{}^4}{\omega_\mathrm{m}{}^4} + C_{46}\frac{A^4\omega_0{}^6}{\omega_\mathrm{m}{}^6} \right\} \tag{5.71}$$

for different matrix sizes.

The low-energy effective theory via the Magnus expansion is consistent with the standard Floquet solution up to the order$(\omega_0/\omega_\mathrm{m})^4 A^4$. Furthermore, the Magnus approach can be extended to more complicated potentials and driving protocols without the need of an elaborated ansatz. In the subsequent section, a heat bath will be coupled to the parametric oscillator system, which can still be treated within the alternative Magnus expansion.

5.1.3 Alternative Magnus expansion for the classical parametric oscillator with heat beath

The classical parametric oscillator is extended by a heat bath and treated in terms of the Kramers-Equation (KE). The KE is a bivariate master equation which takes into account the dynamics of the two conjugate variables x, p. Hence, the full dynamics of the system is describable and the parameters are not restricted to the overdamped

limit, like in the Smoluchowski equation case [3].
This equation assumes the form of a linear master equation

$$\partial_t P(x,p,t) = L_K P(x,p,t) \tag{5.72}$$

for the probability density distribution $P(x,p,t)$ and the alternative Magnus expansion can be applied. The Kramers operator L_K is defined as

$$L_K = L_{\text{rev}} + L_{\text{ir}} + L_{\text{dr}}(t). \tag{5.73}$$

The reversible part of the dynamics is described by

$$L_{\text{rev}} = -\partial_x \left[(\partial_p H_0) \cdot \right] + \partial_p \left[(\partial_x H_0) \cdot \right] \tag{5.74}$$

$$= -\frac{p}{m}\partial_x + m{\omega_0}^2 x \partial_p, \tag{5.75}$$

which incorporates essentially the classical equations of motion from the Hamilton formalism. The inner brackets () in (5.74) represent $\dot{x} = \partial_p H_0$ and $\dot{p} = -\partial_x H_0$. L_{rev} describes the flow of an incompressible or conserved probability distribution in the phase space of x and p.
The irreversible contribution to the master equation is

$$L_{\text{ir}} = \gamma \partial_p \left(p \ \cdot \ + mT\partial_p \cdot \right), \tag{5.76}$$

where γ is the friction or damping coefficient, which describes the coupling to the bath. Assuming a Gaussian white noise, the bath correlations lead to the diffusion coefficient $m\gamma T$. The parametric driving is

$$L_{\text{dr}}(t) = f(t) \underbrace{m{\omega_0}^2 x \partial_p}_{L_{\text{dr},0}} \tag{5.77}$$

$$= f(t) L_{\text{dr},0}. \tag{5.78}$$

As usual, $f(t)$ is the driving protocol. Therefore, the Kramers equation for the driven parametric oscillator is

$$\dot{\rho} = L_K \rho \tag{5.79}$$

$$L_K = \underbrace{-\frac{p}{m}\partial_x + m{\omega_0}^2 x \partial_p}_{L_{\text{rev}}} + \underbrace{\gamma \partial_p \left(p \ \cdot \ + mT\partial_p \cdot \right)}_{L_{\text{ir}}} + \underbrace{f(t) m{\omega_0}^2 x \partial_p}_{L_{\text{dr}}(t)}. \tag{5.80}$$

[3] In the Hamiltonian language, the equations of motion are two first-order differential equations for q and p, or, combined, one second-order equation. Hence, setting the conjugate variable constant or neglecting it, is related to the omission of the second-order derivative.

By defining the unperturbed part

$$L_0 = L_{\mathrm{rev}} + L_{\mathrm{ir}} \tag{5.81}$$

and the driving part

$$L_{\mathrm{dr}}(t) = f(t) L_{\mathrm{dr},0}, \tag{5.82}$$

the given formulas are applied order by order to the Magnus expansion. The commutators are now interpreted as the Poisson brackets $[A, B] \equiv \partial_x A \partial_p B - \partial_p A \partial_x B$. The effective first-order terms is

$$L_{\mathrm{eff},1} = 0. \tag{5.83}$$

The low-frequency component of the second-order terms yields

$$L^{2,2}_{\mathrm{eff},2} = m{\omega_0}^2 x \frac{A^2 {\omega_0}^2}{2{\omega_{\mathrm{m}}}^2} \partial_p \tag{5.84}$$

$$L^{2,4}_{\mathrm{eff},2} = m{\omega_0}^2 x \frac{A^2 {\omega_0}^2 (4{\omega_0}^2 - \gamma^2)}{2{\omega_{\mathrm{m}}}^4} \partial_p + m\gamma T \frac{2A^2 {\omega_0}^4}{{\omega_{\mathrm{m}}}^4} \partial_{pp}. \tag{5.85}$$

The fourth-order correction is derived via the formula (4.54) with the coefficients (E.19)-(E.28) given in the Appendix. After projection onto the low-frequency part, the effective contribution is

$$L^{4,6}_{\mathrm{eff},4} = m{\omega_0}^2 x \frac{9A^4 {\omega_0}^6}{8{\omega_{\mathrm{m}}}^6} \partial_p. \tag{5.86}$$

The effective time-independent operator to $L_K(t)$ is therefore

$$L_{\mathrm{eff}} = L_0 + L^{2,2}_{\mathrm{eff},2} + L^{2,4}_{\mathrm{eff},2} + L^{4,6}_{\mathrm{eff},4}. \tag{5.87}$$

By comparing the prefactor ∂_p in L_{rev}, one finds again a renormalization of the eigenfrequency ω_0 in the presence of the driving. Due to the expansion of the master equation for an open system, one additionally obtains contributions which depend on γ. Rewriting the effective eigenfrequency for L_{eff} yields

$$\frac{{\omega_{\mathrm{eff}}}^2}{{\omega_0}^2} = 1 + \frac{A^2 {\omega_0}^2}{2{\omega_{\mathrm{m}}}^2} + \frac{2A^2 {\omega_0}^2}{{\omega_{\mathrm{m}}}^4} \underbrace{\left({\omega_0}^2 - \frac{\gamma^2}{4} \right)}_{:=\omega^2_{\mathrm{open}}} + \frac{9A^4 {\omega_0}^6}{8{\omega_{\mathrm{m}}}^6}. \tag{5.88}$$

The first effect is the strengthening of the oscillator frequency, which means that by increasing the driving amplitude, the effective frequency is also increased. For

$\gamma = 0$ the second order Magnus contributions from the isolated quantum system and the classical system coincide (5.71). In the case $\gamma \neq 0$, there is an additional term proportional to the renormalized frequency of a damped harmonic oscillator $\omega_{\text{open}} = \sqrt{{\omega_0}^2 - \gamma^2/4}$.
The temperature in the system is initially set by the Gaussian white noise correlation, which enters via the diffusion coefficient into the Fokker-Planck equation. This diffusion coefficient is also renormalized as compared the original undriven system, the prefactor of ∂_{pp} in Eq. (5.85) is namely

$$\frac{T_{\text{eff}}}{T} = 1 + \frac{2A^2{\omega_0}^4}{{\omega_{\text{m}}}^4}. \tag{5.89}$$

To illustrate the consequences of these two renormalizations, the fluctuations in the variables x and p are studied. The thermodynamic observables are computed analytically via the definition given in Eq. (5.94) and the definition of the variance in Eq. (5.95). This requires the construction of the effective underlying probability density distribution $P(x, p, t)$. In the thermal equilibrium case, the distribution is known to be

$$\rho_{\text{th}}(x, p) = \frac{\exp[-\beta H_0(x, p)]}{Z}, \tag{5.90}$$

with $\beta = 1/(k_{\text{B}}T)$. Z is the canonical partition function

$$Z = \int_{-\infty}^{\infty}\int_{-\infty}^{\infty} \exp[-\beta H_0(x, p)]dxdp, \tag{5.91}$$

which just normalizes the probability distribution.
Employing the renormalizations from Eqs. (5.88), (5.89), one sets up an effective Hamiltonian and assumes a putative low-energy effective steady state of the system with

$$H_{\text{eff}} = \frac{m\omega_{\text{eff}}^2}{2}x^2 + \frac{1}{2m}p^2. \tag{5.92}$$

Compared to the thermal equilibrium distribution, one also takes into account the renormalized temperature. Hence the effective distribution for the driven state is

$$\rho_{\text{eff}}(x, p) = \frac{\exp\left[-\beta_{\text{eff}} H_{\text{eff}}(x, p)\right]}{Z_{\text{eff}}}, \tag{5.93}$$

explicitly using the renormalized quantity $\beta_{\text{eff}} = 1/(k_{\text{B}}T_{\text{eff}})$. The terms in the partition function are also renormalized accordingly.
For illustration, the probability density distribution $\rho_{\text{eff}}(x, p, t)$ with p being inte-

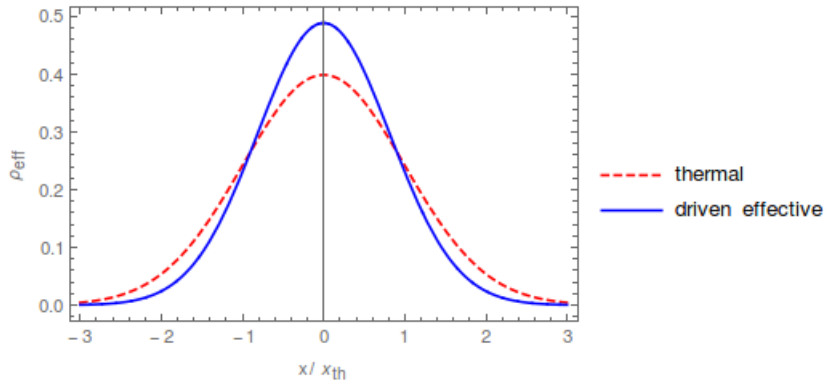

Figure 5.3: The effective steady state probability density distribution ρ_{eff} integrated over p (blue) compared to the thermal equilibrium one ρ_{th} (red dashed). The distribution is clearly narrowed in driven case (blue line). The FWHM is reduced, because the strengthened oscillator frequency (5.88) overcomes the effectively enhanced temperature (5.89).

grated out is shown and compared to the thermal equilibrium distribution ρ_{th}, see Fig.5.3. Furthermore, the difference between $\rho_{\text{eff}}(x,p,t) - \rho_{\text{eff}}$ with x being integrated out is shown in Fig.5.4. Due to the presence of the parametric driving, the densities are redistributed. The momentum distribution is slighly broadened and the spatial distrubtion is narrowed due to the stiffened oscillator frequency (5.88). The analytical results of the redistributed probability density for the parametric oscillator is further confirmed by numerical results presented in Ref. [16].

5.1.4 Variances and comparison to numerics

Based on the constructed effective distribution ρ_{eff}, the variances can also be computed analytically and compared to the numerical results. The expectation value for the observable O is defined as

$$\langle O \rangle_{\text{any}} = \int_{-\infty}^{\infty} \int_{-\infty}^{\infty} O(x,p) \rho_{\text{any}}(x,p,t) dx dp, \tag{5.94}$$

where the sub index any indicates the underlying probability distribution. The definition of the variance is

$$Var(O) = \langle O^2 \rangle - \langle O \rangle^2. \tag{5.95}$$

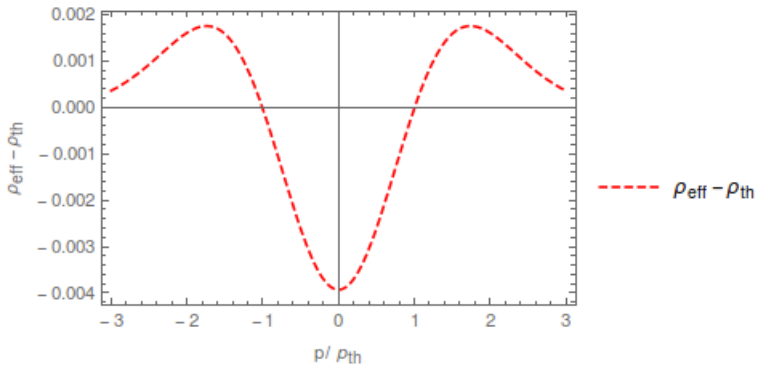

Figure 5.4: Difference between the effective steady state probability density distribution ρ_{eff} for integrated x and the thermal equilibrium one ρ_{th} (red dashed). The driven effective distribution is broadened compared to the thermal one due to the renormalized effective higher temperature(5.89). Hence it is flattened out in the center region and enhanced in the outer regions.

It is a measure of fluctuations around the mean value. The thermal variances for the undriven system are respectively

$$Var_{\text{th}}(x) = \frac{k_{\text{B}}T}{m{\omega_0}^2} \tag{5.96}$$

$$Var_{\text{th}}(p) = k_{\text{B}}Tm, \tag{5.97}$$

where $\langle x\rangle_{\text{th}} = \langle p\rangle_{\text{th}} = 0$. The expectation values

$$x_T = \sqrt{\frac{k_{\text{B}}T}{m{\omega_0}^2}}, \tag{5.98}$$

$$p_T = \sqrt{k_{\text{B}}Tm}, \tag{5.99}$$

can be used to rescale x and p. With this choice, many quantities appear without the temperature or just with a remaining renormalization and it also provides an appropriate energy scale for the system. The rescaling is not suitable for open quantum mechanical oscillators since there is an additonal regime where quantum fluctuations dominate $k_{\text{B}}T \ll \hbar\omega_0$. However, here the focus is on the thermal regime $k_{\text{B}}T \sim \hbar\omega_0$.

The effective steady state variance is

$$
\begin{aligned}
Var_{\text{eff}}(x) &= \langle x^2 \rangle_{\text{eff}} - \langle x \rangle_{\text{eff}}^2 && (5.100)\\
&= \frac{k_{\text{B}} T_{\text{eff}}}{m \omega_{\text{eff}}^2} && (5.101)\\
&= \frac{k_{\text{B}} T \left(1 + \frac{2A^2 {\omega_0}^4}{{\omega_{\text{m}}}^4}\right)}{m {\omega_0}^2 \left(1 + \frac{A^2 {\omega_0}^2}{2{\omega_{\text{m}}}^2} + \frac{2A^2 {\omega_0}^2}{{\omega_{\text{m}}}^4}\left({\omega_0}^2 - \frac{\gamma^2}{4}\right) + \frac{9A^4 {\omega_0}^6}{8{\omega_{\text{m}}}^6}\right)} && (5.102)\\
&\approx \frac{k_{\text{B}} T}{m {\omega_0}^2}\left(1 - \frac{A^2 {\omega_0}^2}{2{\omega_{\text{m}}}^2} + \frac{2A^2 {\omega_0}^2 \gamma^2}{4{\omega_{\text{m}}}^4} - \frac{9A^4 {\omega_0}^6}{8{\omega_{\text{m}}}^6}\right) && (5.103)\\
Var_{\text{eff}}(p) &= k_{\text{B}} T_{\text{eff}} m && (5.104)\\
&= k_{\text{B}} T m \left(1 + \frac{2A^2 {\omega_0}^4}{{\omega_{\text{m}}}^4}\right). && (5.105)
\end{aligned}
$$

In Eq. (5.103) a $1/\omega_{\text{m}}$ expansion was used, assuming $\gamma, \omega_0 \ll \omega_{\text{m}}$. The fluctuations in the momentum variable p are enhanced and the fluctuations in spatial variable x are reduced as compared to the undriven thermal equilibrium values.

5.1.4.1 Low-frequency part of the variance

Before one compares the analytical and numerical results for the variances of the parametric oscillator system, the projection onto the low-frequency or constant part is considered. For this purpose, one computes the variances by integration over the frequency in the power spectral density (PSD). In this way, one achieves a frequency controlled access to the variance, which allows to filter up to a certain cut-off frequency ω_{c} [4].

Often it is not possible or very hard to obtain an explicit analytical expression for the PSD of the nonequilibrium system. By definition, the PSD is defined as the Fourier transform (FT) of the auto-correlation function in time of, for example, the position variable $x(t)$. This requires knowledge of the solution $x(t)$ of the equations of motion of the explicitly time-dependent Hamiltonian $H(t)$. To reduce the complexity of this task one works with the effective time-independent Hamiltonian derived from the Magnus expansion. With the simplified dynamics for $x(t)$, the PSD might be easier to compute. However, it lacks information in the high-frequency regime $\omega \gg \omega_{\text{c}}$. The effective model for the parametric oscillator is a renormalized harmonic oscillator with the frequency $\omega_0 \to \omega_{\text{eff}}$ (5.88) and the renormalized temperature $T \to T_{\text{eff}}$ (5.89). The computation of the power specral density for a harmonic oscillator is a

[4] A comparison between the variance from the full spectral range of the PSD to one with the cut-off can exhibit large deviations for driven systems, see also Fig. 5.8. Furthermore the derived analytic expressions are only valid in the low-frequency regime $\omega_0 < \omega_{\text{c}} < \omega_{\text{m}}$.

straightforward task.
Starting from a Langevin equation for the harmonic oscillator with random noise ξ and noise correlation $\langle \xi(t)\xi(t')\rangle = 2\gamma m T \delta(t-t')$,

$$\ddot{x} + {\omega_0}^2 x + \gamma \dot{x} = \xi, \tag{5.106}$$

the solution is formally written as

$$x(t) = \int_0^t e^{\frac{\gamma}{2}(s-t)} \frac{\sin[\Omega(t-s)]}{m\Omega} \xi(s) ds, \tag{5.107}$$

see Appendix A. The open system eigenfrequency is $\Omega = \sqrt{{\omega_0}^2 - \gamma^2/4}$. One sets the initial conditions to $x(0) = 0$ and $p(0) = 0$. The auto-correlation function is

$$\begin{aligned}
\langle x(t_1)x(t_2)\rangle =& \int_0^{t_1}\int_0^{t_2} e^{\frac{\gamma}{2}[(s_1+s_2)-(t_1+t_2)]} \frac{\sin[\Omega(t_1-s_1)]}{m^2\Omega^2} \cdot \\
& \times \sin[\Omega(t_2-s_2)] \langle \xi(s_1)\xi(s_2)\rangle ds_2 ds_1 \qquad (5.108) \\
=& \frac{2\gamma T}{m\Omega^2} \int_0^{t_1}\int_0^{t_2} e^{\frac{\gamma}{2}[(s_1+s_2)-(t_1+t_2)]} \sin[\Omega(t_1-s_1)] \cdot \\
& \sin[\Omega(t_2-s_2)] \delta(s_2-s_1) ds_2 ds_1. \qquad (5.109)
\end{aligned}$$

Substituting $t_1 - s_1 = \tau_1$ and $t_2 - s_2 = \tau_2$ yields

$$\langle x(t_1)x(t_2)\rangle = \frac{2\gamma T}{m\Omega^2} \int_0^{t_1}\int_0^{t_2} e^{-\frac{\gamma}{2}(\tau_1+\tau_2)} \sin[\Omega(\tau_1)] \sin[\Omega(\tau_2)] \delta(\tau_1 + t_2 - t_1 - \tau_2) d\tau_2 d\tau_1 \tag{5.110}$$

$$= \frac{2\gamma T}{m\Omega^2} \int_0^{t_1} e^{-\frac{\gamma}{2}(2\tau_1 + \underbrace{t_2 - t_1}_{-\tau})} \sin[\Omega(\tau_1)] \sin[\Omega(\tau_1 + \underbrace{t_2 - t_1}_{-\tau})] d\tau_1 \tag{5.111}$$

$$G_{xx}(\tau) = \frac{2\gamma T}{m\Omega^2} \int_0^{\tau} e^{-\frac{\gamma}{2}(2\tau_1 - \tau)} \sin[\Omega(\tau_1)] \sin[\Omega(\tau - \tau_1)] d\tau_1. \tag{5.112}$$

The equation (5.112) is the convolution of the function $e^{-\gamma\tau/2}\sin\Omega\tau$ with itself. Via the Fourier transformation (FT) of this convolution the xx power spectral density yields

$$\begin{aligned}
S_{xx}(\omega) =& \int d\tau G_{xx}(\tau) e^{i\omega\tau} \qquad (5.113) \\
=& \frac{2\gamma T}{m\Omega^2} \left\| FT\left[e^{(-\gamma/2\tau)} \sin\Omega\tau\right] \right\|^2 \qquad (5.114) \\
=& \frac{2\gamma T}{m} \frac{1}{({\omega_0}^2 - \omega^2)^2 + \gamma^2\omega^2}. \qquad (5.115)
\end{aligned}$$

By taking the derivative of $x(t)$ (5.107) and multiplying by m one gets the conjugate momentum $p(t)$. The according PSD is computed analogously. The correlation function is

$$G_{pp}(\tau) = 2m\gamma T \int_0^\tau e^{-\frac{\gamma}{2}(2\tau_1-\tau)} \left(\cos[\Omega(\tau_1)] - \frac{\gamma \sin[\Omega(\tau_1)]}{2\Omega}\right) \cdot \left(\cos[\Omega(\tau_1-\tau)] - \frac{\gamma \sin[\Omega(\tau_1-\tau)]}{2\Omega}\right) d\tau_1. \tag{5.116}$$

Again one finds a convolution in equation (5.116) and performs the FT to find

$$S_{pp}(\omega) = \int d\tau G_{pp}(\tau) e^{i\omega\tau} \tag{5.117}$$

$$= 2m\gamma T \left\| FT\left[\omega^2 e^{-\gamma/2\tau}\left(\cos[\Omega(\tau)] - \frac{\gamma \sin[\Omega(\tau)]}{2\Omega}\right)\right]\right\|^2 \tag{5.118}$$

$$= 2m\gamma T \frac{\omega^2}{({\omega_0}^2 - \omega^2)^2 + \gamma^2\omega^2}. \tag{5.119}$$

The above formulas (5.115) and (5.119) allow to compare the numerical results for the PSD of the parametric oscillator to the effective model of a renormalized harmonic oscillator with frequency $\omega_{\text{eff}}[A, \omega_{\text{m}}]$. This is even possible without the explicit solution of the original parametric oscillator problem $x(t)$.
The numerical power spectra in the low-frequency sector $\omega < \omega_{\text{c}}$ confirm the renormalized oscillator model, as demonstrated in Fig. 5.5 and 5.6. The two pronounced features at the first side bands around the driving frequency $\omega_{\text{m}} \pm \omega_0$ are not included, which is in accordance with the low-energy effective theory, as shown in Fig. 5.5 and 5.6. By refining the stroboscopic time window $T_c = 2\pi/\omega_{\text{c}}$ with $\omega_{\text{c}} \gg \omega_{\text{m}}$ one could try to resolve the higher frequency part of the spectrum. However, averaging way above ω_{m} does not contain any further relevant information, because there is no additional fast degree of freedom and one has effectively only slow time scales. This amounts to the question how does the slow ω_0 part interact with the ω_{m} part on the time scale T_c and which Magnus contributions with spectral factors c_{ijk} are relevant [5].

[5] As always the intermediate regime between the adiabatic regime and the high-frequency regime is difficult to treat analytically.

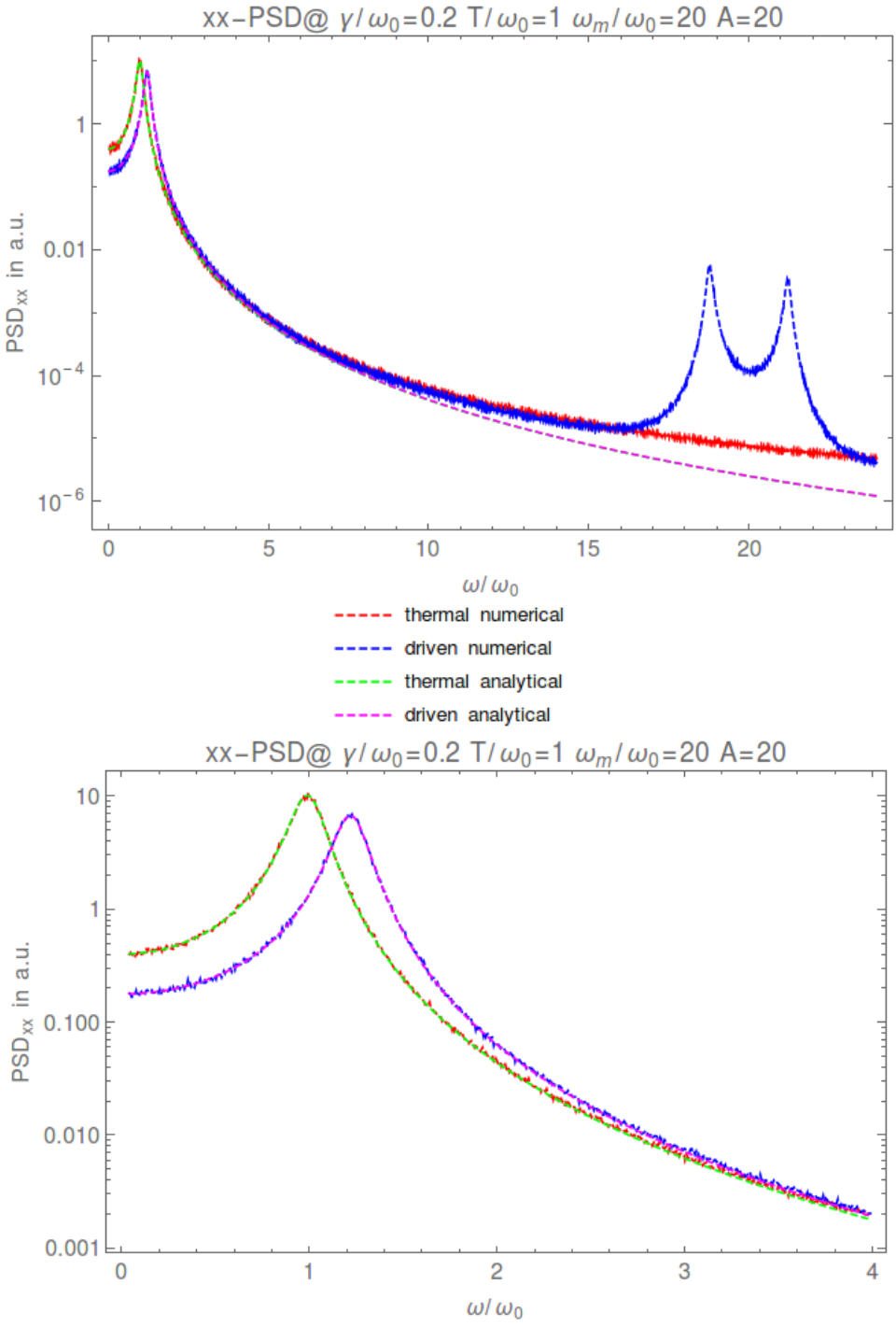

Figure 5.5: Comparison of the PSD from numerical results of the parametric oscillator to the PSD for the effective model. There is a shift of the resonance peak at the eigenfrequency ω_0 which is also featured in the analytical model. The model is an effective low-energy model, therefore the resonance with its splitting at the driving frequency $\omega_\mathrm{m} \pm \omega_0$ is not captured. However, the description is consistent for small frequencies (zoom in the right panel). There is a redistribution of the spectral weight towards higher frequencies. This effect is the reason for the reduced fluctuations in the low-energy degrees of freedom. Ref.[25] reports about the similar effect for the parametrically driven Josephson junction.[7]

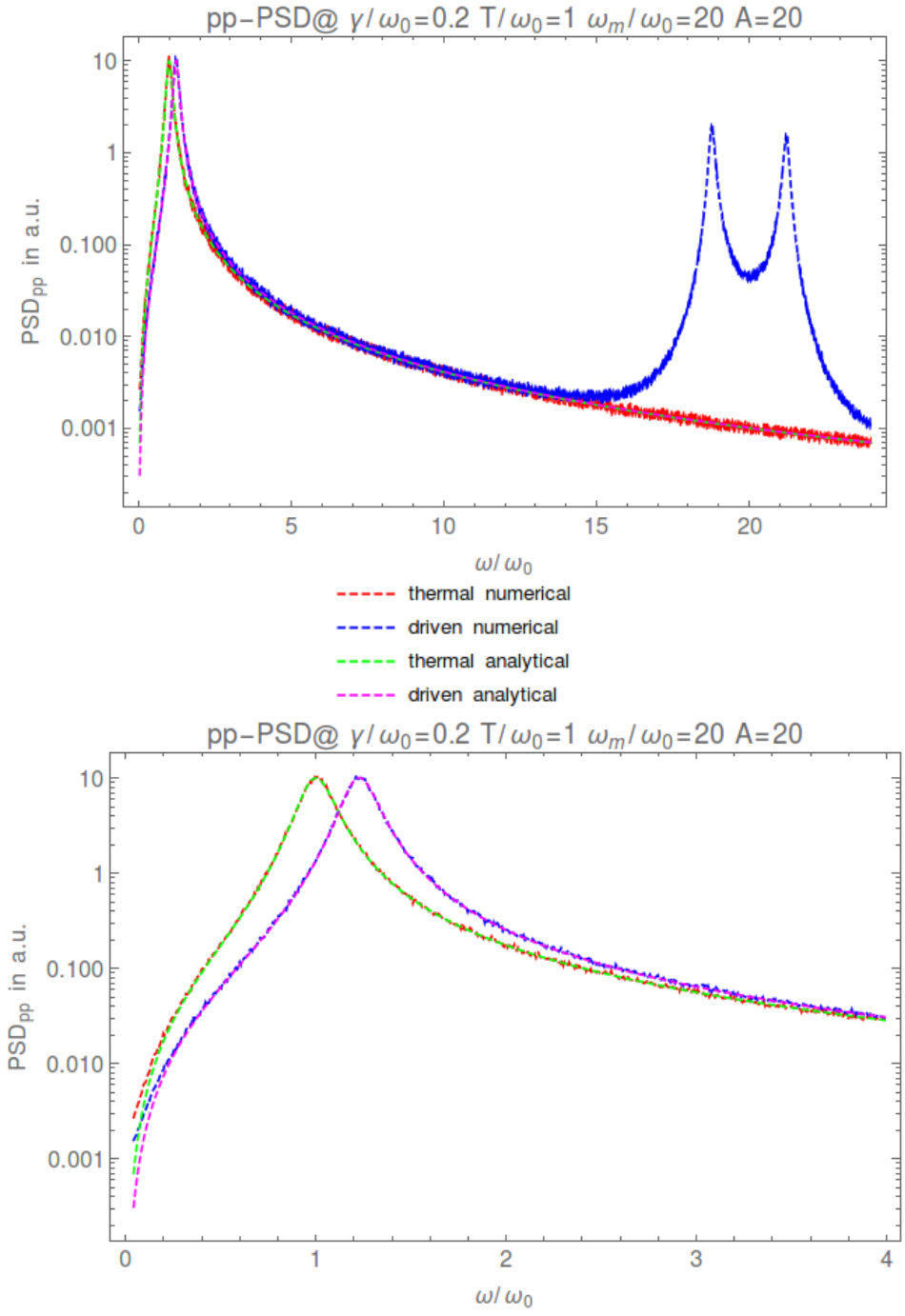

Figure 5.6: Comparison of the pp-PSD from numerical results of the parametric oscillator to the PSD for the effective model. The effects are similiar to the ones mentioned in the previous Fig. 5.5. The numerical data matches quantitatively and qualitatively the analytical prediction for the renormalized harmonic oscillator as in Fig. 5.5.

[7] In Ref.[25], which is about the Josephson junction system, the numerical simulation was performed by my colleagues R.Höppner and B.Zhu. I contributed to the analytical computation of the variances, which were solved by a direct exponential ansatz proposed by Prof. Ludwig Mathey.

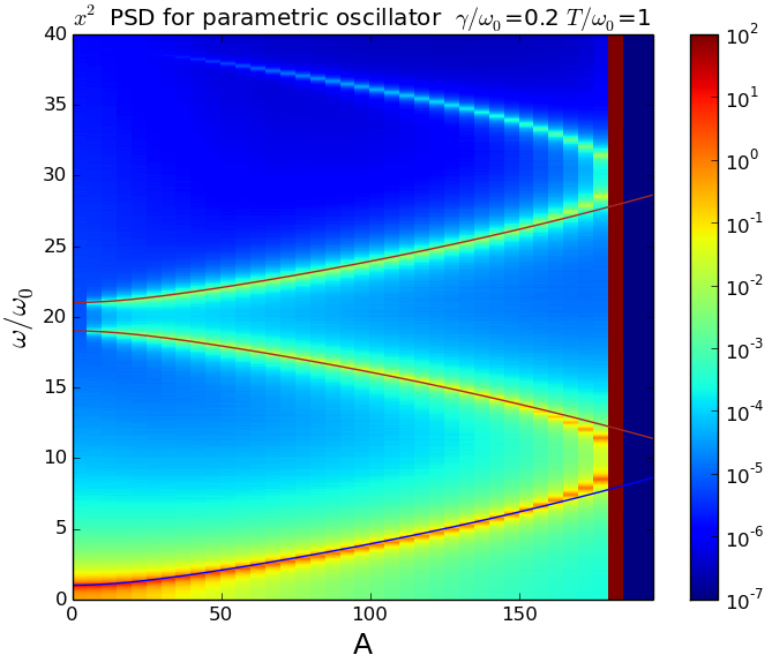

Figure 5.7: Mapping of the power spectra as a function of ω and the driving amplitude A. The driving frequency is $\omega_\mathrm{m}/\omega_0 = 20$. The brown lines indicate the shifted first harmonic frequencies at $\omega_\mathrm{m} \pm \omega_\mathrm{eff}$. The blue one is the effective frequency ω_eff according to Eq. (5.88). These lines perfectly follow the peaks in the PSD. At $A = 180$ the peak from the effective frequency ω_eff merges with the first side band $\omega_\mathrm{m} - \omega_\mathrm{eff}$ and the numerics breaks down. However, this plot illustrates the matching of the analytical derived effective frequencies and the numerical simulations. The similiar plot for the numerical data was first created by colleague Beilei Zhu in Ref. [16]. The data here is my own.

The mapping of the power spectrum from Fig. 5.5 as a function of the frequency ω and additionally the driving amplitude A yields Fig. 5.7. It shows how the stiffened effective eigenfrequency ω_eff merges at critical driving amplitude A_c with the first side band at the frequency $\omega_\mathrm{m} - \omega_\mathrm{eff}$. By setting the condition for the merging of the frequency peaks one determines A_c, i.e,

$$\omega_\mathrm{m} - \omega_\mathrm{eff}(A) = \omega_\mathrm{eff}(A) \tag{5.120}$$

$$\Leftrightarrow \omega_\mathrm{m} = 2\omega_\mathrm{eff}(A) \tag{5.121}$$

$$= 2\omega_0 \sqrt{1 + \frac{A^2{\omega_0}^2}{2{\omega_\mathrm{m}}^2} + \frac{2A^2{\omega_0}^2}{{\omega_\mathrm{m}}^4}\left({\omega_0}^2 - \frac{\gamma^2}{4}\right) + \frac{9A^4{\omega_0}^6}{8{\omega_\mathrm{m}}^6}}. \tag{5.122}$$

Equation (5.121) is the typical resonance condition for the parametric oscillator. However the resonance is not matched by tuning the driving frequency but rather

by forcing the effective eigenfrequency $\omega_{\text{eff}}(A)$ to match the condition. There one may call it effective parametric resonance. The eigenfrequency has been derived in the high frequency regime and under far off-resonant conditions $\omega_{\text{m}} \gg \omega_0$. For large driving amplitudes $A \gg 1$, the hierarchy of the frequencies breaks down, the power broadened eigenfrequency matches the driving frequency. In Ref. [16], it was only stated that accordingly the Magnus expansion breaks down, but the precise point is determined by the effective parametric resonance.
In the second order of A one obtains a quadratic equation and takes the positive real solution for $A_{c,2}$, i.e,

$$A_{c,2} = \sqrt{\frac{{\omega_{\text{m}}}^4}{2{\omega_0}^4} - 2\frac{{\omega_{\text{m}}}^2}{{\omega_0}^2}}. \tag{5.123}$$

In the fourth order of A, one obtains a quartic equation and takes the positive real solution for $A_{c,4}$, i.e,

$$A_{c,4} = \frac{1}{3}\sqrt{\frac{{\omega_{\text{m}}}^2\sqrt{2(11{\omega_{\text{m}}}^4 - 20{\omega_{\text{m}}}^2{\omega_0}^2 + 32{\omega_0}^4)}}{{\omega_0}^4} - \frac{8{\omega_{\text{m}}}^2}{{\omega_0}^2} - \frac{2{\omega_{\text{m}}}^4}{{\omega_0}^4}}. \tag{5.124}$$

The comparison with the numerical exact result A_c for a given value $\omega_{\text{m}}/\omega_0 = 20$ yields

$$A_c = 180 \tag{5.125}$$

$$A_{c,2} = 281 \tag{5.126}$$

$$A_{c,4} = 217. \tag{5.127}$$

The numerical exact value A_c is read off from the PSD map in Fig. 5.7. Hence the fourth order Magnus correction shows the correct tendency, but there is a strong hint that higher order Magnus contributions (e.g $A^6, \dots$) stiffen the effective frequency ω_{eff} even further, such that the merging occurs at around $A_c = 180$.

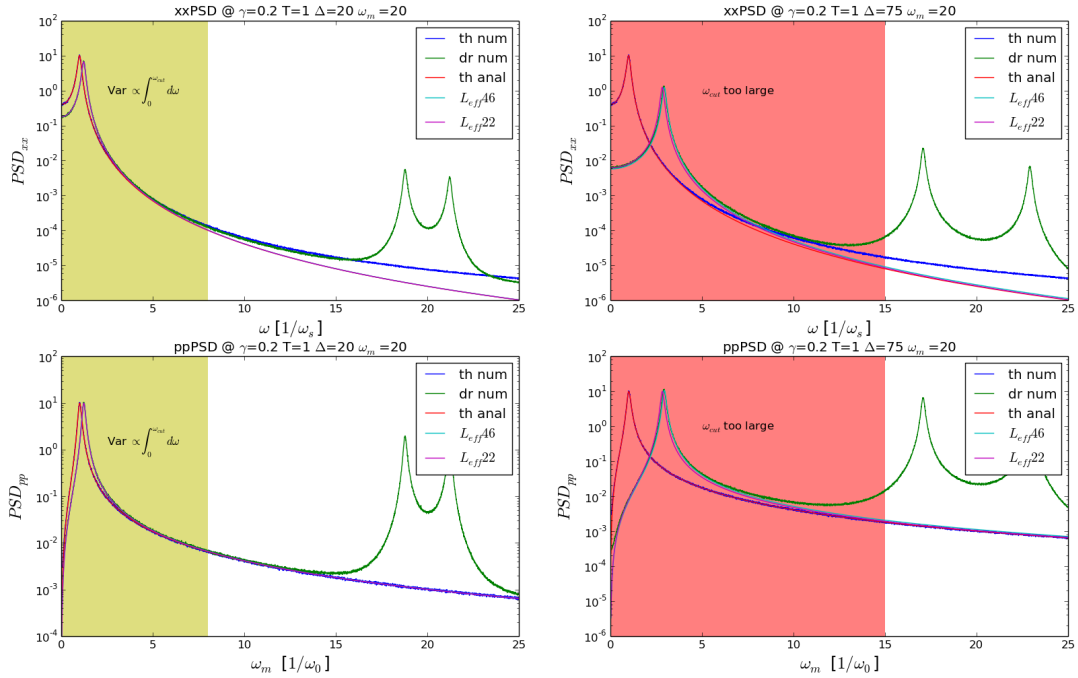

Figure 5.8: **Left panel** shaded area (yellow) indicates the contribution to the low-frequency part of variance from the PSD. The cut-off frequency is set to $\omega_c/\omega_0 = 8$, the driving frequency is $\omega_m/\omega_0 = 20$. **Right panel** the shaded area (red) reaches up to the tails of the first harmonic resonance at $\omega_m \pm \omega_0$. The cut-off frequency is $\omega_c/\omega_0 = 15$, the driving frequency is $\omega_m/\omega_0 = 20$. Due to the higher driving amplitude A the splitting of the resonance peaks is larger and the tails of the shifted resonance from $\omega_m - \omega_0$ reach towards lower frequencies. Hence the hierarchy of the frequencies breaks down and one ends up with highly increased fluctuations.

One expects the variance to depend on the cut-off frequency, as it is the Fourier transform of the PSD. For the numerical data, the Fourier back transformation of the PSD is performed with a frequency cut-off ω_c. Hence, one selects the frequency contribution to the resulting variance. This is a crucial point, since the usual variance contains information from all the frequencies. The numerical variance from PSD with cut-off ensures comparability to the results of the effective model. This can be seen in Fig. 5.5, the PSD for the analytical model lacks the resonance peaks at $\omega_m \pm \omega_0$, hence a contribution to the variance is missing. The redistribution of the spectral weight towards higher frequencies in the right panel of Fig. 5.5 is the remarkable feature in this plot. This feature gives rise to reduced fluctuations in the low-energy degrees of freedom, which is confirmed by the analytical results (brown lines) in Fig. 5.9.

For the low-energy effective theory one derived the Magnus contributions, necces-

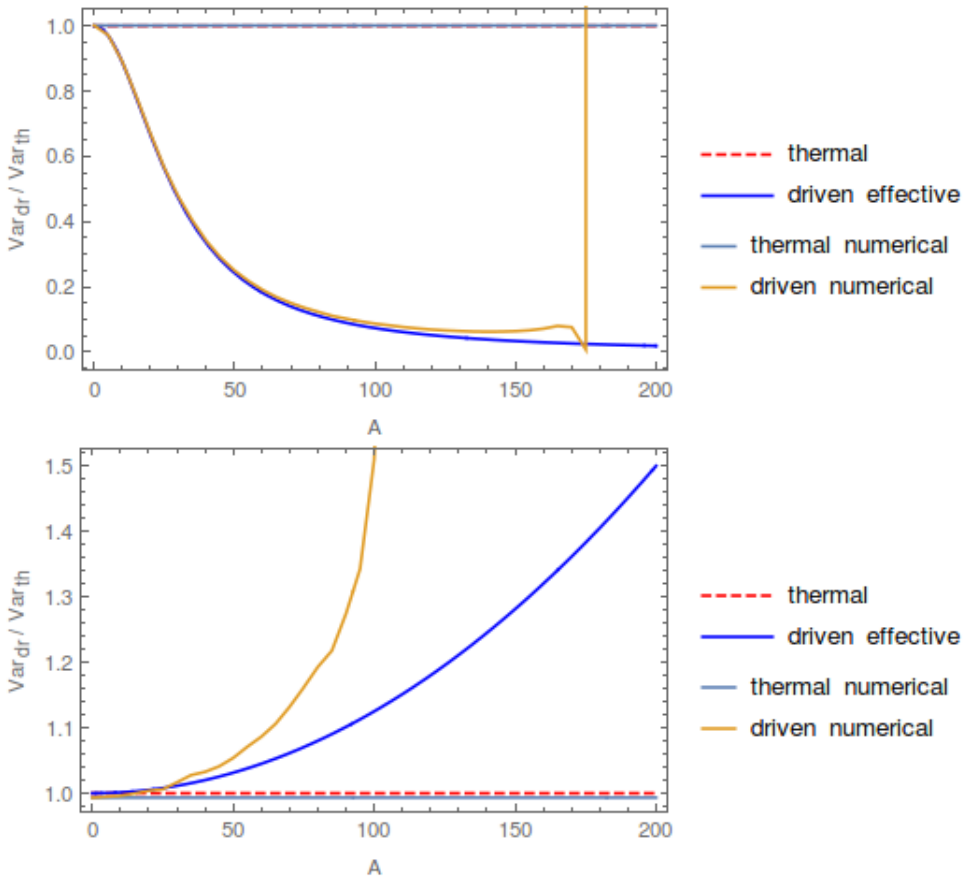

Figure 5.9: Comparison of the analytical and numerical results for the variances of x and p in thermal equilibrium $\mathrm{Var}_{\mathrm{th}}$ and in the effective steady state $\mathrm{Var}_{\mathrm{dr}}$. The quantities are normalized to the respective thermal equilibrium values in Eqs. (5.96), (5.97). The driving frequency is $\omega_{\mathrm{m}}/\omega_0 = 20$ and the cut-off frequency for the numerical computation of the variance is chosen to be $\omega_{\mathrm{c}}/\omega_0 = 8$. The numerical data of the driven system (brown line) diverges for large driving amplitudes A. Again this point of the divergence at about $A = 180$ takes place when the effective frequency ω_{eff} merges with the first side band $\omega_{\mathrm{m}} - \omega_{\mathrm{eff}}$. The low-energy effective theory (blue line) does not include this resonance since the assumption was ω_0 was far off-resonant to ω_{m}. However one runs into the resonance condition due to the strong renormalization of the eigenfrequency Eq. (5.88). Since all contributions to the analytically derived effective frequency Eq.(5.16) are positive, there is a decrease of the variance with increasing driving amplitude A. Note that even for large $A > 1$ the agreement between the theoretical and numerical data is quanitatively correct. This large range of validity for A arises from the perturbative expansion in terms of $(\omega_0/\omega_{\mathrm{m}})^n A^m < 1$, so if the frequency ratio is small, the amplitude term can become larger.

sary to set up a time-independent effective operator. The Magnus expansion was performed in the interaction picture. Afterwards, a perturbative back transformation into the Schrödinger picture yielded the constant contributions to the effective operator. The compact formulas can be applied to various example systems. In the case of the parametric oscillator one finds a renormalization of the eigenfrequency ω_0.

5.2 Parametrically driven Josephson junction with alternative Magnus expansion

The parametrically driven harmonic oscillator model demonstrated how the alternative Magnus expansion works and showed agreement up to the order $(\omega_0/om)^4 A^4$. In this particular case, the results of the Magnus expansion are directly comparable to the results from the straightforward ansatz given in Eq. (5.10). In this section the complexity of the model is increased. Aiming for an effective description of a driven superconductor, one considers a parametrically driven Josephson junction with a full $\sin\theta$-potential. Originally this is related to the classical pendulum with a parametric driving, also known as the Kaptiza pendulum [74]. The respective Hamiltonian for the systems is

$$H = H_0 + H_{dr} \tag{5.128}$$

$$H_0 = \frac{E_c}{2} n^2 - J\cos\theta \tag{5.129}$$

$$H_{dr} = H_d \cdot f(t) = -J\cos\theta \cdot f(t), \tag{5.130}$$

with the two conjugate variables n and θ and the Poisson bracket $[\theta, n] = 1$. n is the density difference between the two sides of the junction and θ is the relative phase of the densities between layers. $f(t)$ is any kind of an amplitude driving protcol, for the present case one assumes $f(t) = A\cos\omega_{\mathrm{m}} t$. The formulas for the different orders of the low-energy effective Magnus contributions yield

$$H_{\mathrm{eff},1} = 0 \tag{5.131}$$

$$H_{\mathrm{eff},2} = J\frac{{\omega_0}^2 A^2}{4{\omega_{\mathrm{m}}}^2}\sin^2\theta + \frac{{\omega_0}^4 A^2(3E_c n^2 + 4J\cos\theta)}{4{\omega_{\mathrm{m}}}^4}\sin^2\theta \tag{5.132}$$

$$H_{\mathrm{eff},3} = 0 \tag{5.133}$$

$$H_{\mathrm{eff},4} = J\frac{{\omega_0}^6 A^4}{{\omega_{\mathrm{m}}}^6}\left(\frac{9}{16}\sin^2\theta - \frac{161}{384}\sin^4\theta\right), \tag{5.134}$$

with the definition of the Josephson plasmon frequency for a single junction $\omega_0 = \sqrt{E_c J}$. Applying the addition theorems $\sin x \sin y = 1/2\,[\cos(x-y) - \cos(x+y)]$ and $\sin x \cos y = 1/2\,[\sin(x-y) + \sin(x+y)]$ reduces the powers of the trigonometric functions in (5.131)-(5.134) which makes the upcoming computation of the variance and other observables more convenient. The reshaped effective Hamiltonian

is

$$H_{\text{eff}} = J\left(\frac{{\omega_0}^2A^2}{8{\omega_\text{m}}^2} + \frac{127{\omega_0}^6A^4}{1024{\omega_\text{m}}^6}\right) + \frac{E_c}{2}n^2\left(1 + \frac{3{\omega_0}^4A^2}{4{\omega_\text{m}}^4}\right)$$
$$- J\left(1 - \frac{{\omega_0}^4A^2}{4{\omega_\text{m}}^4}\right)\cos\theta - J\left(\frac{{\omega_0}^2A^2}{8{\omega_\text{m}}^2} + \frac{55{\omega_0}^6A^4}{768{\omega_\text{m}}^6}\right)\cos 2\theta, \tag{5.135}$$

where the higher harmonics proportional to $\cos 3\theta, \cos 4\theta$ and the cross term $n^2\cos 2\theta$ were neglected, because the coefficients become negligible compared to the second order $\cos 2\theta$ or $n^2J \ll J$. Due to the nonlinear periodic cos-potential, the nested Poisson brackets for the Magnus contributions, e.g. $[\sin\theta, [\cos\theta, n]]$, never hit the identity 1. Thus more and more higher harmonics appear in the higher orders of the Magnus terms and a nontrivial potential landscape is created, whereas for the parametric oscillator one just finds an effective renormalization of the harmonic potential frequency ω_0.

This effective Hamiltonian has several interesting features. First of all, the parametric driving in J affects effectively E_c, as shown by the prefactor of E_c in Eq. (5.135). Without an ansatz by just applying the alternative Magnus scheme for certain parameters, the former instable point at $\theta = \pi$ can become a stable one. Taking the second derivative of (5.135) with respect to θ and plugging in the two extremal points $\{\theta = 0, \theta = \pi\}$, one obtains the conditions for the minima

$$\partial_\theta^2 H_{\text{eff}}|_{\theta=0} = J\left(1 + \frac{{\omega_0}^2A^2}{2{\omega_\text{m}}^2} - \frac{{\omega_0}^4A^2}{4{\omega_\text{m}}^4} + \frac{55{\omega_0}^6A^4}{192{\omega_\text{m}}^6}\right) > 0 \tag{5.136}$$

$$\partial_\theta^2 H_{\text{eff}}|_{\theta=\pi} = J\left(-1 + \frac{{\omega_0}^2A^2}{2{\omega_\text{m}}^2} + \frac{{\omega_0}^4A^2}{4{\omega_\text{m}}^4} + \frac{55{\omega_0}^6A^4}{192{\omega_\text{m}}^6}\right) > 0. \tag{5.137}$$

A and ω_m are the parameters originating from the parametric driving $J(t) = J(1 + A\cos\omega_\text{m}t)$. The minimum at $\theta = 0$ is also present in the undriven system with $A = 0$. The second extremal point, which is a maximum for $A = 0$, only becomes a minimum for

$$A \geq \sqrt{\frac{8}{55}}\sqrt{\frac{{\omega_\text{m}}^2\sqrt{3(3{\omega_0}^4 + 67{\omega_0}^2{\omega_\text{m}}^2 + 12{\omega_\text{m}}^4)}}{{\omega_0}^4} - \frac{3{\omega_\text{m}}^2}{{\omega_0}^2} - \frac{6{\omega_\text{m}}^4}{{\omega_0}^4}}. \tag{5.138}$$

The stabilization of a formerly instable point via driving is called dynamical stabilization. In the present case, the dynamical stabilization in a Josephson junction is achieved via parametric driving. Citro et al. derived a similar effect for the many-body version [121].

The single junction is analogous to the Kapitza pendulum [74], a full non-linear classic pendulum with a parametrically driven pivot. The stability analysis for the

Kapitza pendulum involves a separation of time scales for a slowly varying and a fastly oscillating contribution of the variable θ. Kapitza already predicted the occurence of another minimum apart from $\theta = 0$. The criterion for a second minimum according to the Kapitza approach yields

$$A \geq \sqrt{\frac{2{\omega_\mathrm{m}}^2}{{\omega_0}^2}}. \tag{5.139}$$

This is in accordance with Eq. (5.138). The leading-order correction of the effective Hamiltonian yields the same result. By applying the alternative Magnus expansion one has further access to the next order terms and can refine the condition for the minimum.

5.2.1 Effective distribution of the parametrically driven Josephson junction

The known equilibrium distribution is

$$\rho_\mathrm{th}(\theta, n) = \frac{1}{Z} \exp[-\beta(E_c/2n^2 - J\cos\theta)]. \tag{5.140}$$

The time-independent effective Hamiltonian again allows for a quasi steady state treatment in exponential form and yields

$$\rho_\mathrm{eff}(\theta, n) = \frac{1}{Z_\mathrm{eff}} \exp[-\beta H_\mathrm{eff}]. \tag{5.141}$$

The distribution is illustrated for $n = 0$ in Fig. 5.10 with parameters such that the side minimum occurs. The effective potential landscape in Eqs. (5.132) and (5.134) provides further localization of the distribution around $\theta = 0$ and $\theta = \pi$, whereas the density distribution around $\theta = \pi$ is strongly reduced. The strong enhancement around $\theta = 0$ is investigated by Taylor expanding the full effective Hamiltonian $H_0 + H_{\mathrm{eff},2} + H_{\mathrm{eff},4}$ given in Eqs. (5.132),(5.134) and isolating the prefactor of $\theta^2/2$. The resulting effective Josephson tunneling is

$$J_\mathrm{eff} = J\left(1 + \frac{{\omega_0}^2 A^2}{2{\omega_\mathrm{m}}^2} + \frac{2{\omega_0}^4 A^2}{{\omega_\mathrm{m}}^4} + \frac{9{\omega_0}^6 A^4}{8{\omega_\mathrm{m}}^6}\right) > J. \tag{5.142}$$

The expression ${\omega_0}^2 A^2/2{\omega_\mathrm{m}}^2$ is exactly the leading order Kapitza term [122] and it is also consistent with the term from the renormalized paramtric oscillator frequency (5.71), as it should be. Yet, the Magnus expansion yields additional terms, which

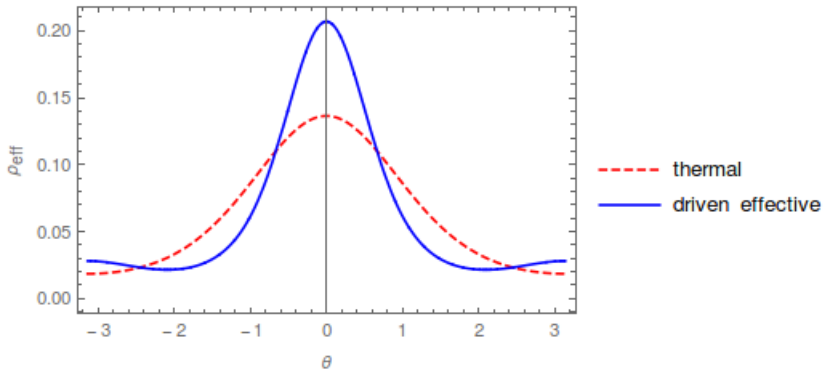

Figure 5.10: The effective steady state probability density distribution ρ_{eff} for a parametrically driven Josesphson junction at $n = 0$ compared to the thermal equilibrium one (red dashed). In the plot the condition for the side minimum (5.138) is fulfilled and there is an enhanced probability density at $\theta = \pi$. The general distribution at $\theta = 0$ is strongly enhanced, indicating that the renormalized is $J_{\text{eff}} > J$ (5.148). The parameters were $E_c/J = T/J = 1, \omega_{\text{m}}/J = 10, J = 1, A = 20$.

lead to an even deeper potential around $\theta = 0$. Due to the enhanced probability density around $\theta = 0$ and $\theta = \pi$ the total density is more localized and thus can be associated with an effectively more ordered and less thermally spread system. For comprison the infinite temperature distribution is totally flattened out and the underlying periodic cosine-potential is negligible, as the distributed electron pairs have enough energy to travel across the potential hills multiple times. At finite temperature and in the low-frequency regime, the effective terms next to the leading order become relevant and enforce the effectively narrowed distribution, especially for large drivings $A > \omega_{\text{m}}/\omega_0$.
Furthermore some of these terms do not only influence the distribution of θ, but also the distribution of n. To illustrate this, the difference between the effective steady state probability density distribution ρ_{eff} and the thermal one ρ_{th} is shown in Fig. 5.11.

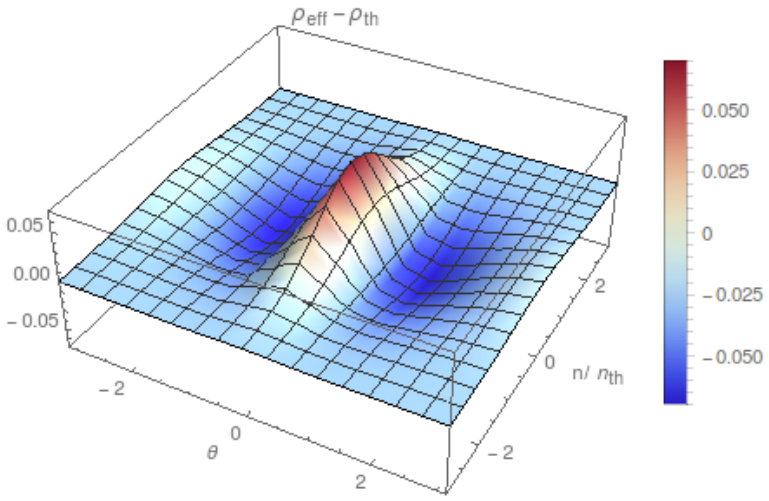

Figure 5.11: Difference between the effective steady state probability density distribution ρ_{eff} and the thermal one ρ_{th}. Close to $\theta = \pm\pi/2$ the nonequilibrium distribution is reduced. The parameters were chosen to visualize all features $E_c/J = T/J = 1, \omega_{\text{m}}/J = 10, J = 1, A = 20$.

5.2.2 Variance of the parametrically driven Josephson junction

Using the effective steady state distribution ρ_{eff}, the fluctuations of the current $\sim \sin\theta$ across a parametrically driven Josephson junction are computed analytically. The result is then compared to the undriven thermally distributed system with the underlying distribution ρ_{th}. The current fluctuations are related to the phase stiffness and phase correlations of a superconductor, see Eq. 1.8. In the context of driven high-T_c superconductors the literature describes the effects of the driving as transiently enhanced coherent transport or tunneling [4, 5, 6, 7, 11, 27, 28].
The equilibrium variance was already computed in (2.63) and is

$$Var_{\text{eq}}(\sin\theta) = \langle \sin^2\theta \rangle_{\text{eq}} - \langle \sin\theta \rangle_{\text{eq}}^2 = \frac{T}{J}\frac{I_1[J/T]}{I_0[J/T]}. \tag{5.143}$$

The $I_n[x]$ is again the modified Bessel function of n^{th} order. In Chapter 2, so before the introduction of the low-energy effective theory, the nonequilibrium distribution for the overdamped case was approximated by the smart ansatz $\exp[f(\theta_{\text{w}}, t)]$, where f was

$$f(\theta_{\text{w}}, t) = \frac{J_{\text{w}}}{T}\left[(1 + a_{\text{c}}(t))\cos\theta_{\text{w}} + a_{\text{s}}(t)\sin\theta_{\text{w}}\right]. \tag{5.144}$$

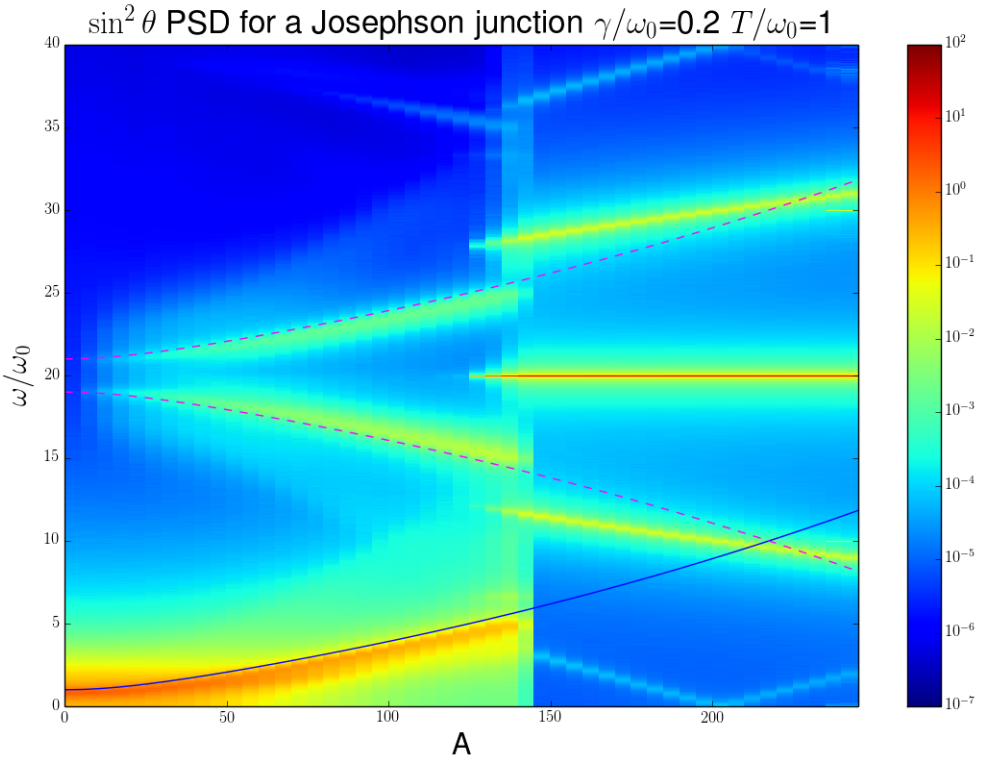

Figure 5.12: Mapping of the power spectral density of the current squared $\sim \sin^2\theta$ of a driven Josephson junction as a function of ω and the driving amplitude A. The blue line is the effective frequency ω_{eff}, as deduced from a linear potential (5.148). The dashed magenta lines indicate the first harmonic frequencies at $\omega_{\text{m}} \pm \omega_{\text{eff}}$. These lines follow the peaks in the PSD for small amplitudes A. A similiar mapping of the power spectral density of the parametric oscillator has been used by my colleague Beilei Zhu in Ref. [16].

The low-energy effective theory with the alternative Magnus scheme yields the following result

$$\begin{aligned} H_{\text{eff}} = & -J\cos\theta + \frac{E_{\text{c}}}{2}n^2 \\ & + J\frac{{\omega_0}^2 A^2}{4{\omega_{\text{m}}}^2}\sin^2\theta + \frac{{\omega_0}^4 A^2(3E_c n^2 + 4J\cos\theta)}{4{\omega_{\text{m}}}^4}\sin^2\theta \\ & + J\frac{{\omega_0}^6 A^4}{{\omega_{\text{m}}}^6}\left(\frac{9}{16}\sin^2\theta - \frac{161}{384}\sin^4\theta\right). \end{aligned} \tag{5.145}$$

By means of this time-independent Hamiltonian one constructs an effective nonequilibrium distribution $\rho_{\text{eff}} = \exp(-\beta H_{\text{eff}})$ and computes the variance of the Josephson current accordingly, i.e.,

$$Var_{\text{eff}}(\sin\theta) = \langle\sin^2\theta\rangle_{\text{eff}} - \langle\sin\theta\rangle^2_{\text{eff}}, \tag{5.146}$$

Since the exponent of ρ_{eff} is slighly more complex, the lengthy expressions for the variances will be ordered in powers of A^n and $(\omega_0/\omega_{\text{m}})^m$. The result for the variance up the order $n = 2$ and $m = 4$ is

$$\begin{aligned} Var_{\text{eff}}(\sin\theta) = & \frac{T}{J}\frac{I_1[J/T]}{I_0[J/T]}\left(1 + \frac{{\omega_0}^2 A^2}{{\omega_{\text{m}}}^2}\frac{3T}{2J} - \frac{{\omega_0}^4 A^2}{{\omega_{\text{m}}}^4}\left(2 + \frac{39T^2}{2J^2}\right)\right) + \\ & \frac{TI_1[J/T]^2}{JI_0[J/T]^2}\left(\frac{{\omega_0}^2 A^2}{4{\omega_{\text{m}}}^2} - \frac{{\omega_0}^4 A^2}{{\omega_{\text{m}}}^4}\frac{5T}{4J}\right) + \frac{{\omega_0}^4 A^2}{{\omega_{\text{m}}}^4}\frac{39T}{4J} - \frac{{\omega_0}^2 A^2}{{\omega_{\text{m}}}^2}\frac{3}{4} \end{aligned} \tag{5.147}$$

The analytical result for the variance with the Hamiltonian in the exponent H_{eff} is fully evaluated without any Taylor series and plotted in Fig. 5.13. Even for large amplitudes up to $A = 50$ the analytical prediction has good qualitative and quantitative agreement with the full numerical simulations. The variance of the current of a parametrically driven Josephson junction can be reduced and therefore the phase coherence between two layers of superconductors can be enhanced.
Numerically one should try to resolve the bump in the variance at $A = 140$ in Fig. 5.13 a little more, as this seems to be the crucial part where the resonance peaks from linearized approximation suddenly stop and some new unknown frequencies appear, see Fig.5.8. Maybe these effects are related to some phase slips in this nonlinear non-trivial cos potential landscape.

The application of the alternative Magnus expansion to parametrically driven Josephson junction yields an effective system Hamiltonian H_{eff}, which has several interesting features. First off all, a new side minimum at $\theta = \pi$ appears for critical value of A. This is the Kapitza effect which is referred as dynamical stabilization, where the former instable point $\theta = \pi$ becomes stable under the fast periodic driv-

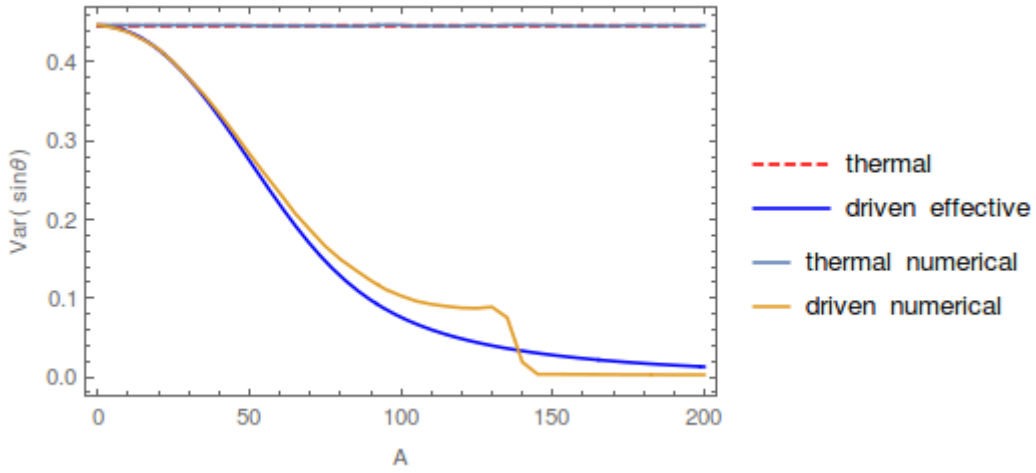

Figure 5.13: Variance of the Josephson current, which is proportional to $\sin\theta$ plotted versus the driving amplitude A. The key feature of the driven Josephson junction is a reduction of the variance as a function of the driving amplitude A. The numerical results for the thermal equilibrium (dark green line) and for the driven case (brown line) quantitatively coincide with analytic predictions from the lower-energy effective theory. The analytic solution for the driven case (blue line) lacks the resonance bump at $A = 135$, apart from that it accurately describes the variance for driving amplitudes up to $A = 50$. The driving frequency ω_{m} was 20 times the Josephson plasmon frequency $\omega_{\mathrm{m}}/\omega_{\mathrm{p}} = 20$. In Ref. [25], my colleagues computed the variances numerically for the single Josephson junction system and the bulk system of Josephson junctions. Here the numerical data for the single Josephson junction are my own product.

ing. So the Magnus expansion can automatically derive the Kapitza effect [121]. Furthermore due to the *cos* function the Magnus expansion generated higher and higher harmonic potentials, e.g. $\cos 2\theta, \cos 3\theta$, whereas compared to the parametric oscillator one only obtained a frequency renormalization. By linearizing the H_{eff} with respect to θ one estimates the renormalized effective Joesphson tunneling

$$J_{\text{eff}} = J\left(1 + \frac{{\omega_0}^2 A^2}{2{\omega_{\text{m}}}^2} + \frac{2{\omega_0}^4 A^2}{{\omega_{\text{m}}}^4} + \frac{9{\omega_0}^6 A^4}{8{\omega_{\text{m}}}^6}\right) > J, \tag{5.148}$$

and finds an effective enhancement. As it is already known from nonequilibrium distribution ρ_{eff}, the systems seem to favor the alignment of the relative phases $\theta = 0$ or for some critical driving amplitude also allow for an anti-alignment of the phases, where other configurations of phases are further suppressed under the driving.

Chapter 6

Summary and conclusion

Phase fluctuations of the wave function of the order parameter play a crucial role in highly anisotropic high T_c supercondcutors around the critical temperature. Based on the Lawrence-Doniach model, the layered high T_c superconductors were described as stacks of Josephson junctions. These Josephson junction arrays were considered as a thermodynamic ensemble. The central extension is the addition of a time-dependent external driving, which creates a state away from the equilibrium in these materials. In order to study the effects the thesis presented an alternative Magnus expansion, which is especially siutable in the high-frequency regime $\omega_m \gg \omega_0$.
At first the equilibrium distribution ρ_{eq} is directly analytically computed. This probability distribution shows the spread of the relative phases of the order parameter between the layers at a given temperature T and allows to compute the phase fluctuations. For the nonequilibrium situation a master equation was derived and solved by a simple exponential ansatz. For the overdamped case it was analytically shown that phase fluctuations in layered superconductors can be suppressed in the presence of the driving [25], effectively enhancing the phase coherence between the layers, supporting the observed experiments from [6, 7].
Inspired by the direct exponential solution, the idea was to find a general scheme for solutions of driven systems. Therefore, the main result of this thesis is an alternative Magnus expansion approach, which was used to derive Floquet Hamiltonians in the high-frequency approximation. In Chapter 3 a formalism to derive effective gauge-invariant Floquet Hamiltonians has been developed. This involved the introduction of spectral factors from the nested integrals of the Magnus series such as

$$c_{klm} = \frac{1}{3!(i\hbar)^2 T} \int_{t_0}^{t_0+T} dt_1 \int_{t_0}^{t_1} dt_2 \int_{t_0}^{t_2} dt_3 \left(e^{ik\omega t_1} e^{il\omega t_2} e^{im\omega t_3} + e^{ik\omega t_3} e^{il\omega t_2} e^{im\omega t_1} \right). \tag{6.1}$$

To obtain the constant, t_0-independent contributions, the condition $k+l+m=0$ has to be fulfilled. Given a time-dependent Hamiltonian system in Fourier decomposition $H(t)=\sum_k e^{ik\omega t}H_k$, this method yields a short cut to the effective Hamiltonian without the requirement of gauge transformations [15].
In Chapter 4 the Magnus series was perturbatively rearranged such that it provides a systematic expansion in the driving amplitude A and the inverse driving frequency $1/\omega_{\mathrm{m}}$. Apart from having a systematic expansion, the alternative Magnus expansion approach is a little more robust as compared to the standard Magnus scheme, because the perturbation parameter is always a controllable polynomial of $(\omega_0/om)^n A^m$. Especially in the high-frequency limit, this allows to study rather large driving amplitudes $A>1$.
Furthermore, a scheme and explicit formulas to construct the effective Floquet Hamiltonian in the high-frequency limit up fourth order is presented. With these closed formulas, one can then easily check whether a certain driving as non-trivial impact on the low-frequency effective system. It also enables to test different coupling and driving scenarios by just substituting $L_{\mathrm{dr}}(t)=f(t)L_{\mathrm{dr},0}$.
Applications of these general schemes are presented in Chapter 5. Applying the alternative Magnus formalism to a linear master equation, the initial problem with an explicitly time-dependent operator $L(t)$ is approximated by an effective time-independent operator $L(t)\approx L_{\mathrm{eff}}$. Exploiting the exponential form of the solution, one approximates a putative steady-state distribution for example as $\rho_{dr}=\exp[-\beta H_{\mathrm{eff}}]$. With time-independent operators for driven systems, one can transfer concepts and techniques only available for time-independent systems to periodically driven systems, as stated in Ref. [78].
As a first benchmark for the developed theory the Magnus expansion is explicitly applied to the parametric oscillator, which led to an effectively renormalized harmonic oscillator. This allowed to construct analytically a non-equilibrium power spectral density for the low-frequency sector. The quantitative agreement of the spectra from the full numerical simulation with solution from the Magnus expansion just confirms, that the scheme works.
Studying the parametric oscillator via the power spectra also revealed, that the reduced effective low-energy variance $Var_{\mathrm{dr(x)<Var_{th}}}(x)$ is caused by a redistribution of the spectral weight towards higher frequencies. Analytically this is also confirmed by the dynamical stabilization of the renormalized eigenfrequency $\omega_{\mathrm{eff}}>\omega_0$, see Eq. (5.88). The redistribution of spectral weight can therefore be interpreted as an effective cooling for the low-energy degrees of freedom. A related observation has been reported in Ref. [25] for the driven Josephson junction.

In the paper Ref. [16][1], the Magnus expansion is used to derive dynamical stabilization and to provide an approach to the parametric instability. The breakdown of the Magnus expansion indicates only a breakdown in the hierarchy of time scales which is now explained in this thesis. It is demonstrated that the numercial observed instability is nothing but the effective parametric resonance, namely the point where the first side band meets the effective eigenfrequency

$$\omega_{\mathrm{m}} - \omega_{eff}[A, \omega_{\mathrm{m}}] = \omega_{eff}[A, \omega_{\mathrm{m}}]. \tag{6.2}$$

The effect is called effective parametric resonance, because it is not the driving frequency ω_{m} which is tuned to $2\omega_0$, but the effective dressed eigenfrequency which matches for some critical A_{crit} the resonance condition. Keep in mind that this only happens for really large driving amplitudes $A \gg 1$, since one is usually in the high-frequency off-resonant regime $\omega_{\mathrm{m}} \gg \omega_0$. The final result of the thesis is the analytical derivation of the reduced phase fluctuations for the parametrically driven Josephson junction. The effective Hamiltonian, which encompasses the renormalization of system parameters and effects like dynamical stabilization, leads to enhanced phase coherence between the layers of anisotropic superconductors and is a hint towards the explanation of the transiently enhanced coherent transports in driven high T_{c} materials such as YBCO, see also Refs. [6, 7, 8]. By means of the Magnus expansion it was shown, that the non-equilibrium θ distribution of a parametrically driven Josephson junction has an enhanced probability around $\theta = 0$ or at the anti-aligned $\theta = \pi$. The distribution is increased around the two preferred phases and reduced close to $\theta = \pm\pi/2$, this can be interpreted as an effective cooling or enhanced phase coherence via an enhanced Josephson parameter $J_{\mathrm{eff}} > J$.
The thesis provides an instruction how to compute effective Hamiltonians without any elaborated ansatz up to the fourth order in Magnus terms and it also works for nonlinear potentials. The only required input is the undriven system Hamiltonian H_0 and the driven system part $H_{\mathrm{dr}}(t) = f(t)H_{\mathrm{dr},0}$ comprising a time-dependent driving protocol $f(t)$ and a coupling to the system $H_{\mathrm{dr},0}$. Even the explicit knowledge of the Floquet states is not required. By keeping formulas for the driving protocols and the coupling general, this thesis provides an ideal test ground for driven systems in the high frequency limit [17]. This allows for example to explore different driving scenarios for the cuprate superconductors such as an $U(t), J(t)$ or simply a linear coupling. With the growing number of pump-probe experiments and the advancement in experimental techniques in cold atom systems and solid state systems, there will be a broad spectrum of non-equilibrium setups which can be treated within the

[1]My contribution was to set up scheme and derive the formulas and prefactors. My former supervisor Ludwig Mathey gave valuable hints and advice here.

presented low-energy effective theory.
Possible further directions could be the extension of the scheme towards multi-mode driving which is a further step towards Floquet engineering [14].

Appendix A

Green's function for the externally driven harmonic oscillator

In this section, the solution for the externally driven harmonic oscillator, i.e.,

$$\ddot{\theta}_\mathrm{s} + \gamma\dot{\theta}_\mathrm{s} + \omega_\mathrm{s}^2\theta_\mathrm{s} = F(t). \tag{A.1}$$

is derived. γ is a damping term and $F(t) = F_0 \sin\omega_\mathrm{m} t$ is the external driving. First, one solves the homogeneous differential equation

$$\ddot{\theta}_\mathrm{s} + \omega_\mathrm{s}^2\theta_\mathrm{s} + \gamma\dot{\theta}_\mathrm{s} = 0 \tag{A.2}$$

with the exponential ansatz

$$\theta_\mathrm{s,hom} = \exp(i\lambda t). \tag{A.3}$$

Inserting (A.3) into Eq. (A.2) yields an algebraic equation for λ in the form

$$\exp(i\lambda t)(\lambda^2 - i\gamma\lambda - \omega_\mathrm{s}^2) \stackrel{!}{=} 0, \tag{A.4}$$

$$\tag{A.5}$$

which has the two solutions

$$\lambda_\pm = i\frac{\gamma}{2} \pm \underbrace{\sqrt{\omega_\mathrm{s}^2 - \frac{\gamma^2}{4}}}_{\omega}. \tag{A.6}$$

The general solution of the homogeneous problem is

$$\theta_{\mathrm{s,hom}} = e^{-\frac{\gamma}{2}t}\left(\tilde{A}e^{i\omega t} + \tilde{B}e^{-i\omega t}\right) \tag{A.7}$$

$$= e^{-\frac{\gamma}{2}t}\left[A\cos(\omega t) + B\sin(\omega t)\right] \tag{A.8}$$

where the unknown constants A and B are fixed by the initial conditions. In the next step, one solves the inhomogeneous differential equation with the Green's function formalism

$$\ddot{\theta}_{\mathrm{s}} + \gamma\dot{\theta}_{\mathrm{s}} + \omega_{\mathrm{s}}^2\theta_{\mathrm{s}} = F(t) \tag{A.9}$$

$$\hat{L}\theta = F(t) \tag{A.10}$$

with the linear differential operator

$$\hat{L} = \frac{d^2}{dt^2} + \gamma\frac{d}{dt} + \omega_{\mathrm{s}}^2. \tag{A.11}$$

The fundamental solution is defined by the equation

$$\hat{L}G(t) = \delta(t). \tag{A.12}$$

First one Fourier transforms Eq. (A.12) from the time domain to the frequency domain

$$\mathscr{F}\left[\hat{L}G(t)\right] = \frac{1}{\sqrt{2\pi}} \tag{A.13}$$

$$\frac{1}{\sqrt{2\pi}}\int_{-\infty}^{\infty} e^{i\lambda t}\hat{L}G(t) = \frac{1}{\sqrt{2\pi}} \tag{A.14}$$

$$-\left(\lambda^2 - i\gamma\lambda - \omega_{\mathrm{s}}^2\right)\mathscr{F}\left[G(t)\right] = \frac{1}{\sqrt{2\pi}} \tag{A.15}$$

$$G(t) = -\frac{1}{\sqrt{2\pi}}\mathscr{F}^{-1}\left(\frac{1}{\lambda^2 - i\gamma\lambda - \omega_{\mathrm{s}}^2}\right) \tag{A.16}$$

which means by performing the Fourier backtransform, one obtains the fundamental solution

$$G(t) = -\mathscr{F}^{-1}\left(\frac{1}{\lambda^2 - i\gamma\lambda - \omega_{\mathrm{s}}^2}\right) \tag{A.17}$$

$$G(t) = -\frac{1}{2\pi}\int_{-\infty}^{\infty}\frac{e^{i\lambda t}}{\lambda^2 - i\gamma\lambda - \omega_{\mathrm{s}}^2}d\lambda. \tag{A.18}$$

Applying the residue theorem for integration in the complex plane yields

$$G(t) = \lim_{\eta\to 0} -\frac{1}{2\pi}\int_0^\infty \frac{e^{i\lambda(t+i\eta)}}{\left(\lambda - i\frac{\gamma}{2} - \omega\right)\left(\lambda - i\frac{\gamma}{2} + \omega\right)} d\lambda \tag{A.19}$$

$$- \frac{1}{2\pi}\int_{-\infty}^0 \frac{e^{i\lambda(t-i\eta)}}{\left(\lambda - i\frac{\gamma}{2} - \omega\right)\left(\lambda - i\frac{\gamma}{2} + \omega\right)} d\lambda \tag{A.20}$$

$$= -\frac{2\pi i}{2\pi}\left[\frac{e^{i\left(i\frac{\gamma}{2}+\omega\right)}\left(\lambda - i\frac{\gamma}{2} - \omega\right)}{\left(\lambda - i\frac{\gamma}{2} - \omega\right)2\omega} + \frac{e^{i\left(i\frac{\gamma}{2}-\omega\right)}\left(\lambda - i\frac{\gamma}{2} + \omega\right)}{-2\omega\left(\lambda - i\frac{\gamma}{2} + \omega\right)}\right] \tag{A.21}$$

$$= \frac{e^{-\frac{\gamma}{2}t}}{\omega}\sin\omega t \tag{A.22}$$

$$G(t) = \underbrace{\Theta(t)}_{\text{for causality}} \frac{e^{-\frac{\gamma}{2}t}}{\omega}\sin\omega t \tag{A.23}$$

Now one can construct any solution for the inhomogeneous differential equation (A.30) by folding the inhomogeneity with the fundamental solution

$$\theta_{\mathrm{s},inh} = \int_{-\infty}^t dt' G(t-t')F(t') \tag{A.24}$$

$$= -\frac{e^{-\frac{\gamma}{2}t}\omega_\mathrm{m}}{\omega}\int_{-\infty}^t dt' e^{-\frac{\gamma}{2}t'}\sin\omega(t-t')F_0\sin\omega_\mathrm{m}t' \tag{A.25}$$

$$= \frac{\omega_\mathrm{m}^2\gamma F_0}{(\omega_\mathrm{s}^2-\omega_\mathrm{m}^2)^2+\omega_\mathrm{m}^2\gamma^2}\cos\omega_\mathrm{m}t - \frac{\omega_\mathrm{m}(\omega_\mathrm{s}^2-\omega_\mathrm{m}^2)F_0}{(\omega_\mathrm{s}^2-\omega_\mathrm{m}^2)^2+\omega_\mathrm{m}^2\gamma^2}\sin\omega_\mathrm{m}t. \tag{A.26}$$

Hence the general solution to the inhomogeneous differential equation is given by

$$\theta_\mathrm{s} = \theta_{\mathrm{s},h} + \theta_{\mathrm{s},inh} \tag{A.27}$$

$$= e^{-\frac{\gamma}{2}t}\left(B_1\cos\left[\sqrt{\omega_\mathrm{s}^2 - \frac{\gamma^2}{4}}t\right] + B_2\sin\left[\sqrt{\omega_\mathrm{s}^2 - \frac{\gamma^2}{4}}t\right]\right) \tag{A.28}$$

$$+ \frac{\omega_\mathrm{m}^2\gamma F_0}{(\omega_\mathrm{s}^2-\omega_\mathrm{m}^2)^2+\omega_\mathrm{m}^2\gamma^2}\cos\omega_\mathrm{m}t - \frac{\omega_\mathrm{m}(\omega_\mathrm{s}^2-\omega_\mathrm{m}^2)F_0}{(\omega_\mathrm{s}^2-\omega_\mathrm{m}^2)^2+\omega_\mathrm{m}^2\gamma^2}\sin\omega_\mathrm{m}t, \tag{A.29}$$

where the coefficients B_1 and B_2 have to be determined by the initial conditions. The Langevin equation for a harmonic oscillator with external driving is

$$\ddot{\theta}_\mathrm{s} + \gamma\dot{\theta}_\mathrm{s} + \omega_\mathrm{s}^2\theta_\mathrm{s} + \xi = F(t). \tag{A.30}$$

with the Gaussian white noise ξ and its noise correlation $\langle\xi(t)\xi(t')\rangle = 2\gamma mT\delta(t-t')$ and expectation value $\langle\xi(t)\rangle = 0$.
Hence, in order to solve the Langevin Equation (A.30) one has to fold the stochastic

noise term with the fundamental solution

$$\theta_{\mathrm{s},inh,stoch} = \int_{-\infty}^{t} dt' G(t-t')\xi(t') \tag{A.31}$$

and add this expression to the solution θ_{s}.

Appendix B

Solution of the forced quartic (or Duffing) oscillator

The response of the high-frequency mode in Eq. (2.33) can be described analytically via a Duffing oscillator approximation

$$\ddot{\theta}_{\mathrm{s}} \approx -\gamma\,\dot{\theta}_{\mathrm{s}} - {\omega_{\mathrm{s}}}^2\left(\theta_{\mathrm{s}} - \frac{{\theta_{\mathrm{s}}}^3}{6}\right) + \tilde{F} + \xi + \mathcal{O}({\omega_{\mathrm{w}}}^2), \tag{B.1}$$

where the backaction of weak Josephson junction to strong Josephson junction has been neglected, because for $\omega_{\mathrm{s}} \gg \omega_{\mathrm{w}}$ the term ${\omega_{\mathrm{w}}}^2 \sin\theta_{\mathrm{w}}$ is a rather weak perturbation to the strong junction, than vice versa. The solution of (B.1) for the strongly coupled degree of freedom θ_{s} then acts as driving term for the weak junction (2.40)

$$\ddot{\theta}_{\mathrm{w}} = -\gamma\,\dot{\theta}_{\mathrm{w}} - {\omega_{\mathrm{w}}}^2 \sin\theta_{\mathrm{w}} + \left({\omega_{\mathrm{s}}}^2 \sin\theta_{\mathrm{s}} - \tilde{F} + \xi\right). \tag{B.2}$$

This section provides the stationary solution of a Duffing oscillator which describes the strong junction, i.e.,

$$\ddot{\theta}_{\mathrm{s}} = -\gamma\,\dot{\theta}_{\mathrm{s}} - {\omega_{\mathrm{s}}}^2\left(\theta_{\mathrm{s}} - \frac{{\theta_{\mathrm{s}}}^3}{6}\right) + F(t). \tag{B.3}$$

Introducing the van der Pol transformation leads to variables (u, v) rotating in the $(\theta_{\mathrm{s}}, \dot{\theta}_{\mathrm{s}}/\omega_{\mathrm{m}})$-plane. The transformation is

$$u = \theta_{\mathrm{s}} \cos\omega_{\mathrm{m}} t - \frac{\dot{\theta}_{\mathrm{s}}}{\omega_{\mathrm{m}}} \sin\omega_{\mathrm{m}} t \tag{B.4}$$

$$v = -\theta_{\mathrm{s}} \sin\omega_{\mathrm{m}} t - \frac{\dot{\theta}_{\mathrm{s}}}{\omega_{\mathrm{m}}} \cos\omega_{\mathrm{m}} t. \tag{B.5}$$

Taking the derivative of Eqs. (B.4), (B.5) with respect to t and substituting (B.3) for $\ddot{\theta}_\mathrm{s}$ yields

$$\begin{aligned}\dot{u} &= \tfrac{1}{\omega}\left[-\Delta(u\cos\omega_\mathrm{m}t - v\sin\omega_\mathrm{m}t) - \omega_\mathrm{m}\gamma(u\sin\omega_\mathrm{m}t + v\cos\omega_\mathrm{m}t)\right. \\ &\qquad \left. + \tfrac{{\omega_\mathrm{s}}^2}{6}(u\cos\omega_\mathrm{m}t - v\sin\omega_\mathrm{m}t)^3 - F(t)\right]\sin\omega_\mathrm{m}t \qquad \text{(B.6)} \\ \dot{v} &= \tfrac{1}{\omega}\left[-\Delta(u\cos\omega_\mathrm{m}t - v\sin\omega_\mathrm{m}t) - \omega_\mathrm{m}\gamma(u\sin\omega_\mathrm{m}t + v\cos\omega_\mathrm{m}t)\right. \\ &\qquad \left. + \tfrac{{\omega_\mathrm{s}}^2}{6}(u\cos\omega_\mathrm{m}t - v\sin\omega_\mathrm{m}t)^3 - F(t)\right]\cos\omega_\mathrm{m}t \qquad \text{(B.7)}\end{aligned}$$

where $\Delta = {\omega_\mathrm{m}}^2 - {\omega_\mathrm{s}}^2$.
Averaging (B.6) and (B.7) over the small period $2\pi/\omega_\mathrm{m}$ we get equations for the slow varying amplitudes u, v

$$\begin{aligned}\dot{u} &= \frac{1}{2\omega_\mathrm{m}}\left[-\omega_\mathrm{m}\gamma u + \Delta v + \frac{3}{24}{\omega_\mathrm{s}}^2\left(u^2+v^2\right)v\right] \qquad \text{(B.8)} \\ \dot{v} &= \frac{1}{2\omega_\mathrm{m}}\left[-\Delta u - \omega_\mathrm{m}\gamma v - \frac{3}{24}{\omega_\mathrm{s}}^2\left(u^2+v^2\right)u - F_0\right]. \qquad \text{(B.9)}\end{aligned}$$

Expressed in polar coordinates $r = \sqrt{u^2+v^2}$ and $\phi = \arctan(v/u)$ this amounts to

$$\begin{aligned}\dot{r} &= \frac{1}{2\omega_\mathrm{m}}\left(-\omega_\mathrm{m}\gamma r - F_0\sin\phi\right) \qquad \text{(B.10)} \\ r\dot{\phi} &= \frac{1}{2\omega_\mathrm{m}}\left(-\Delta r - \frac{3}{24}{\omega_\mathrm{s}}^2 r^3 - F_0\cos\phi\right). \qquad \text{(B.11)}\end{aligned}$$

By checking the stationary states of (B.10), (B.11), one can analyze the response of the strong junction to the periodic external applied field $V(t)$ which leads to the equation

$$\left(-\omega_\mathrm{m}\gamma r - \sqrt{F_0^2 - \left(-\Delta r - \frac{3}{24}{\omega_\mathrm{s}}^2 r^3\right)^2}\right) \stackrel{!}{=} 0 \qquad \text{(B.12)}$$

for the amplitude r. Note that, if the cubic expression in (B.12) is zero, the standard solution to the amplitude of the harmonic oscillator is retrieved

$$\begin{aligned}r &= \frac{F_0}{\sqrt{\gamma^2{\omega_\mathrm{m}}^2 + ({\omega_\mathrm{m}}^2 - {\omega_\mathrm{s}}^2)^2}} \qquad \text{(B.13)} \\ & \qquad \text{(B.14)}\end{aligned}$$

Taking into account the non-linearity, e.g., the cubic term, the amplitude r can bifurcate, meaning for a certain given frequency ω_b it has a high and low amplitude solution.

Appendix C

Generalization of the stroboscopic time evolution

The non-stroboscopic time evolution for times which do not exactly match a multiple of the driving period $t \neq nT$ can be defined via

$$\begin{aligned} U(t_2,t_1) &= U(t_2,t_0+nT)e^{iH_F[t_0](t_2-t_0-nT)}e^{-iH_F[t_0](t_2-t_0-nT)}e^{-iH_F[t_0]nT}. \\ &\quad e^{-iH_F[t_0](t_0-t_1)}e^{iH_F[t_0](t_0-t_1)}U(t_0,t_1) && \text{(C.1)} \\ &= P(t_2,t_0)e^{-iH_F[t_0](t_2-t_1)}P^\dagger(t_1,t_0) && \text{(C.2)} \\ &= e^{-iK[t_0](t_2)}e^{-iH_F(t_1-t_2)}e^{iK[t_0](t_1)}. && \text{(C.3)} \end{aligned}$$

The unitary operator P, which does not necessarily come in exponential representation, is defined here as

$$P(t_2,t_0) = U(t_2,t_0)e^{iH_F[t_0](t_2-t_0)} = e^{-iK[t_0](t_2)}. \tag{C.4}$$

This implicitly defines the stroboscopic kick operator $K[t_0](t)$. The operator P contains the dynamics of the fast varying contributions on time scales $t < T$ and yields a temporal translation such that one keeps the stroboscopic Floquet Hamiltonian H_F in the time evolution operator. By construction P is periodic, i.e, $P(t,t_0) = P(t,t_0+nT) = P(t+nT,t_0)$ and fulfills $P(t_0+nT,t_0) = \mathrm{I}$. Equation (C.4) directly relates the stroboscopic kick operator $K[t_0](t) = i\log[P(t,t_0)]$ to the fast varying motion operator P. Hence, K satisfies $K[t_0](t_0+nT) = 0$ for an integer n.

By choosing one of the times t_1 or t_2 to coincide with t_0, we reduce equation (C.2) by one P operator This simplification comes at a cost, namely the Floquet Hamiltonian is either tied to the initial or final time of the evolution. Regarding experiments in the high-frequency limit, the initial and final time of a measurement often fluctuate

within a period, accordingly the Floquet Hamiltonian changes. In these cases, it is more convenient to define the Floquet Hamiltonian with respect to some fixed Floquet gauge t_0, independent of t_1 and t_2. In this way, the kick operators may differ, but the Floquet Hamiltonian H_F for the "middle part" of the time evolution remains unchanged.

Appendix D

Numerics

This section provides a few remarks on a few techniques and assumptions for the numerical computation.

D.1 Definition of power spectral density (PSD)

For a stationary time random process $X(t)$ the first moment fulfills

$$m_x[t] = \langle X[t] \rangle = m_x[t+\tau] = \langle X[t+\tau] \rangle \qquad \forall\, \tau \in \mathbb{R} \tag{D.1}$$

and the centered second moment, the autocovariance, suffices

$$acov[t,t'] = \langle (X[t] - m_x[t])(X[t'] - m_x[t']) \rangle = acov[t-t', 0]. \tag{D.2}$$

As usual, the expectation value $\langle \cdot \rangle$ is understood as a trajectory or ensemble average. The first statement implies that the mean is constant. The second one states that the autocovariance only depends on the time difference of $t - t'$. This is the standard setting, for example, for the Gaussian white noise ξ with its properties $\langle \xi(t)\xi(t') \rangle = 2\gamma m T \delta(t-t')$ and mean $\langle \xi(t) \rangle = 0$. It holds at thermal equilibrium. If one considers driven noise, the statements no longer hold.
In this thesis, the Langevin equation is studied, which is a stochastic differential equation with its noise term as external driving. Therefore, the solution of this equation comprises generally three contributions -the deterministic homogeneous part $X_{h,d}(t)$, the deterministic inhomogeneous part $X_{i,d}(t)$, the stochastic inhomogeneous part $X_{i,s}(t)$.
The PSD is defined via the Fourier transform of the observable $X(t)$

$$X(\omega) = \lim_{T\to\infty} \frac{1}{\sqrt{T}} \int_0^T X(t) e^{-i\omega t} dt, \tag{D.3}$$

namely

$$S_{xx}(\omega) = \langle |X(\omega)|^2 \rangle = \left\langle \frac{1}{T} \int_0^T X(t) e^{-i\omega t} dt \int_0^T X(t') e^{-i\omega t'} dt' \right\rangle . \tag{D.4}$$

Note here that t and t' are independent variables. Numerically one considers the case for $t' = t + \tau$. This means technically one computes the quantity

$$S_{xx}(\omega, \tau) = \langle X_t(\omega) X_{t+\tau}(\omega) \rangle, \tag{D.5}$$

where the constant shift τ is a free parameter. The dependence on τ is shown for the PSD from $\langle \sin x(t) \sin x(t+\tau) \rangle$ in Fig. (D.2). In order to obtain the PSD one first ensemble averages the considered variable at each time slice t_n. Afterwards the time intervall is Fast Fourier transformed.

D.2 Remark on the FFT

The computation of the PSD involves the Fast Fourier transformation of the computed trajectories $x(t)$ and $p(t)$. In some examples the numerical thermal equilibrium PSD did not match perfectly with the thermal analytical PSD. Also in the driven case the thermal back ground was a little overrated. One reason for this is the acquisition time for the Fourier sample, which leads to deviations in particular in the high-frequency part. The acquisition time T_{ac} limits the spectral resolution

$$df = \frac{1}{T_{\mathrm{ac}}}. \tag{D.6}$$

In the example (D.2) the PSD of the parametric oscillator in the long term steady state is studied. With longer acquisition times the PSD converges towards the thermal equilibrium values

D.3 Remarks on PSDs

The numerical ensemble preparation consists of a large number of independent trajectories, usually around 500-20000 depending on signal to noise ratio (SNR) needed to provide useful data. The SNR is defined as

$$SNR = \frac{\mu}{\sigma} \tag{D.7}$$

where μ is the expectation value and $\sigma \propto 1/\sqrt{N}$ the standard deviation and N the number of trajectories. This means the standard deviation gets smaller by the

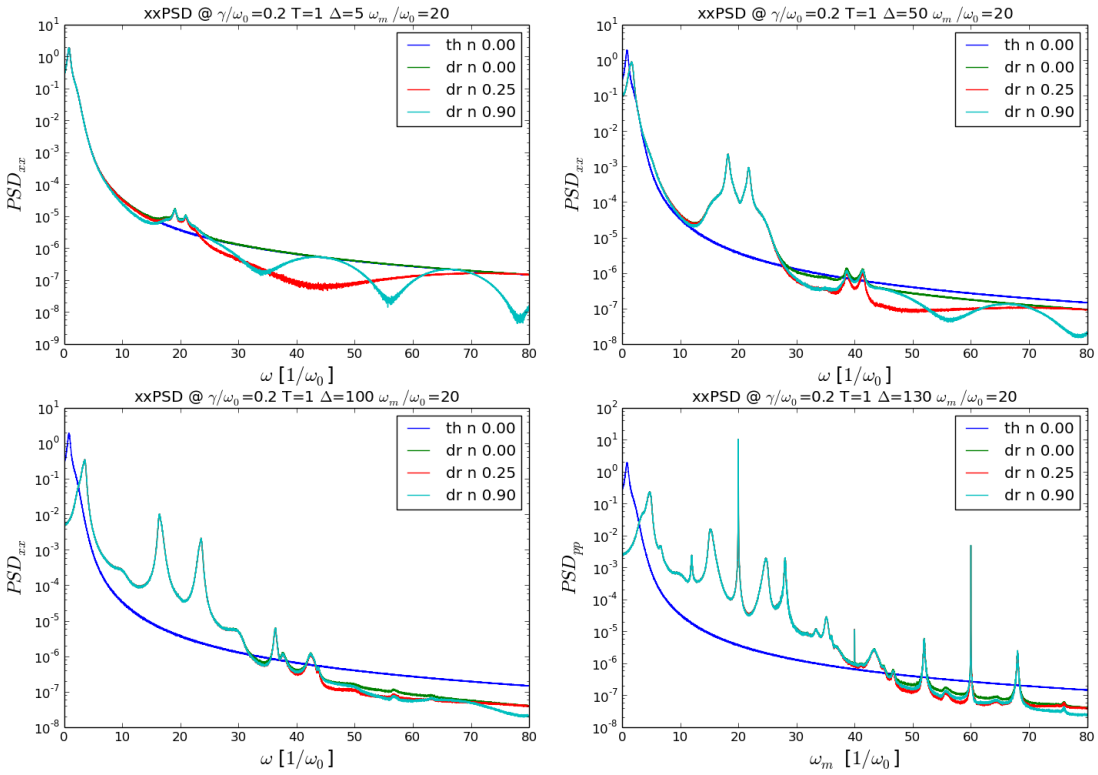

Figure D.1: PSD for a single Josephson junction computed from different correlation times $\langle \sin x(t) \sin x(t+\tau) \rangle$, here specified as in terms of $\tau = 2\pi n/\omega_0$ where n labels the fraction of the period (last number in the plot labels). As expected the PSDs strongly differ in the high frequency part $\omega > 10\omega_0$ of the spectrum but the low frequency part is almost not affected. The plots show this effect for different driving amplitudes.

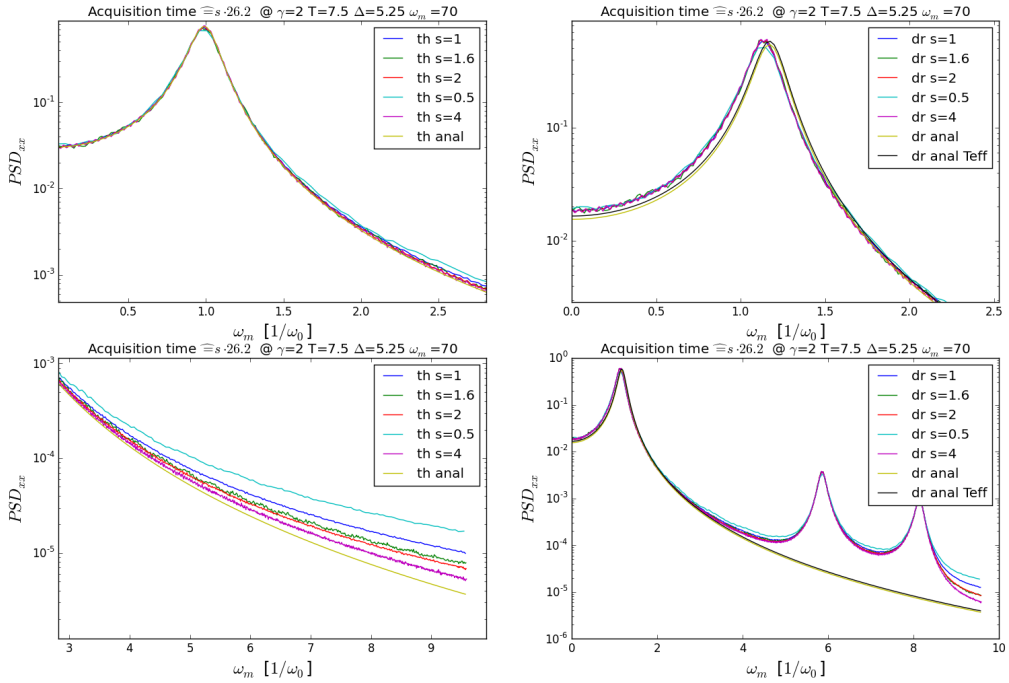

Figure D.2: Acquisition time dependence of the PSD

factor $1/\sqrt{N}$ and the SNR grows as $\sqrt{N}$. In order to keep the computational time handable the number of trajectories was limited to 20000.

Appendix E

General fourth order Magnus term

This section summarizes the general fourth-order Magnus term after the backtransformation into the Schrödinger picture. For a linear operator $L(t) = L_0 + f(t)L_{\mathrm{dr},0}$ the fourth-order term assumes the form

$$
\begin{aligned}
L_4 &= \exp[L_0 t]\dot{\Omega}_{4,I}(t)\exp[-L_0 t] && \text{(E.1)}\\
&= \frac{1}{12}\exp[L_0 t]\int_{t_0} dt_2 \int_{t_0}^{t_2} dt_3 \int_{t_0}^{t_3} dt_4 \\
&([L_{\mathrm{dr,I}}(t),[L_{\mathrm{dr,I}}(t_2),[L_{\mathrm{dr,I}}(t_3),L_{\mathrm{dr,I}}(t_4)]]] && \text{(E.2)}\\
&+[L_{\mathrm{dr,I}}(t_2),[L_{\mathrm{dr,I}}(t_3),[L_{\mathrm{dr,I}}(t_4),L_{\mathrm{dr,I}}(t)]]] && \text{(E.3)}\\
&+[L_{\mathrm{dr,I}}(t),[L_{\mathrm{dr,I}}(t_4),[L_{\mathrm{dr,I}}(t_3),L_{\mathrm{dr,I}}(t_2)]]] && \text{(E.4)}\\
&+[L_{\mathrm{dr,I}}(t_4),[L_{\mathrm{dr,I}}(t_3),[L_{\mathrm{dr,I}}(t),L_{\mathrm{dr,I}}(t_2)]]])\exp[-L_0 t]. && \text{(E.5)}
\end{aligned}
$$

Omitting the common integral prefactor

$$
\frac{1}{12}\int_{t_0}^{t} dt_2 \int_{t_0}^{t_2} dt_3 \int_{t_0}^{t_3} dt_4 f(t)f(t_2)f(t_3)f(t_4)\cdot, \tag{E.6}
$$

one sorts the occurring expression according to their order in perturbation theory of the back transformation into the Schrödinger picture. The nested commutators only differ by their time arguments. In particular, one can always exchange the innermost commutator and just get a different temporal argument and a negative sign. For example, the line (E.2) has two contributions to the first order of the perturbative back transformation to the Schrödinger picture, namely

$$
\begin{aligned}
[L_4]^{(1)}_{(\mathrm{E.2})} &= [L_{\mathrm{dr},0},[L_{\mathrm{dr},0},[{L_{\mathrm{dr},0}}^1,L_{\mathrm{dr},0}]]](t-t_3) + [L_{\mathrm{dr},0},[L_{\mathrm{dr},0},[L_{\mathrm{dr},0},{L_{\mathrm{dr},0}}^1]]](t-t_4) && \text{(E.7)}\\
&= [L_{\mathrm{dr},0},[L_{\mathrm{dr},0},[{L_{\mathrm{dr},0}}^1,L_{\mathrm{dr},0}]]](t_4-t_3). && \text{(E.8)}
\end{aligned}
$$

Collecting all the terms carefully, one arrives at

$$[L_4]^{(1)}_{0010} = [L_{\mathrm{dr},0}, [L_{\mathrm{dr},0}, [{L_{\mathrm{dr},0}}^1, L_{\mathrm{dr},0}]]]2(t_2 - t_3) \tag{E.9}$$

for the first order contribution after the back transformation. The second order has the following contributions

$$\begin{aligned}[L_4]^{(2)}_{0110} &= [L_{\mathrm{dr},0}, [{L_{\mathrm{dr},0}}^1, [{L_{\mathrm{dr},0}}^1, L_{\mathrm{dr},0}]]] \\ &\quad \times \{(t-t_2)(t_4-t_3) + (t-t_3)(t-t_4) + (t-t_4)(t_2-t_3) + (t-t_3)(t_2-t)\}\end{aligned} \tag{E.10}$$

$$[L_4]^{(2)}_{1010} = [{L_{\mathrm{dr},0}}^1, [L_{\mathrm{dr},0}, [{L_{\mathrm{dr},0}}^1, L_{\mathrm{dr},0}]]] \{(t-t_2)(t-t_4) + (t-t_4)(t_2-t)\} \tag{E.11}$$

$$[L_4]^{(2)}_{0020} = \frac{1}{2} L_{\mathrm{dr},0}, [L_{\mathrm{dr},0}, [{L_{\mathrm{dr},0}}^2, L_{\mathrm{dr},0}]]2\{(t-t_3)^2 - (t-t_2)^2\}. \tag{E.12}$$

The third order is a more involved, since one has to deal with different orders $(1, 2, 3)$ in the perturbative back transformation on different 'slots' in the nested commutators

$$\begin{aligned}[L_4]^{(3)}_{0021} &= \frac{1}{2} L_{\mathrm{dr},0}, [L_{\mathrm{dr},0}, [{L_{\mathrm{dr},0}}^2, {L_{\mathrm{dr},0}}^1]]] \\ &\quad \times \left\{(t-t_3)^2(t-t_4) - (t-t_4)^2(t-t_3) + (t-t_3)^2(t-t_2) - (t-t_2)^2(t-t_3)\right\}\end{aligned} \tag{E.13}$$

$$\begin{aligned}[L_4]^{(3)}_{0120} &= \frac{1}{2}[L_{\mathrm{dr},0}, [{L_{\mathrm{dr},0}}^1, [{L_{\mathrm{dr},0}}^2, L_{\mathrm{dr},0}]]] \\ &\quad \times \left\{(t-t_2)[(t-t_3)^2 - (t-t_4)^2] + (t-t_3)[(t-t_4)^2]\right. \\ &\quad \left.+(t-t_4)[(t-t_3)^2 - (t-t_2)^2] + (t-t_3)[-(t-t_2)^2]\right\}\end{aligned} \tag{E.14}$$

$$\begin{aligned}[L_4]^{(3)}_{1020} &= \frac{1}{2}[{L_{\mathrm{dr},0}}^1, [L_{\mathrm{dr},0}, [{L_{\mathrm{dr},0}}^2, L_{\mathrm{dr},0}]]] \\ &\quad \times \left\{(t-t_2)[(t-t_4)^2] + (t-t_4)[-(t-t_2)^2]\right\}\end{aligned} \tag{E.15}$$

$$\begin{aligned}[L_4]^{(3)}_{0210} &= \frac{1}{2}[L_{\mathrm{dr},0}, [{L_{\mathrm{dr},0}}^2, [{L_{\mathrm{dr},0}}^1, L_{\mathrm{dr},0}]]] \\ &\quad \times \left\{(t-t_2)^2(t_4-t_3) + (t-t_3)^2(t-t_4) + (t-t_4)^2(t_2-t_3) + (t-t_3)^2(t_2-t)\right\}\end{aligned} \tag{E.16}$$

$$\begin{aligned}[L_4]^{(3)}_{2010} &= \frac{1}{2}[{L_{\mathrm{dr},0}}^2, [L_{\mathrm{dr},0}, [{L_{\mathrm{dr},0}}^1, L_{\mathrm{dr},0}]]] \\ &\quad \times \left\{(t-t_2)^2(t-t_4) + (t-t_4)^2(t_2-t)\right\}\end{aligned} \tag{E.17}$$

$$[L_4]^{(3)}_{0030} = \frac{1}{3!}[L_{\mathrm{dr},0}, [L_{\mathrm{dr},0}, [{L_{\mathrm{dr},0}}^3, L_{\mathrm{dr},0}]]]2\{(t-t_3)^3 - (t-t_2)^3\}. \tag{E.18}$$

The above expressions are the contributions to the fourth-order Magnus term. For a better overview, the time-dependent coefficients are specified here as

$$C_{0010}(t) = \frac{1}{12}\int_{t_0}^{t} dt_2 \int_{t_0}^{t_2} dt_3 \int_{t_0}^{t_3} dt_4 f(t)f(t_2)f(t_3)f(t_4)2(t_2 - t_3) \tag{E.19}$$

$$\begin{aligned} C_{0110}(t) = \frac{1}{12}\int_{t_0}^{t} dt_2 \int_{t_0}^{t_2} dt_3 \int_{t_0}^{t_3} dt_4 f(t)f(t_2)f(t_3)f(t_4)\cdot \\ \{(t-t_2)(t_4-t_3) + (t-t_3)(t-t_4) + (t-t_4)(t_2-t_3) + (t-t_3)(t_2-t)\} \end{aligned} \tag{E.20}$$

$$C_{1010}(t) = \frac{1}{12}\int_{t_0}^{t} dt_2 \int_{t_0}^{t_2} dt_3 \int_{t_0}^{t_3} dt_4 f(t)f(t_2)f(t_3)f(t_4)\left\{(t-t_2)(t-t_4) + (t-t_4)(t_2-t)\right\} \tag{E.21}$$

$$C_{0020}(t) = \frac{1}{12}\int_{t_0}^{t} dt_2 \int_{t_0}^{t_2} dt_3 \int_{t_0}^{t_3} dt_4 f(t)f(t_2)f(t_3)f(t_4)\{(t-t_3)^2 - (t-t_2)^2\} \tag{E.22}$$

$$\begin{aligned} C_{0021}(t) = \frac{1}{12}\int_{t_0}^{t} dt_2 \int_{t_0}^{t_2} dt_3 \int_{t_0}^{t_3} dt_4 f(t)f(t_2)f(t_3)f(t_4)\frac{1}{2} \\ \times \left\{(t-t_3)^2(t-t_4) - (t-t_4)^2(t-t_3) + (t-t_3)^2(t-t_2) - (t-t_2)^2(t-t_3)\right\} \end{aligned} \tag{E.23}$$

$$\begin{aligned} C_{0120}(t) = \frac{1}{12}\int_{t_0}^{t} dt_2 \int_{t_0}^{t_2} dt_3 \int_{t_0}^{t_3} dt_4 f(t)f(t_2)f(t_3)f(t_4)\frac{1}{2} \\ \times \left\{(t-t_2)[(t-t_3)^2 - (t-t_4)^2] + (t-t_3)[(t-t_4)^2]\right. \\ \left.+(t-t_4)[(t-t_3)^2 - (t-t_2)^2] + (t-t_3)[-(t-t_2)^2]\right\} \end{aligned} \tag{E.24}$$

$$\begin{aligned} C_{1020}(t) = \frac{1}{12}\int_{t_0}^{t} dt_2 \int_{t_0}^{t_2} dt_3 \int_{t_0}^{t_3} dt_4 f(t)f(t_2)f(t_3)f(t_4)\frac{1}{2} \\ \times \left\{(t-t_2)(t-t_4)^2 - (t-t_4)(t-t_2)^2\right\} \end{aligned} \tag{E.25}$$

$$\begin{aligned} C_{0210}(t) = \frac{1}{12}\int_{t_0}^{t} dt_2 \int_{t_0}^{t_2} dt_3 \int_{t_0}^{t_3} dt_4 f(t)f(t_2)f(t_3)f(t_4)\frac{1}{2} \\ \times \left\{(t-t_2)^2(t_4-t_3) + (t-t_3)^2(t-t_4)\right. \\ \left.+(t-t_4)^2(t_2-t_3) + (t-t_3)^2(t_2-t)\right\} \end{aligned} \tag{E.26}$$

$$C_{2010}(t) = -C_{1020}(t) \tag{E.27}$$

$$C_{0030}(t) = \frac{1}{12}\int_{t_0}^{t} dt_2 \int_{t_0}^{t_2} dt_3 \int_{t_0}^{t_3} dt_4 f(t)f(t_2)f(t_3)f(t_4)\frac{1}{3}\{(t-t_3)^3 - (t-t_2)^3\}. \tag{E.28}$$

Bibliography

[1] Julian Struck, Malte Weinberg, Christoph Ölschläger, Patrick Windpassinger, Juliette Simonet, Klaus Sengstock, Robert Höppner, Philipp Hauke, André Eckardt, Maciej Lewenstein, et al. Engineering ising-xy spin-models in a triangular lattice using tunable artificial gauge fields. *Nature Physics*, 9(11):738–743, 2013.

[2] Claudio Giannetti, Massimo Capone, Daniele Fausti, Michele Fabrizio, Fulvio Parmigiani, and Dragan Mihailovic. Ultrafast optical spectroscopy of strongly correlated materials and high-temperature superconductors: a non-equilibrium approach. *Advances in Physics*, 65(2):58–238, 2016.

[3] Daniele Nicoletti and Andrea Cavalleri. Nonlinear light–matter interaction at terahertz frequencies. *Advances in Optics and Photonics*, 8(3):401–464, 2016.

[4] A Dienst, Matthias C Hoffmann, Daniele Fausti, Jesse C Petersen, S Pyon, T Takayama, H Takagi, and Andrea Cavalleri. Bi-directional ultrafast electric-field gating of interlayer charge transport in a cuprate superconductor. *Nature Photonics*, 5(8):485, 2011.

[5] Daniele Fausti, RI Tobey, Nicky Dean, Stefan Kaiser, A Dienst, Matthias C Hoffmann, S Pyon, T Takayama, H Takagi, and Andrea Cavalleri. Light-induced superconductivity in a stripe-ordered cuprate. *science*, 331(6014):189–191, 2011.

[6] Wanzheng Hu, Stefan Kaiser, Daniele Nicoletti, Cassandra R Hunt, Isabella Gierz, Matthias C Hoffmann, M Le Tacon, T Loew, B Keimer, and Andrea Cavalleri. Optically enhanced coherent transport in yba 2 cu 3 o 6.5 by ultrafast redistribution of interlayer coupling. *Nature materials*, 13(7):705, 2014.

[7] Stefan Kaiser, Cassandra R Hunt, Daniele Nicoletti, Wanzheng Hu, Isabella Gierz, HY Liu, M Le Tacon, T Loew, D Haug, B Keimer, et al. Optically induced coherent transport far above t c in underdoped yba 2 cu 3 o 6+ δ. *Physical Review B*, 89(18):184516, 2014.

[8] Michael Först, A Frano, Stefan Kaiser, Roman Mankowsky, Cassandra R Hunt, JJ Turner, GL Dakovski, MP Minitti, J Robinson, T Loew, et al. Femtosecond x rays link melting of charge-density wave correlations and light-enhanced coherent transport in yb a 2 c u 3 o 6.6. *Physical Review B*, 90(18):184514, 2014.

[9] Roman Mankowsky, Michael Först, and Andrea Cavalleri. Non-equilibrium control of complex solids by nonlinear phononics. *Reports on Progress in Physics*, 79(6):064503, 2016.

[10] R Mankowsky, M Fechner, M Först, A von Hoegen, J Porras, T Loew, GL Dakovski, M Seaberg, S Möller, G Coslovich, et al. Optically induced lattice deformations, electronic structure changes, and enhanced superconductivity in yba2cu3o6. 48. *Structural Dynamics*, 4(4):044007, 2017.

[11] Matteo Mitrano, Alice Cantaluppi, Daniele Nicoletti, Stefan Kaiser, A Perucchi, S Lupi, P Di Pietro, D Pontiroli, M Riccò, Stephen R Clark, et al. Possible light-induced superconductivity in k 3 c 60 at high temperature. *Nature*, 530(7591):461, 2016.

[12] Wanzheng Hu, D Nicoletti, AV Boris, B Keimer, and A Cavalleri. Optical melting of the transverse josephson plasmon: A comparison between bilayer and trilayer cuprates. *Physical Review B*, 95(10):104508, 2017.

[13] Andrea Cavalleri. Photo-induced superconductivity. *Contemporary Physics*, 59(1):31–46, 2018.

[14] Marin Bukov, Luca D'Alessio, and Anatoli Polkovnikov. Universal high-frequency behavior of periodically driven systems: from dynamical stabilization to floquet engineering. *Advances in Physics*, 64(2):139–226, 2015.

[15] André Eckardt and Egidijus Anisimovas. High-frequency approximation for periodically driven quantum systems from a floquet-space perspective. *New Journal of Physics*, 17(9):093039, 2015.

[16] Beilei Zhu, Tobias Rexin, and Ludwig Mathey. Magnus expansion approach to parametric oscillator systems in a thermal bath. *Zeitschrift für Naturforschung A*, 71(10):921–932, 2016.

[17] André Eckardt. Colloquium: Atomic quantum gases in periodically driven optical lattices. *Reviews of Modern Physics*, 89(1):011004, 2017.

[18] Roman Mankowsky, Alaska Subedi, Michael Först, SO Mariager, M Chollet, HT Lemke, JS Robinson, JM Glownia, MP Minitti, A Frano, et al. Nonlinear lattice dynamics as a basis for enhanced superconductivity in yba2cu3o6. 5. *Nature*, 516(7529):71–73, 2014.

[19] M Först, Roman Mankowsky, and Andrea Cavalleri. Mode-selective control of the crystal lattice. *Accounts of chemical research*, 48(2):380–387, 2015.

[20] Andreas Komnik and Michael Thorwart. Bcs theory of driven superconductivity. *The European Physical Journal B*, 89(11):244, 2016.

[21] Zachary M Raines, Valentin Stanev, and Victor M Galitski. Enhancement of superconductivity via periodic modulation in a three-dimensional model of cuprates. *Physical Review B*, 91(18):184506, 2015.

[22] Aavishkar A Patel and Andreas Eberlein. Light-induced enhancement of superconductivity via melting of competing bond-density wave order in underdoped cuprates. *Physical Review B*, 93(19):195139, 2016.

[23] Michael A Sentef, Akiyuki Tokuno, Antoine Georges, and Corinna Kollath. Theory of laser-controlled competing superconducting and charge orders. *Physical review letters*, 118(8):087002, 2017.

[24] Mehrtash Babadi, Michael Knap, Ivar Martin, Gil Refael, and Eugene Demler. Theory of parametrically amplified electron-phonon superconductivity. *Physical Review B*, 96(1):014512, 2017.

[25] Robert Hoeppner, Beilei Zhu, Tobias Rexin, Andrea Cavalleri, and L Mathey. Redistribution of phase fluctuations in a periodically driven cuprate superconductor. *Physical Review B*, 91(10):104507, 2015.

[26] SJ Denny, SR Clark, Y Laplace, A Cavalleri, and D Jaksch. Proposed parametric cooling of bilayer cuprate superconductors by terahertz excitation. *Physical review letters*, 114(13):137001, 2015.

[27] Jun-ichi Okamoto, Andrea Cavalleri, and Ludwig Mathey. Theory of enhanced interlayer tunneling in optically driven high-t c superconductors. *Physical review letters*, 117(22):227001, 2016.

[28] Jun-ichi Okamoto, Wanzheng Hu, Andrea Cavalleri, and Ludwig Mathey. Transiently enhanced interlayer tunneling in optically driven high-t c superconductors. *Physical Review B*, 96(14):144505, 2017.

[29] H Kamerlingh Onnes. The resistance of pure mercury at helium temperatures. *Commun. Phys. Lab. Univ. Leiden, b*, 120, 1911.

[30] Dirk Van Delft and Peter Kes. The discovery of superconductivity. *Physics Today*, 63(9):38–43, 2010.

[31] George F Hardy and John K Hulm. Superconducting silicides and germanides. *Physical Review*, 89(4):884, 1953.

[32] JR Gavaler. Superconductivity in nb–ge films above 22 k. *Applied Physics Letters*, 23(8):480–482, 1973.

[33] John Bardeen. J. bardeen, ln cooper, and jr schrieffer, phys. rev. 108, 1175 (1957). *Phys. Rev.*, 108:1175, 1957.

[34] LD Landau. 545; vl ginzburg and ld landau. *Zh. Eksp. Teor. Fiz*, 20:1064, 1950.

[35] Anthony J Leggett. *Quantum liquids: Bose condensation and Cooper pairing in condensed-matter systems*. Oxford University Press, 2006.

[36] Lev Petrovich Gor'kov. Microscopic derivation of the ginzburg-landau equations in the theory of superconductivity. *Sov. Phys. JETP*, 9(6):1364–1367, 1959.

[37] David Dew-Hughes. The critical current of superconductors: an historical review. *Low Temperature Physics*, 27(9):713–722, 2001.

[38] Fritz London and Heinz London. The electromagnetic equations of the supraconductor. *Proc. R. Soc. Lond. A*, 149(866):71–88, 1935.

[39] W Meissner and R Ochsenfeld. A new effect in penetration of superconductors. *Die Naturwissenschaften*, 21:787–788, 1933.

[40] Thorsten Fredrick Stromberg. The superconducting properties of high purity niobium. 1965.

[41] J George Bednorz and K Alex Müller. Possible hight c superconductivity in the ba- la- cu- o system. *Zeitschrift für Physik B Condensed Matter*, 64(2):189–193, 1986.

[42] A Schilling, M Cantoni, JD Guo, and HR Ott. Superconductivity above 130 k in the hg–ba–ca–cu–o system. *Nature*, 363(6424):56, 1993.

[43] Alexey Y Ganin, Yasuhiro Takabayashi, Yaroslav Z Khimyak, Serena Margadonna, Anna Tamai, Matthew J Rosseinsky, and Kosmas Prassides. Bulk superconductivity at 38 k in a molecular system. *Nature materials*, 7(5):367, 2008.

[44] Yoichi Kamihara, Takumi Watanabe, Masahiro Hirano, and Hideo Hosono. Iron-based layered superconductor la [o1-x f x] feas (x= 0.05- 0.12) with t c= 26 k. *Journal of the American Chemical Society*, 130(11):3296–3297, 2008.

[45] modified and saved as png. Illustration from wikipedia. *https://commons.wikimedia.org/wiki/File:Ybco.jpg*.

[46] T Valla, AV Fedorov, PD Johnson, BO Wells, SL Hulbert, Qiang Li, GD Gu, and N Koshizuka. Evidence for quantum critical behavior in the optimally doped cuprate bi2sr2cacu2o8+ δ. *Science*, 285(5436):2110–2113, 1999.

[47] J Orenstein and AJ Millis. Advances in the physics of high-temperature superconductivity. *Science*, 288(5465):468–474, 2000.

[48] Anthony J Leggett. What do we know about high t c? *Nature Physics*, 2(3):134, 2006.

[49] VJ Emery and SA Kivelson. Importance of phase fluctuations in superconductors with small superfluid density. *Nature*, 374(6521):434–437, 1995.

[50] SD Brorson, A Kazeroonian, JS Moodera, DW Face, TK Cheng, EP Ippen, MS Dresselhaus, and G Dresselhaus. Femtosecond room-temperature measurement of the electron-phonon coupling constant γ in metallic superconductors. *Physical Review Letters*, 64(18):2172, 1990.

[51] RD Averitt, G Rodriguez, AI Lobad, JLW Siders, SA Trugman, and AJ Taylor. Nonequilibrium superconductivity and quasiparticle dynamics in yba 2 cu 3 o 7- δ. *Physical Review B*, 63(14):140502, 2001.

[52] Gino P Segre, Nuh Gedik, Joseph Orenstein, Doug A Bonn, Ruixing Liang, and Walter N Hardy. Photoinduced changes of reflectivity in single crystals of yba 2 cu 3 o 6.5 (ortho ii). *Physical review letters*, 88(13):137001, 2002.

[53] S Dal Conte, CLAUDIO Giannetti, Giacomo Coslovich, Federico Cilento, Davide Bossini, Tadesse Abebaw, FRANCESCO Banfi, Gabriele Ferrini, Hiroshi Eisaki, Martin Greven, et al. Disentangling the electronic and phononic glue in a high-tc superconductor. *Science*, 335(6076):1600–1603, 2012.

[54] WE Lawrence and S Doniach. Proceedings of the 12th international conference on low temperature physics. 1971.

[55] L Bulaevskii and John R Clem. Vortex lattice of highly anisotropic layered superconductors in strong, parallel magnetic fields. *Physical Review B*, 44(18):10234, 1991.

[56] LN Bulaevskii, M Zamora, D Baeriswyl, H Beck, and John R Clem. Time-dependent equations for phase differences and a collective mode in josephson-coupled layered superconductors. *Physical Review B*, 50(17):12831, 1994.

[57] Mihail D Croitoru and Alexandre I Buzdin. Extended lawrence-doniach model: The temperature evolution of the in-plane magnetic field anisotropy. *Physical Review B*, 86(22):224508, 2012.

[58] Denis Feinberg, Stavros Theodorakis, and Abdel Mouneim Ettouhami. Model for layered superconductors: From josephson coupling to three-dimensional behavior. *Physical Review B*, 49(9):6285, 1994.

[59] Alexei E Koshelev and Matthew JW Dodgson. Josephson vortex lattice in layered superconductors. *Journal of Experimental and Theoretical Physics*, 117(3):449–479, 2013.

[60] CS Owen and DJ Scalapino. Vortex structure and critical currents in josephson junctions. *Physical Review*, 164(2):538, 1967.

[61] Dirk van der Marel and A Tsvetkov. Transverse optical plasmons in layered superconductors. *Czechoslovak Journal of Physics*, 46(6):3165–3168, 1996.

[62] L Benfatto, C Castellani, and Thierry Giamarchi. Doping dependence of the vortex-core energy in bilayer films of cuprates. *Physical Review B*, 77(10):100506, 2008.

[63] VJ Emery and SA Kivelson. Crossovers and phase coherence in cuprate superconductors. *Journal of Physics and Chemistry of Solids*, 59(10-12):1705–1710, 1998.

[64] TP Devereaux, A Virosztek, and A Zawadowski. Charge-transfer fluctuation, d-wave superconductivity, and the b 1 g raman phonon in cuprates. *Physical Review B*, 51(1):505, 1995.

[65] EW Carlson, SA Kivelson, VJ Emery, and E Manousakis. Classical phase fluctuations in high temperature superconductors. *Physical review letters*, 83(3):612, 1999.

[66] S Jonathan Chapman, Qiang Du, and Max D Gunzburger. On the lawrence–doniach and anisotropic ginzburg–landau models for layered superconductors. *SIAM Journal on Applied Mathematics*, 55(1):156–174, 1995.

[67] Zhiming Chen, K-H Hoffmann, and Lishang Jiang. On the lawrence–doniach model for layered superconductors. *European Journal of Applied Mathematics*, 8(4):369–387, 1997.

[68] Alaska Subedi, Andrea Cavalleri, and Antoine Georges. Theory of nonlinear phononics for coherent light control of solids. *Physical Review B*, 89(22):220301, 2014.

[69] Ali H Nayfeh and Dean T Mook. *Nonlinear oscillations*. John Wiley & Sons, 2008.

[70] Nicolaas Godfried Van Kampen. *Stochastic processes in physics and chemistry*, volume 1. Elsevier, 1992.

[71] HA Kramers. Ha kramers, physica 7, 284 (1940). *Physica*, 7:284, 1940.

[72] Hannes Risken. Fokker-planck equation. In *The Fokker-Planck Equation*. Springer, 1996.

[73] M Matti Maricq. Equilibrium in periodically time-dependent two-level systems. *Physical review letters*, 56(14):1433, 1986.

[74] P.L. Kapitza. Dynamic stability of a pendulum when its point of suspension vibrate. *Soviet Phys. JETP*, 21:588–592, 1951.

[75] Saar Rahav, Ido Gilary, and Shmuel Fishman. Time independent description of rapidly oscillating potentials. *Physical review letters*, 91(11):110404, 2003.

[76] Wolfgang Paul. Electromagnetic traps for charged and neutral particles. *Reviews of modern physics*, 62(3):531, 1990.

[77] Q Su and JH Eberly. Suppression of ionization and atomic electron localization by short intense laser pulses. *Physical Review A*, 43(5):2474, 1991.

[78] Martin Holthaus. Floquet engineering with quasienergy bands of periodically driven optical lattices. *Journal of Physics B: Atomic, Molecular and Optical Physics*, 49(1):013001, 2015.

[79] N Goldman and J Dalibard. Periodically driven quantum systems: effective hamiltonians and engineered gauge fields. *Physical Review X*, 4(3):031027, 2014.

[80] EB Feldman, AK Hitrin, and BN Provotorov. On the equivalence of different effective hamiltonians which determine the dynamics of a spin system in rapidly oscillating periodic fields. *Physics Letters A*, 99(2-3):114–116, 1983.

[81] Saar Rahav, Ido Gilary, and Shmuel Fishman. Effective hamiltonians for periodically driven systems. *Physical Review A*, 68(1):013820, 2003.

[82] Luca D'Alessio and Marcos Rigol. Long-time behavior of isolated periodically driven interacting lattice systems. *Physical Review X*, 4(4):041048, 2014.

[83] M Matti Maricq. Application of average hamiltonian theory to the nmr of solids. *Physical Review B*, 25(11):6622, 1982.

[84] Felix Bloch. Über die quantenmechanik der elektronen in kristallgittern. *Zeitschrift für Physik A Hadrons and Nuclei*, 52(7):555–600, 1929.

[85] AK Khitrin, Jiadi Xu, and Ayyalusamy Ramamoorthy. Coherent averaging in the frequency domain. *The Journal of chemical physics*, 136(21):214504, 2012.

[86] L.D. Landau and E.M. Lifshitz. Mechanics. *Pergamon Press*, 1:95, 1969.

[87] Sergio Blanes, Fernando Casas, JA Oteo, and José Ros. The magnus expansion and some of its applications. *Physics Reports*, 470(5):151–238, 2009.

[88] Wilhelm Magnus. On the exponential solution of differential equations for a linear operator. *Communications on pure and applied mathematics*, 7(4):649–673, 1954.

[89] André Nauts and Robert E Wyatt. Theory of laser-molecule interaction: The recursive-residue-generation method. *Physical Review A*, 30(2):872, 1984.

[90] TP Grozdanov and MJ Raković. Quantum system driven by rapidly varying periodic perturbation. *Physical Review A*, 38(4):1739, 1988.

[91] M Matti Maricq. Relaxation and equilibrium of a spin system coupled to a radiation field. *Physical Review B*, 37(13):7215, 1988.

[92] Heinz Peter Breuer and Martin Holthaus. A semiclassical theory of quasienergies and floquet wave functions. *Annals of Physics*, 211(2):249–291, 1991.

[93] Malay Bandyopadhyay and Sushanta Dattagupta. Quantum mechanics of rapidly and periodically driven systems. *Pramana–J. Phys*, 70(3), 2008.

[94] Albert Verdeny, Andreas Mielke, and Florian Mintert. Accurate effective hamiltonians via unitary flow in floquet space. *Physical review letters*, 111(17):175301, 2013.

[95] Freeman J Dyson. The radiation theories of tomonaga, schwinger, and feynman. *Physical Review*, 75(3):486, 1949.

[96] Richard P Feynman. An operator calculus having applications in quantum electrodynamics. *Physical Review*, 84(1):108, 1951.

[97] Sergio Blanes, Fernando Casas, JA Oteo, and J Ros. A pedagogical approach to the magnus expansion. *European Journal of Physics*, 31(4):907, 2010.

[98] Matthias W Reinsch. A simple expression for the terms in the baker–campbell–hausdorff series. *Journal of Mathematical Physics*, 41(4):2434–2442, 2000.

[99] S Klarsfeld and JA Oteo. The baker-campbell-hausdorff formula and the convergence of the magnus expansion. *Journal of Physics A: Mathematical and General*, 22(21):4565, 1989.

[100] RM Wilcox. Exponential operators and parameter differentiation in quantum physics. *Journal of Mathematical Physics*, 8(4):962–982, 1967.

[101] D Prato and PW Lamberti. A note on magnus formula. *The Journal of chemical physics*, 106(11):4640–4643, 1997.

[102] DP Burum. Magnus expansion generator. *Physical Review B*, 24(7):3684, 1981.

[103] S Klarsfeld and JA Oteo. Recursive generation of higher-order terms in the magnus expansion. *Physical Review A*, 39(7):3270, 1989.

[104] Philip Pechukas and John C Light. On the exponential form of time-displacement operators in quantum mechanics. *The Journal of Chemical Physics*, 44(10):3897–3912, 1966.

[105] I Bialynicki-Birula, B Mielnik, and J Plebański. Explicit solution of the continuous baker-campbell-hausdorff problem and a new expression for the phase operator. *Annals of Physics*, 51(1):187–200, 1969.

[106] WAB Evans. On some applications of the magnus expansion in nuclear magnetic resonance. *Annals of Physics*, 48(1):72–93, 1968.

[107] U Haeberlen and JS Waugh. Coherent averaging effects in magnetic resonance. *Physical Review*, 175(2):453, 1968.

[108] Albert Verdeny, Lukasz Rudnicki, Cord A Müller, and Florian Mintert. Optimal control of effective hamiltonians. *Physical review letters*, 113(1):010501, 2014.

[109] Fernando Casas. Sufficient conditions for the convergence of the magnus expansion. *Journal of Physics A: Mathematical and Theoretical*, 40(50):15001, 2007.

[110] F Casas, JA Oteo, and J Ros. Floquet theory: exponential perturbative treatment. *Journal of Physics A: Mathematical and General*, 34(16):3379, 2001.

[111] Per Christian Moan and Jitse Niesen. Convergence of the magnus series. *Foundations of Computational Mathematics*, 8(3):291–301, 2008.

[112] M Matti Maricq. Convergence of the magnus expansion for time dependent two level systems. *The Journal of chemical physics*, 86(10):5647–5651, 1987.

[113] EB Fel'dman. On the convergence of the magnus expansion for spin systems in periodic magnetic fields. *Physics Letters A*, 104(9):479–481, 1984.

[114] Francisco M Fernández. Convergence of the magnus expansion. *Physical Review A*, 41(5):2311, 1990.

[115] WR Salzman. An alternative to the magnus expansion in time-dependent perturbation theory. *The Journal of chemical physics*, 82(2):822–826, 1985.

[116] Luca D'Alessio and Anatoli Polkovnikov. Many-body energy localization transition in periodically driven systems. *Annals of Physics*, 333:19–33, 2013.

[117] Anatoli Polkovnikov. Phase space representation of quantum dynamics. *Annals of Physics*, 325(8):1790–1852, 2010.

[118] Milton Abramowitz, Irene A Stegun, et al. *Handbook of mathematical functions: with formulas, graphs, and mathematical tables*, volume 55. Dover publications New York, 1972.

[119] J Casas-Vázquez and D Jou. Temperature in non-equilibrium states: a review of open problems and current proposals. *Reports on Progress in Physics*, 66(11):1937, 2003.

[120] Gaston Floquet. Sur les équations différentielles linéaires à coefficients périodiques. 12:47–88, 1883.

[121] Roberta Citro, Emanuele G Dalla Torre, Luca D'Alessio, Anatoli Polkovnikov, Mehrtash Babadi, Takashi Oka, and Eugene Demler. Dynamical stability of a many-body kapitza pendulum. *Annals of Physics*, 360:694–710, 2015.

[122] P.L. Kapitza. Dynamical stability of a many-body kapitza pendulum. *Usp. Fiz. Nauk*, 44:7–15, 1951.

Muchas gracias

Eigentlich bin ich kein Fan von viel Pathos, aber ein paar Menschen lassen mich nicht daran vorbeikommen.

Michael, ich ziehe meinen Hut vor so einer großen aufrichtigen Persönlichkeit
Paulina, du hast mich ausgehalten
meiner Familie

Eidesstattliche Versicherung

Hiermit versichere ich an Eides statt, die vorliegende Dissertationsschrift selbst verfasst und keine anderen als die angegebenen Hilfsmittel und Quellen benutzt zu haben.

Die eingereichte schriftliche Fassung entspricht der auf dem elektronischen Speichermedium.

Die Dissertation wurde in der vorgelegten oder einer ähnlichen Form nicht schon einmal in einem früheren Promotionsverfahren angenommen oder als ungenügend beurteilt.

Hamburg, den 28. Juni 2019

Tobias Rexin